공학박사 학위논문

Enriching Simultaneous Transmission in High-Density WLAN

고밀도 무선랜 동시 전송 향상 기법

2017년 8월

서울대학교 대학원

전기·컴퓨터공학부

김 성 원

공학박사 학위논문

Enriching Simultaneous Transmission in High-Density WLAN

고밀도 무선랜 동시 전송 향상 기법

2017년 8월

서울대학교 대학원

전기·컴퓨터공학부

김 성 원

Enriching Simultaneous Transmission in High-Density WLAN

지도교수 최 성 현

이 논문을 공학박사 학위논문으로 제출함

2017년 7월

서울대학교 대학원

전기·컴퓨터공학부

김 성 원

김성원의 공학박사 학위 논문을 인준함

2017년 6월

위 원 장: 박 세 웅 (인)

부위원장: 최 성 현 (인)

위 원: 심 병 효 (인)

위 원: 김 효 일 (인)

위 원: 채 찬 병 (인)

Abstract

With increasing demand for wireless connectivity, IEEE 802.11 wireless local area network (WLAN), a.k.a. Wi-Fi, has become ubiquitous and continues to grow in number. This leads to the high density of WLAN, where many access points (APs) and client stations (STAs) operate on the same frequency channel. In a densely deployed WLAN, greater emphasis is placed on the importance of spatial reuse as well as spectral efficiency. In other words, it is of particular importance how many simultaneous transmissions are possible in a given area.

In this dissertation, we consider the following three strategies to increase the number of successful simultaneous transmissions: (i) Transmit power control for medium access control (MAC) acknowledgment (ACK) and clear-to-send (CTS) frames, (ii) carrier sense threshold (CST) adaptation, and (iii) simultaneous transmit and receive (STR), i.e., in-band full-duplex communication.

First, this dissertation sheds light on the co-channel interference (CCI) caused by 802.11 MAC ACK frames, which has been less studied than the CCI caused by data frames. Based on stochastic geometry analysis, we propose Quiet ACK (QACK), a dynamic transmit power control algorithm for ACK frames. Fine-grained transmit power adjustment is enabled by CCI detection and CCI power estimation in the middle of a data frame reception. A power control algorithm for clear-to-send (CTS) frame transmission, namely Quiet CTS (QCTS) is also proposed based on QACK. Our prototype using software-defined radio shows the feasibility and performance gain of QACK, i.e., $1.5\times$ higher throughput than the legacy 802.11 WLAN. The performance of QACK and QCTS is further evaluated in more general WLAN environments via extensive simulations using ns-3.

Second, a fine-grained CST adaptation method, which controls CST depending on both interferer and destination nodes, is proposed to improve spatial reuse in WLAN.

The proposed method utilizes pre-defined functions in the WLAN standard, thus making itself easily implementable in commercial WLAN devices. Supplementary clear channel assessment (CCA) method is also proposed to further enhance network performance by reducing CCA overhead. The performance of the proposed methods is comparatively evaluated via ns-3 simulation. Simulation results show that the proposed methods significantly improve network throughput compared with the legacy method.

Finally, a novel MAC protocol that enables STR in 802.11 WLAN, namely MASTaR, is proposed based on standard-compliant methods. Also, a digital self-interference cancellation (SIC) strategy is proposed to support the operation of MASTaR. The feasibility and the performance of MASTaR are extensively evaluated via 3D ray tracing-based simulation. The simulation results demonstrate that significant performance enhancement, e.g., up to 2.58$\times$ higher throughput than the current 802.11 MAC protocol, can be achieved by an STR-capable access point.

In summary, we propose an algorithm for ACK and CTS transmission power control and two protocols each for CST adaptation and STR which enhance the efficiency of WLAN by enriching simultaneous transmission. The feasibility and the performance of the algorithm and protocols are demonstrated via various methodologies including numerical analysis, 3D ray-tracing, ns-3 based system-level simulation, and prototype using a software-defined radio.

keywords: Wi-Fi, spatial reuse, power control, clear channel assessment (CCA), full duplex

student number: 2013-30962

Contents

List of Tables

List of Figures

Chapter 1

Introduction

1.1 Motivation

IEEE 802.11 wireless local area network (WLAN), a.k.a. Wi-Fi, has become a major wireless access technology in our daily lives, along with the soaring demand for mobile traffic. In 2015, mobile offload traffic via WLAN exceeded cellular traffic for the first time, and it will increase to 38.1 Exabytes per month by 2020, accounting for 55 percent of total mobile traffic [1]. Accordingly, total public WLAN hotspots including homespots will also grow 7-fold globally from 2015 to 2020.

Such proliferation of WLANs leads to high density of basic service sets (BSSs)[1] with the significant co-channel interference (CCI). In such a densely deployed WLAN, the need to enable more simultaneous transmission is emphasized on top of existing efforts to deliver large amount of information in one transmission. In this regard, a task group (TG) named TGax was launched in 2014 to develop IEEE 802.11ax, which is the next amendment for IEEE 802.11 WLAN, claiming for high-efficiency WLANs especially in dense deployment scenarios.

To increase the number of successful simultaneous transmissions in an environ-

[1] A BSS is composed of an access point and a number of associated stations.

ment with multiple overlapping BSSs (OBSSs),[2] we need to manage the CCI among the OBSSs effectively. The CCI between OBSSs harms the network performance in two respects. First, if the power of a CCI from an OBSS is smaller than carrier sense threshold (CST), the CCI deteriorates signal-to-interference-plus-noise-ratio (SINR) in the network, thus yielding more frame errors. On the other hand, the CCI whose power is greater than CST intensifies the channel access contention among BSSs, thus limiting transmission opportunities.

This brings up the question: *How can we reduce the network performance degradation due to CCI?* The first candidate solution is to lower transmit power. Since a transmission in a BSS acts as CCI to other BSS, a lower transmit power in the BSS leads to a smaller CCI power in OBSSs and fewer frame errors due to the CCI consequently. The second possible solution is to adjust CST, which gives the criteria for whether to initiate a new transmission or not.

Meanwhile, in cell-based wireless networks such as cellular networks and infrastructure WLAN, it has been assumed that either uplink (UL) transmission or downlink (DL) transmission is possible at a certain moment. However, the recent advances in self-interference cancellation (SIC) are realizing simultaneous transmit and receive (STR), a.k.a. in-band full-duplex communication, in wireless networks, i.e., a wireless node is expected to successfully receive a signal while transmitting another signal. This is also another way to increase simultaneous transmission. While insufficient suppression of self-interference (SI) has been a major obstacle to enable STR in WLAN, an even bigger obstacle is the fact that enabling STR involves significant modification to the current IEEE 802.11 MAC protocol.

[2] A neighboring BSS using the same frequency channel is called an OBSS.

1.2 Overview of Existing Approaches

1.2.1 Transmit power control for CCI reduction

Most studies on transmit power control have focused on data frame transmissions, which occupy the medium longer than control and management frame transmissions in general. Such approaches focusing on data frame control transmit power jointly with data rate adaptation [2], carrier sensing [3, 4], and scheduling [5] to resolve the performance degradation due to CCIs.

However, 802.11 MAC ACK frame transmission, which follows successful delivery of a data frame, can also cause a strong CCI to OBSSs depending on the topology. A recent work [6], based on measurements, revealed that ACK frames give rise to performance degradation and starvation in OBSSs especially in densely deployed WLAN environments. To reduce such damage caused by ACK interference, a heuristic algorithm named *MinPACK* is proposed in [6]. MinPACK periodically adapts ACK transmit power by comparing the ACK frame error rate (AFER) with reduced ACK power and the AFER with the maximum transmit power. It is also shown in [6] that device driver of off-the-shelf devices supports fine-grained power control for ACK frames independently from data frames.

1.2.2 CST adaptation for better spatial reuse

Many studies have been conducted on controlling CST to improve spatial reuse. Analytic schemes proposed in [7, 8] focus on hidden terminal problem. These schemes assume that nodes are aware of link distances and the received signal power is determined by a pathloss model, thus limiting their practicality. Meanwhile, heuristic schemes based on packet error rate (PER) are proposed in [9], [10]. These schemes increase/decrease CST by comparing the maximum per-link PER with a target PER [9] or by comparing PER of the recent window with that of the previous window [10]. Due to the nature of heuristic approaches, the schemes take time to converge, thus

improperly working in volatile channel condition. Also, using a global value of CST regardless of an *interferer*, i.e., the transmitter of the current CCI, and a *destination*, i.e., the receiver of the packet at the head of the queue, these schemes have a limitation in improving spatial reuse when multiple interferers and destinations exist.

1.2.3 MAC protocol for STR in WLAN

In recent years, many studies have developed new MAC protocols to support STR in WLANs [11]. In this section, we review the protocols in the literature while focusing on (i) whether channel access is conducted in a distributed manner or a centralized manner, (ii) whether the asymmetric mode is supported, and (iii) whether UL-to-DL interference (UDI)[3] is considered. The protocols designed for infrastructure network are mainly considered, since the target environment in this dissertation is infrastructure-based WLAN.

Protocol Based on Centralized Channel Access

Proposed in [12] is *Janus*, a MAC protocol scheduling both UL and DL transmissions based on a conflict map, which describes the amount of interference a node experiences when another node transmits. At each round, initiated by a probe packet from an AP, the AP and its associated STAs exchange a set of information in a predefined order and, using the information, the AP coordinates both UL and DL transmissions. Janus, however, requires significant modifications to the current behavior of WLANs, which operate in a distributed manner.

Distributed Protocols for Symmetric Mode

Distributed approaches focusing on symmetric modes are proposed in [13, 14]. The proposed protocols in [13] enable STR in WLAN based on collision avoidance by utilizing RTS/CTS. The authors also addressed the fairness issue between the nodes

[3] A detailed description of UDI is provided in Chapter 5.

involved in STR transmission, i.e., FD nodes, and the nodes overhearing the transmission, i.e., overhearing nodes. The overhearing nodes may not decode the overlapping transmitted frames, thus waiting for extended inter-frame space (EIFS) after the STR transmission. Since EIFS is considerably longer than DCF inter-frame space (DIFS), which is used after successful reception, the FD nodes would have a higher opportunity to win the channel again. To solve the unfairness problem, the authors make the FD nodes wait for EIFS instead of DIFS even after a successful transmission.

FuMAC [14] initiates bi-directional transmission by checking the destination field of primary transmission. If no responding transmission is observed, the PTX infers that a collision has occurred at PRX, and thus aborts the primary transmission. The authors also modified the packet preamble to convey a pseudo noise (PN) sequence as a transmitter identifier, and use the sequence for the transmitter-side collision detection.

Distributed Protocols for Both Modes

Proposed in [15–20] are MAC protocols that consider the asymmetric modes. In [15], a synchronized channel access based on shared random back-off is proposed on top of the current CSMA/CA based channel access. The authors added a new header carrying a set of information. By using the information, two nodes can share the same back-off counter and start transmission simultaneously.

The proposed protocol in [16] arranges symmetric and asymmetric modes by exchanging full duplex acknowledgments (FDAs) in the middle of a packet. After receiving the PLCP header and MAC header of a data frame, the target receiver notifies the transmitter of the feasibility of the transmission by sending FDA. The transmitter then decides whether to keep or stop the transmission. The authors in [16] do not, however, consider the feasibility of ACK transmission, which follows a successful delivery of the data transmission. Therefore, the simultaneous ACK transmissions are not protected. RCTC [17] enables STR by transmitting two PN signatures, which carry the identifiers of PTX and PRX, respectively, before data transmission. The target receiver

Table 1.1: Comparison of STR MAC protocols.

	Year	Distr.	Asymm. mode	UDI	ACK protection	Standard-comp.
FD-MAC [15]	2011	O	O	△[4]	O*	X
[16]	2013	O	O	O	X	X
Janus [12]	2013	X	O	O	X	X
RCTC [17]	2013	O	O	O	△[5]	X
[13]	2014	O	X	–	–	X
FuMAC [14]	2014	O	X	–	–	X
RTS/FCTS [18]	2015	O	O	X	X	X
A-Duplex [19]	2015	O	O	O	O*	X
Energy-FDM [20]	2016	O	O	X	X	X
MASTaR	–	O	O	O	O	O

*These protocols transmit ACK frames in half duplex mode.

of the data transmission answers with another signature as in [16]. It also utilizes the previous frame success/failure history and initiates the secondary transmission of the asymmetric mode in a probabilistic manner.

In [18], three-way handshaking using a modified CTS, namely full-duplex CTS (FCTS), is proposed. Data transmission is preceded by the RTS transmission and two consecutive FCTS transmission, where the FCTS frame includes the addresses of PTX, PRX, STX, and SRX along with the duration of both primary and secondary transmissions. STX, i.e., PRX, determines SRX to be the destination of the head packet in its queue, and thus UDI is not considered. Energy-FDM [20] evolves the proposed scheme in [18] to use reduced data transmit power for energy-efficient full duplex communi-

[4]While the existence of UDI is decided by whether a node can receive the MAC header in other nodes' transmission, the amount of the UDI is not considered.

[5]The UDI during ACK transmission is implicitly considered. However, if strong UDI causes ACK failures, the protocol decreases the probability to initiate secondary transmission.

cation. A-Duplex [19] considers UDI; STAs measure i) interference power using RTS frames from other STAs and ii) signal power using CTS frames from an AP, and report the difference of the powers, that is, SIR, via a modified RTS frame. Then, the AP uses the SIR information to choose an appropriate SRX. All protocols in [18], [20], and [19] mandate the use of the modified CTS or RTS, thus requiring the change of the current standard.

While all existing STR MAC protocols require new behaviors of STA devices, MASTaR utilizes the existing functions in the standard, and hence it is implementable in commercial STA devices via only firmware update. Table 1.1 compares the protocols according to five criteria: i) Distr. (distributed channel access), ii) Asymm. mode (asymmetric mode consideration), iii) UDI (UDI consideration), iv) ACK protection (robust ACK transmission consideration after simultaneous data transmission), and v) Standard-comp. (standard-compliance). "O" and "X" represent the satisfied and unsatisfied criteria, respectively. If a clear classification is not possible, we mark "△" with footnotes.

1.3 Main Contributions

1.3.1 Quiet ACK: ACK Transmit Power Control

In order to reduce frame errors caused by CCI in OBSSs, we first propose an ACK transmit power control algorithm, namely Quiet ACK (QACK). QACK is designed to ameliorate OBSSs' data frame errors caused by the CCI from ACK transmission, namely *ACK-driven data errors*, by lowering ACK power while maintaining the power high enough for each ACK frame to be successfully delivered. Our contributions are summarized as follows.

- Based on stochastic geometry analysis, we study the effect of ACK interference compared with data interference. Formulating an optimization problem, we also establish criteria for ACK power reduction to protect OBSSs.

- We develop a method for CCI detection and CCI power estimation using 802.11 pilot tones during a frame reception. Its feasibility is validated using a software-defined radio (SDR) platform, i.e., NI USRP.

- We implement QACK in NI USRP and ns-3, and verify its performance in comparison with the default (maximum power) and existing scheme (MinPACK). Compared with the default, QACK yields up to 55% and 81% throughput gain in the testbed with two BSSs and in the simulation with 19 BSSs, respectively.

1.3.2 FACT: CST adaptation scheme

To enable more simultaneous transmissions in OBSSs by adjusting CST, in addition, we propose a standard-complaint CST adaptation method, called FACT (Fine-grained Adaptation of Carrier sense Threshold). The main advantages of FACT are

- Adaptivity: FACT adapts CST depending on both interferer and destination, thus eliminating exposed terminals. With marginal overhead, it also adapts to channel variation in order to be more robust to channel fading.

- Practicality: FACT utilizes functions defined in IEEE 802.11 standard to identify interferer and measure the effect of the interference at destination. Therefore, it is implementable in commercial WLAN devices via only firmware update.

We also propose a supplementary CCA method which reduces time overhead in identifying interferers.

1.3.3 MASTaR: MAC protocol for STR in WLAN

To enable STR in 802.11 WLAN, we analyze the SIC performance achievable with the 802.11 physical layer convergence protocol (PLCP) frame structure without any modification. By using 3D-ray tracing results and adopting the notion of *dirty estimation* and *clean estimation* as the estimation method for SI channel, we measure the physical

(PHY) layer feasibility of STR in the 802.11 WLANs. We also propose a novel protocol for APs supporting STR in WLANs, named MASTaR (MAC protocol for Access point in Simultaneous Transmit and Receive mode). Designed based on the current IEEE 802.11 standard, MASTaR's main advantage is standard-compliant operation of STAs, i.e., it only requires legacy devices of existing IEEE 802.11 functions and does not change the PLCP/MAC frame structures. To the best of our knowledge, this is the first standard-compliant STR MAC protocol in the 802.11 WLANs, supporting the asymmetric mode with legacy STAs.

1.4 Organization of the Dissertation

The rest of the dissertation is organized as follows.

Chapter 2 presents QACK, the proposed dynamic transmit power control algorithm for ACK frames. The stochastic geometry analysis is provided and followed by the detailed explanation of QACK. We then verify QACK's feasibility via prototyping and evaluate its performance via extensive simulation.

In Chapter 3, we present FACT, the proposed CST adaptation method. We introduce preliminary IEEE 802.11 functions to describe the proposed CST adaptation method and CCA method, and simulation-based performance evaluation follows.

Chapter 4 presents MASTaR, the proposed MAC protocol enabling STR in 802.11 WLAN. We provide the 802.11 functions utilized in the proposed protocol and give the detailed explanation of MASTaR's operation. In addition, we look at the feasibility of MASTaR and evaluate its performance.

Finally, Chapter 5 concludes the dissertation with the summary of contributions and discussion on the future work.

Chapter 2

Quiet ACK: ACK Transmit Power Control in IEEE 802.11 WLANs

2.1 Introduction

The proliferation of WLANs leads to severer co-channel interferences (CCIs) among basic service sets (BSSs). The CCI limits transmission opportunities by intensifying the channel access contention among overlapping BSSs (OBSSs), and causes frame errors by deteriorating signal-to-interference-plus-noise-ratio (SINR). Existing approaches, therefore, control transmit power jointly with data rate adaptation [2], carrier sensing [4], and scheduling [5] to resolve the performance degradation due to CCIs.

Most studies on transmit power control have focused on data frame transmissions, which occupy the medium longer than control and management frame transmissions in general. However, 802.11 medium access control (MAC) acknowledgement (ACK) frame transmission, which follows successful delivery of a data frame, can also cause a strong CCI to OBSSs depending on the topology. A recent work [6], based on measurements, revealed that ACK frames give rise to performance degradation and starvation in OBSSs especially in densely deployed WLAN environments. It shows that the likelihood that a client will experience interference from MAC ACK frames can range

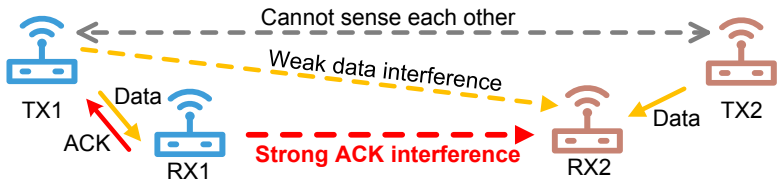

Figure 2.1: Imbalance between data interference and ACK interference.

from 25% to 50% in practical Wi-Fi deployments.

In addition, the large gap between RF parameters of access points (APs) and handheld devices causes uplink/downlink (UL/DL) asymmetry [21], thus leading to considerable imbalance between the CCI caused by data frames—*data interference*—and the CCI caused by ACK frames—*ACK interference*. Specifically, if the transmit power and antenna gain of an AP are much higher than those of its client STA, the AP's ACK interference can be much stronger than the STA's data interference in OBSSs. Fig. 2.1 shows an example with two pairs of a transmitter and a receiver, when simultaneous transmissions occur. RX 2 can fail in receiving TX 2's data frame due to the strong ACK interference from RX 1, after enduring the data interference from TX 1. *Therefore, controlling only the transmit power used for data frame or using the same transmit power for both data and ACK frames cannot effectively manage the network performance degradation caused by ACK interference.*

To reduce such damage caused by ACK interference, a heuristic algorithm named *MinPACK* is proposed in [6]. MinPACK periodically adapts ACK transmit power by comparing the ACK frame error rate (AFER) with reduced ACK power and the AFER with the maximum transmit power. It is also shown in [6] that device driver of off-the-shelf devices supports fine-grained power control for ACK frames independently from data frames. Since MinPACK controls ACK power depending only on AFER statistic, however, it slowly reflects the the fast-changing channel gain and amount of CCIs.

In this chapter, we present QACK (Quiet ACK), a dynamic transmit power control algorithm for ACK frames. Because an ACK frame is transmitted subsequent to a suc-

cessfully delivered data frame, which is longer and transmitted at less robust data rate compared with the ACK frame in general, it can admit of transmit power decrease to some degree. In this regard, we design QACK to ameliorate OBSSs' data frame errors caused by ACK interference, namely *ACK-driven data errors*, by lowering ACK power while maintaining the power high enough for each ACK frame to be successfully delivered. Our contributions are summarized as follows.

- Based on stochastic geometry analysis, we study the effect of ACK interference compared with data interference. Formulating an optimization problem, we also establish criteria for ACK power reduction to protect OBSSs.
- We develop a method for CCI detection and CCI power estimation using 802.11 pilot tones during a frame reception. Its feasibility is validated using a software-defined radio (SDR) platform, i.e., NI USRP.
- We implement QACK in NI USRP and ns-3, and verify its performance in comparison with the default (maximum power) and existing scheme (MinPACK). Compared with the default, QACK yields up to 55% and 81% throughput gain in the testbed with two BSSs and in the simulation with 19 BSSs, respectively.

The rest of this chapter is organized as follows. Section 2.2 presents the stochastic geometry analysis. The proposed algorithm QACK is detailed in Section 2.3. We then verify QACK's feasibility via prototyping and evaluate its performance via extensive simulation in Sections 2.4 and 2.5, respectively. Finally, we give a summary of this chapter in Section 2.7.

2.2 Numerical Analysis

In this section, we study the effect of CCIs based on stochastic geometry to figure out (i) how large area is affected by data and ACK interferences, respectively, (ii) how much data frame errors can be prevented by adjusting ACK power, and (iii) the criteria

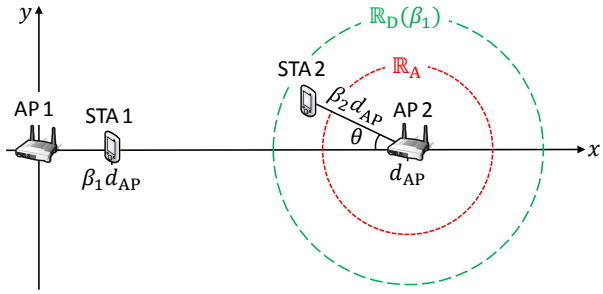

Figure 2.2: System model with two BSSs.

for ACK power control. Table 2.1 provides the description of the parameters used in this numerical analysis.

2.2.1 System Model

We consider a two BSS topology with two APs operating in the same frequency channel as shown in Fig. 2.2. STA 1 is connected to AP 1 and STA 2 is connected to AP 2, respectively. We focus on UL data transmissions, and AP 1 is the main object performing ACK power control in this model. In a coordinate system centered at AP 1's location, AP 2 and STA 1 are located at $(d_{\mathrm{AP}}, 0)$ and $(\beta_1 d_{\mathrm{AP}}, 0)$, respectively, where $-0.5 < \beta_1 < 0.5$. STA 2, on the other hand, is located at a point $\beta_2 d_{\mathrm{AP}}$ away from AP 2 with an angle of θ, where $0 < \beta_2 < 0.5$. The channel gain between any two nodes is modeled by

$$L_{\mathrm{TX,RX}} = \Gamma_{\mathrm{TX,RX}} \cdot L_0 \cdot d_{\mathrm{TX,RX}}^{-\alpha}, \tag{2.1}$$

where $d_{\mathrm{TX,RX}}$ is the distance between them, α is pathloss exponent, L_0 is a fixed loss, and $\Gamma_{\mathrm{TX,RX}} \sim \mathrm{Exp}(1)$ is a Rayleigh fast fading component with a unit average power. It is assumed that $\Gamma_{\mathrm{TX,RX}}$ is reciprocal and mutually independent for any pair of nodes. Then, the power of a signal from a transmitter at a receiver is given as

$$S_{\mathrm{TX}\to\mathrm{RX}} = P_{\mathrm{TX}} \cdot G_{\mathrm{TX}} \cdot G_{\mathrm{RX}} \cdot L_{\mathrm{TX,RX}}, \tag{2.2}$$

where P_{node} and G_{node} represent transmit power and antenna gain of a node, respectively.

In this analysis, we assume that STA 1 and STA 2 start simultaneous transmissions. According to the path-loss model in TGax simulation scenarios [22], if the distance between STA 1 and STA 2 is greater than 35 m and $\Gamma_{\mathrm{TX,RX}} = 1$, they cannot sense each other, thus transmitting simultaneously.[1] This condition for simultaneous transmissions, however, depends heavily on the pathloss model and RF parameters. Therefore, we do not present a mathematical formulation for the condition.

Data interference safe region (DISR)

We first define STA 1's DISR as the region of STA 2's position, where STA 2's UL data transmission is not disrupted by STA 1's data transmission. In terms of the signal-to-interference ratio (SIR)[2] at AP 2 with a signal from STA 2 and a CCI from STA 1, we define *data outage* of STA 2 by *SIR threshold* as

$$\mathrm{SIR}_{\mathrm{AP2}} \triangleq \frac{S_{\mathrm{STA2}\to\mathrm{AP2}}}{I_{\mathrm{STA1}\to\mathrm{AP2}}} \leq \rho^*_{\mathrm{D},10\%}, \tag{2.3}$$

where I represents the CCI power, which is also given by (2.2), and $\rho^*_{\mathrm{D},10\%}$ is the SIR threshold which yields 10% data frame error rate according to [23]. Assuming that the APs employ the same transmit power and antenna gain, i.e., P_{AP} and G_{AP}, and the STAs also have P_{STA} and G_{STA} in common,[3] while a transmit power greater than P_{AP} (P_{STA}) is impossible. (2.3) is further given as

$$\begin{aligned}\mathrm{SIR}_{\mathrm{AP2}} &= \frac{P_{\mathrm{STA}} \cdot G_{\mathrm{STA}} \cdot G_{\mathrm{AP}} \cdot \Gamma_{\mathrm{STA2,AP2}}(L_0 \cdot d^{-\alpha}_{\mathrm{STA2,AP2}})}{P_{\mathrm{STA}} \cdot G_{\mathrm{STA}} \cdot G_{\mathrm{AP}} \cdot \Gamma_{\mathrm{STA1,AP2}}(L_0 \cdot d^{-\alpha}_{\mathrm{STA1,AP2}})} \\ &= \frac{\Gamma_{\mathrm{STA2,AP2}}}{\Gamma_{\mathrm{STA1,AP2}}} \left(\frac{\beta_2}{1-\beta_1}\right)^{-\alpha} \leq \rho^*_{\mathrm{D},10\%}. \end{aligned} \tag{2.4}$$

[1] We assume $P_{\mathrm{TX}} = 15$ dBm, $G_{\mathrm{TX}} = G_{\mathrm{RX}} = -8$ dBi considering hand-grip loss [21], and carrier sense threshold $= -82$ dBm.

[2] We use SIR instead of SINR assuming that the CCI power is much greater than the noise power.

[3] We assume that P_{AP} and P_{STA} are the maximum transmit power. Therefore, an AP (STA) can use a transmit power smaller than P_{AP} (P_{STA}).

Table 2.1: Parameters used in numerical analysis

Parameter	Description
d_{AP}	Distance between AP 1 and AP 2
β_1	Location of STA 1 on the x-axis, normalized to d_{AP}
β_2	Distance between AP 2 and STA 2, normalized to d_{AP}
β_{STA}	Distance between STA 1 and STA 2, normalized to d_{AP}
$d_{\mathrm{A,B}}$	Distance between nodes A and B
α	Pathloss exponent
L_0	Fixed pathloss
$\Gamma_{\mathrm{A,B}}$	Rayleigh fast fading component between nodes A and B with a unit average power, and equal to $\Gamma_{\mathrm{B,A}}$
P_{A}	Transmit power of node A
G_{A}	Antenna gain of node A
$S_{\mathrm{A}\to\mathrm{B}}$	Signal power at node B from node A
$I_{\mathrm{A}\to\mathrm{B}}$	Interference power at node B from node A
$\rho^*_{\mathrm{D},10\%}$	SIR threshold which yields 10% data frame error rate
$\rho^*_{\mathrm{A},10\%}$	SIR threshold which yields 10% ACK frame error rate
ρ^*	$\rho^*_{\mathrm{D},10\%} \cdot \rho^*_{\mathrm{A},10\%}$
δ_{D}	Data outage probability
δ_{A}	ACK outage probability
$\mathbb{R}_{\mathrm{D}}(\beta_1)$	Data interference safe region (DISR) as a function of β_1
$\mathbb{R}_{\mathrm{A}}$	ACK interference safe region (AISR)
$\mathbb{R}_{\mathrm{Q}}(\delta_{\mathrm{A}})$	QACK interference safe region (QISR) as a function of δ_{A}
δ^*_{A}	Optimal ACK outage probability equalizing DISR and QISR
η	Parameter representing the RF asymmetry between AP and STA devices, and equal to $(P_{\mathrm{AP}} \cdot G_{\mathrm{AP}})/(P_{\mathrm{STA}} \cdot G_{\mathrm{STA}})$
ΔP	Reducing factor of ACK power

The ratio of two independent exponential random variables, i.e., $Z \triangleq X/Y$, where X and Y are i.i.d. exponential random variables with a unit variance, has the following cumulative distribution function (CDF).

$$F_Z(z) = \Pr(Z \leq z) = \frac{1}{1+1/z}. \tag{2.5}$$

Since $\Gamma_{\mathrm{STA2,AP2}}$ and $\Gamma_{\mathrm{STA1,AP2}}$ are i.i.d. exponential random variables with a unit variance, we re-define STA 1's DISR using (2.5) as the area inside a circle centered at $(d_{\mathrm{AP}}, 0)$, where the *data outage probability* of STA 2 due to STA 1's data is δ_{D} $(0 \leq \delta_{\mathrm{D}} < 1)$ at the boundary, i.e.,

$$\begin{aligned}&\Pr\left[\frac{\Gamma_{\mathrm{STA2,AP2}}}{\Gamma_{\mathrm{STA1,AP2}}}\left(\frac{\beta_2}{1-\beta_1}\right)^{-\alpha} \leq \rho^*_{\mathrm{D},10\%}\right]\\ &= \Pr\left[Z \leq \rho^*_{\mathrm{D},10\%}\left(\frac{\beta_2}{1-\beta_1}\right)^{\alpha}\right] = \frac{1}{1+\frac{1}{\rho^*_{\mathrm{D},10\%}}\left(\frac{\beta_2}{1-\beta_1}\right)^{-\alpha}} = \delta_{\mathrm{D}}.\end{aligned} \tag{2.6}$$

The DISR, which depends on β_1, is then given as

$$\begin{aligned}\mathbb{R}_{\mathrm{D}}(\beta_1) &= \left\{(x,y)\,\middle|\, \beta_2 = \frac{\sqrt{(x-d_{\mathrm{AP}})^2+y^2}}{d_{\mathrm{AP}}} \leq \beta_{2,\mathrm{DISR}}\right\},\\ &\text{where } \beta_{2,\mathrm{DISR}} = (1-\beta_1)\left(\frac{\delta_{\mathrm{D}}}{\rho^*_{\mathrm{D},10\%}(1-\delta_{\mathrm{D}})}\right)^{\frac{1}{\alpha}}.\end{aligned} \tag{2.7}$$

ACK interference safe region (AISR)

Next, we define AP 1's AISR as the area inside another circle centered at $(d_{\mathrm{AP}}, 0)$, where the data outage probability of STA 2 due to AP 1's ACK on the boundary is δ_{D}, i.e.,

$$\Pr\left[\frac{S_{\mathrm{STA2}\to\mathrm{AP2}}}{I_{\mathrm{AP1}\to\mathrm{AP2}}} \leq \rho^*_{\mathrm{D},10\%}\right] = \delta_{\mathrm{D}}. \tag{2.8}$$

Similar to DISR, AISR is given as

$$\begin{aligned}\mathbb{R}_{\mathrm{A}} &= \left\{(x,y)\,\middle|\, \frac{\sqrt{(x-d_{\mathrm{AP}})^2+y^2}}{d_{\mathrm{AP}}} \leq \beta_{2,\mathrm{AISR}}\right\},\\ &\text{where } \beta_{2,\mathrm{AISR}} = \left(\frac{\delta_{\mathrm{D}}}{\eta\rho^*_{\mathrm{D},10\%}(1-\delta_{\mathrm{D}})}\right)^{\frac{1}{\alpha}},\end{aligned} \tag{2.9}$$

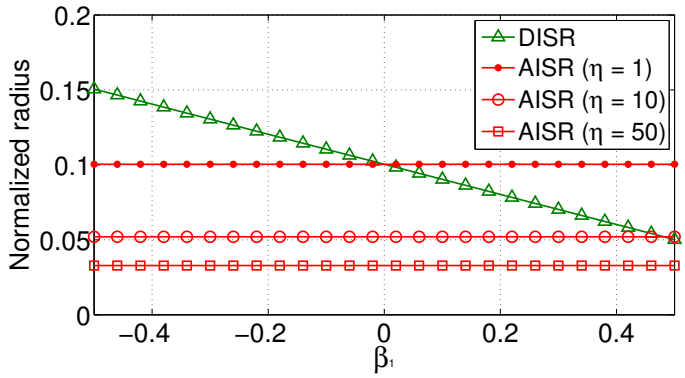

Figure 2.3: Normalized radii of DISR and AISR: $\alpha = 3.5$, $\delta_D = 10\%$, and $\rho^*_{\mathrm{D},10\%} = 25.4$ dB.

and $\eta = \frac{P_{\mathrm{AP}} \cdot G_{\mathrm{AP}}}{P_{\mathrm{STA}} \cdot G_{\mathrm{STA}}}$ is a parameter which represents the RF asymmetry between AP and STA devices. Fig. 2.3 shows the radii of DISR and AISR normalized to d_{AP}, i.e., $\beta_{2,\mathrm{DISR}}$ and $\beta_{2,\mathrm{AISR}}$. For $\eta \geq 10$,[4] the radius of AISR is smaller than the radius of DISR regardless of β_1, i.e., $\mathbb{R}_{\mathrm{A}} \subset \mathbb{R}_{\mathrm{D}}(\beta_1)$. In such a case, if STA 2 is located in the relative complement of AISR and DISR, i.e., STA 2 is in $\left(\mathbb{R}_{\mathrm{D}}(\beta_1) \setminus \mathbb{R}_{\mathrm{A}}\right)$ as in Fig. 2.1, STA 2 may experience ACK-driven data outage caused by AP 1.

Meanwhile, the normalized radius of DISR is smaller than 0.15 for $\forall \beta_1$. It means that if $\beta_2 > 0.15$, STA 2 may experience data-driven data outage regardless of STA 1's location, and hence, AP 2 may not send ACK. Similarly, if $\beta_1 > 0.15$, AP 1 also may not send ACK regardless of STA 2's location, and hence, we do not need to consider ACK interference from AP 1. From now on, therefore, we consider only $\beta_1 \leq 0.15$ for AP 1's ACK power control.

[4] According to the common parameters in TGax simulation scenarios [22] $P_{\mathrm{AP}} = 20$ dBm, $P_{\mathrm{STA}} = 15$ dBm, $G_{\mathrm{AP}} = 0$ dB, and $G_{\mathrm{STA}} = -2$ dBm, respectively. Considering at least 3 dB receive combining gain at APs, which generally have more than one antenna, the parameters yield $\eta = 10$. Hand-grip loss of portable devices [21], in addition, accounts for more than 6 dB additional loss at STAs, thus yielding η of about 50.

2.2.2 AISR Expansion by ACK Power Control

Motivated by the result in the previous subsection, we make AP 1 reduce its ACK power by a factor of Δ_P such that the outage probability of AP 1's ACK, i.e., *ACK outage probability of AP 1*, due to STA 2's data becomes δ_{A},[5] i.e.,

$$\begin{aligned}&\Pr\left[\frac{S_{\mathrm{AP1}\to\mathrm{STA1}}}{I_{\mathrm{STA2}\to\mathrm{STA1}}}\le\rho^*_{\mathrm{A},10\%}\right]\\&=\Pr\left[\frac{\eta}{\Delta_P}\cdot\frac{\Gamma_{\mathrm{AP1,STA1}}}{\Gamma_{\mathrm{STA2,STA1}}}\left(\frac{d_{\mathrm{AP1,STA1}}}{d_{\mathrm{STA1,STA2}}}\right)^{-\alpha}\le\rho^*_{\mathrm{A},10\%}\right]=\delta_{\mathrm{A}},\end{aligned}\tag{2.10}$$

where $\rho^*_{\mathrm{A},10\%}$ is the SIR threshold which yields 10% AFER and δ_{A} $(0\le\delta_{\mathrm{A}}<1)$ is *ACK outage tolerance*. Then, Δ_P is given as

$$\Delta_P=\frac{\eta}{\rho^*_{\mathrm{A},10\%}}\left(\frac{\delta_{\mathrm{A}}}{1-\delta_{\mathrm{A}}}\right)\left(\frac{d_{\mathrm{AP1,STA1}}}{d_{\mathrm{STA1,STA2}}}\right)^{-\alpha}.\tag{2.11}$$

With the power adjustment in (2.11), $I_{\mathrm{AP1}\to\mathrm{AP2}}$ decreases by a factor of Δ_P, and hence, the data outage probability of STA 2 due to AP 1's ACK with the adjusted ACK power is given as

$$\begin{aligned}&\Pr\left[\frac{S_{\mathrm{STA2}\to\mathrm{AP2}}}{I_{\mathrm{AP1}\to\mathrm{AP2}}/\Delta_P}\le\rho^*_{\mathrm{D},10\%}\right]\\&=\Pr\left[\left(\frac{\delta_{\mathrm{A}}}{1-\delta_{\mathrm{A}}}\right)\frac{\Gamma_{\mathrm{STA2,AP2}}}{\Gamma_{\mathrm{AP1,AP2}}}\left(\frac{|\beta_1|\beta_2}{\beta_{\mathrm{STA}}}\right)^{-\alpha}\le\rho^*\right]\\&=\frac{1}{1+\frac{1}{\rho^*}\left(\frac{\delta_{\mathrm{A}}}{1-\delta_{\mathrm{A}}}\right)\left(\frac{|\beta_1|\beta_2}{\beta_{\mathrm{STA}}}\right)^{-\alpha}},\end{aligned}\tag{2.12}$$

where $\beta_{\mathrm{STA}}=\frac{d_{\mathrm{STA1,STA2}}}{d_{\mathrm{AP}}}$ and $\rho^*=\rho^*_{\mathrm{D},10\%}\rho^*_{\mathrm{A},10\%}$. Note that η is canceled out in (2.12). Since $\beta_{\mathrm{STA}}=\sqrt{(1-\beta_1-\beta_2\cos\theta)^2+(\beta_2\sin\theta)^2}$ depends on θ, we define ACK-driven data outage probability (ADDOP) with reduced ACK power for given δ_{A}, β_1, and β_2 as

$$P(\delta_{\mathrm{A}},\beta_1,\beta_2)\triangleq\frac{1}{2\pi}\int_0^{2\pi}\left(\frac{1}{1+\frac{1}{\rho^*}\left(\frac{\delta_{\mathrm{A}}}{1-\delta_{\mathrm{A}}}\right)\left(\frac{|\beta_1|\beta_2}{\beta_{\mathrm{STA}}}\right)^{-\alpha}}\right)\mathrm{d}\theta.\tag{2.13}$$

[5]The failure of AP 1's ACK transmission due to AP 2's ACK frame rarely happens. Therefore, we only consider ACK failures due to STA 2's data frame.

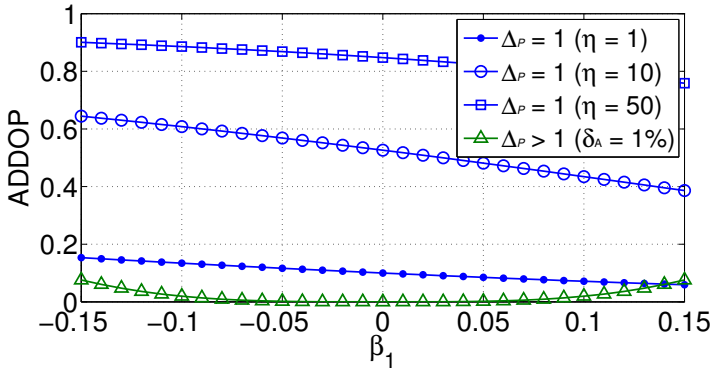

Figure 2.4: ADDOP of STA 2 at DISR boundary: $\alpha = 3.5$, $\delta_D = 10\%$, and $\rho^*_{\mathrm{D},10\%} = 25.4$ dB.

Fig. 2.4 shows ADDOP of STA 2, which is located at the boundary of STA 1's DISR. The upper three curves indicate the ADDOP for $\eta = \{1, 10, 50\}$ when AP 1 does not reduce ACK power, and the lowest curve represents $P(1\%, \beta_1, \beta_{2,\mathrm{DISR}})$. *The results show that ACK-driven data outage is significant when η is greater than one. Reducing ACK power, on the other hand, AP 1 protects the neighboring BSS from ACK-driven data outage*. In other words, ACK power reduction expands AISR and the expansion depends on the determination of δ_{A}. We refer to this expanded AISR as *QACK interference safe region (QISR)*, and denote it as $\mathbb{R}_{\mathrm{Q}}(\delta_{\mathrm{A}})$.

2.2.3 Optimization of ACK Outage Tolerance

As shown in the previous subsection, ADDOP depends on Δ_P, which is determined by δ_{A} in (2.11). With too large δ_{A}, a node excessively sacrifices the robustness of its ACK transmission for protecting OBSS nodes. On the contrary, too small δ_{A} leaves high ADDOP in the network. Therefore, δ_{A} should be optimized considering the tradeoff relation. With complete information about a network topology and all nodes' traffic, δ_{A} can be optimized to maximize the network throughput. The challenge in reality is that, however, a single node is not able to have the complete information needed for such an optimal ACK power control.

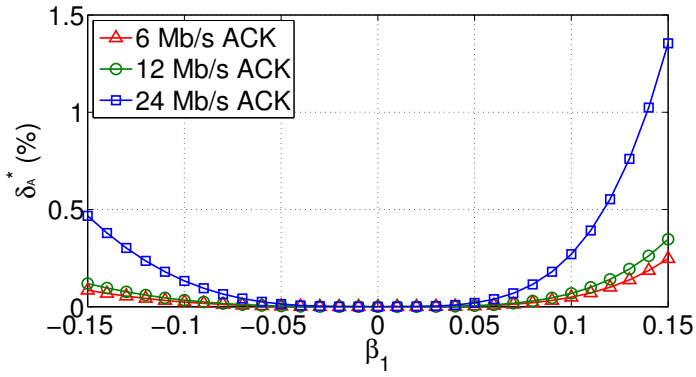

Figure 2.5: δ_A^* equalizing QISR and DISR: $\alpha = 3.5$, $\delta_D = 10\%$, $\rho^*_{\mathrm{D},10\%} = 25.4$ dB, and $\rho^*_{\mathrm{A},10\%} = 7.45$ dB.

We tackle this challenge by determining appropriate δ_{A} in a stochastic manner based on the notion of DISR and QISR.

i) If $\mathbb{R}_{\mathrm{Q}}(\delta_{\mathrm{A}}) \subset \mathbb{R}_{\mathrm{D}}(\beta_1)$, STA 2 in $\big(\mathbb{R}_{\mathrm{D}}(\beta_1) \setminus \mathbb{R}_{\mathrm{Q}}(\delta_{\mathrm{A}})\big)$ may experience ACK-driven data outage caused by AP 1.

ii) If $\mathbb{R}_{\mathrm{Q}}(\delta_{\mathrm{A}}) \supset \mathbb{R}_{\mathrm{D}}(\beta_1)$, STA 2 in $\big(\mathbb{R}_{\mathrm{Q}}(\delta_{\mathrm{A}}) \backslash \mathbb{R}_{\mathrm{D}}(\beta_1)\big)$ may experience data-driven data outage before AP 1's ACK transmission. In such a case, the ACK power reduction is to no avail.

Since both cases are undesirable, we define the optimal δ_{A} as the value equalizing QISR and DISR, i.e.,

$$\delta_{\mathrm{A}}^* \triangleq \big\{\delta_{\mathrm{A}} \big| \, \mathbb{R}_{\mathrm{Q}}(\delta_{\mathrm{A}}) = \mathbb{R}_{\mathrm{D}}(\beta_1)\big\}. \tag{2.14}$$

Fig. 2.5 shows δ_{A}^* depending on β_1 for three basic data rates, which are used for ACK frames. The maximum δ_{A}^* is 1.35% at $\beta_1 = 0.15$. It should be reminded that ACK outage probability is not identical to AFER, because the SIR threshold for outage, i.e., $\rho^*_{\mathrm{A},10\%}$, yields 10% AFER. Using the fading model in this analysis and the frame error probability model in [23], we calculate

$$\mathrm{AFER}(\delta_{\mathrm{A}}) = \int_0^{\rho^*_{\mathrm{A},10\%}} \mathrm{FER}_{\mathrm{A}}(\rho') \cdot f_{\rho,\delta_{\mathrm{A}}}(\rho') \, \mathrm{d}\rho', \tag{2.15}$$

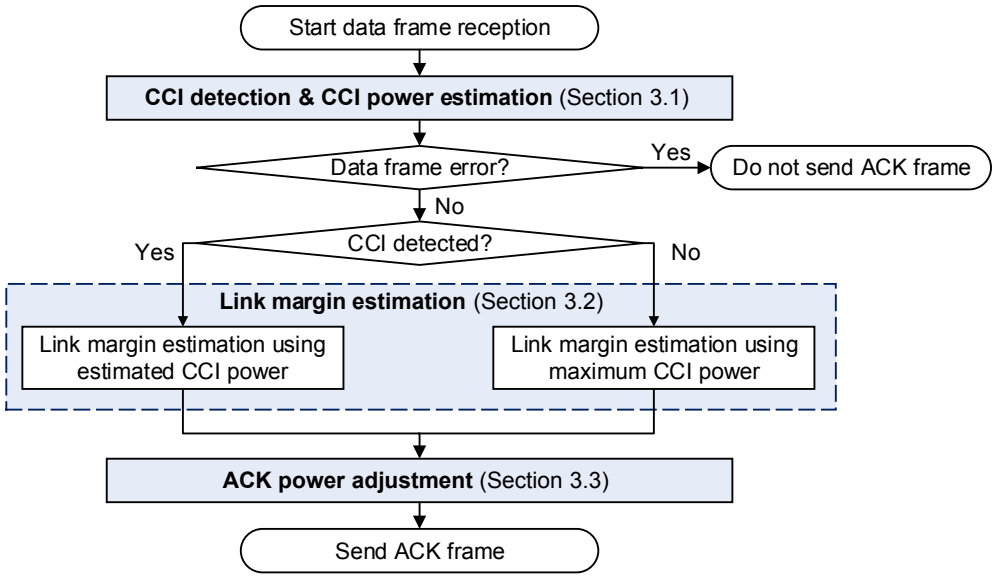

Figure 2.6: Flow chart for QACK.

where ρ' represents SIR value, $\mathrm{FER_A}(\rho')$ is the ACK frame error probability for given ρ', and $f_{\rho,\delta_\mathrm{A}}(\rho')$ is the probability distribution function of SIR which depends on δ_A. Eq. (2.15) yields $\mathrm{AFER}(1.35\%) = 0.0092$, meaning that tolerating 1.35% ACK outage probability results in 0.92% AFER. *Accordingly, a node can prevent ACK-driven data outage in the OBSS by tolerating only 1% AFER.*

2.3 QACK: Proposed ACK power Control

Based on the numerical analysis, the fundamental idea of QACK is reducing ACK power to ameliorate ACK-driven data errors in OBSSs, while maintaining ACK-frame error rate (*AFER*) under 1%. Fig. 2.6 shows the overall procedure of QACK. During a data frame reception, the data frame receiver, equivalently ACK transmitter (aTX), continuously calculates *symbol-level SINR* to detect CCI from an OBSS interferer (iTX), which interposes during the frame reception, and estimate the CCI power. aTX then estimates *link margin* of the data frame transmitter, equivalently ACK receiver

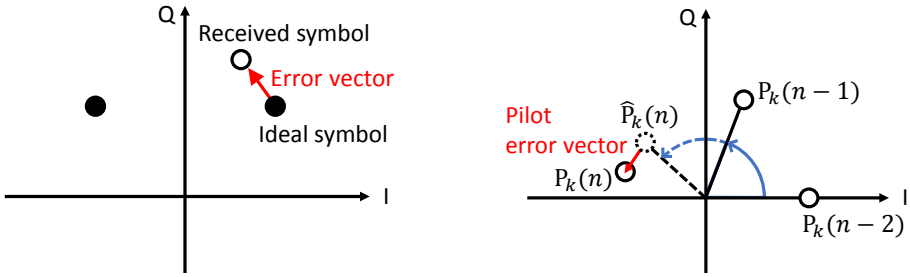

(a) Error vector (b) Pilot error vector

Figure 2.7: Error vector and pilot error vector.

(aRX), depending on the result of CCI detection, where link margin is defined as the ratio of the received SIR during ACK frame reception to the required SIR. Based on the estimation, aTX determines the amount of ACK power adjustment. The detailed operation of each step is presented in the following.

2.3.1 CCI Detection and CCI Power Estimation

To enable appropriate ACK power adjustment, aTX needs to know the presence and power of a CCI. With a frame-level SINR, i.e., a single representative SINR value for the entire frame, a node cannot detect a CCI which intrudes in the middle of the frame reception. In [24, 25], accordingly, error vector magnitude (EVM) is employed to calculate symbol-level SNR, which changes during a frame reception. EVM is the magnitude of error vector, i.e., the vector from the ideal/transmitted symbol to the received symbol (after channel equalization) in the I-Q plane as shown in Fig. 2.7(a).

Obtaining EVM from unknown transmitted data symbols, however, requires complicated calculation, which cannot be performed in real time, or yields inaccurate result especially when SINR is low. We thus exploit the known pilot symbols, the 127-element sequence of 1 and -1, to obtain EVM. With carrier frequency offset (CFO) between transmitter and receiver, the position of a pilot in the I-Q plane changes over time due to phase offset and inter-carrier interference (ICI). The phase offset incurred

by CFO consistently increases over time as

$$\phi_{\text{offset}} = e^{j2\pi f_{\text{offset}} t}, \tag{2.16}$$

where f_{offset} and ϕ_{offset} are CFO and the phase offset incurred by CFO, respectively [26]. If the effects of channel fluctuation, noise, CCI, and ICI are negligible, the pilot symbol rotates with a constant angular velocity in the I-Q plane over time. In such a case, the position of a pilot symbol in the I-Q plane can be estimated with the locations of previous pilot symbols.

We therefore define *pilot error vector* as the vector from the estimated position of pilot symbol to the position of received pilot symbol as illustrated in Fig. 2.7(b). $\mathbf{P}_k(n)$ represents the position vector of a pilot symbol in the kth subcarrier of the nth OFDM symbol, and $\hat{\mathbf{P}}_k(n)$ is the estimated $\mathbf{P}_k(n)$ using the phase of $\mathbf{P}_k(n-1)$ and $\mathbf{P}_k(n-2)$. Specifically, the phase of $\hat{\mathbf{P}}_k(n)$, denoted by $\measuredangle\hat{\mathbf{P}}_k(n)$, is estimated as

$$\begin{aligned}\measuredangle\hat{\mathbf{P}}_k(n) &= \measuredangle\mathbf{P}_k(n-1) + \big(\measuredangle\mathbf{P}_k(n-1) - \measuredangle\mathbf{P}_k(n-2)\big) \\ &= 2 \cdot \measuredangle\mathbf{P}_k(n-1) - \measuredangle\mathbf{P}_k(n-2).\end{aligned} \tag{2.17}$$

$\hat{\mathbf{P}}_k(n)$ is then estimated as

$$\hat{\mathbf{P}}_k(n) = |\mathbf{P}_k(n)| e^{\measuredangle\hat{\mathbf{P}}_k(n)}, \tag{2.18}$$

where $|\mathbf{P}_k(n)|$ is the magnitude of $\mathbf{P}_k(n)$. Pilot error vector of the kth subcarrier of the nth OFDM symbol, denoted by $e_k(n)$, is given as

$$\mathbf{e}_k(n) = \mathbf{P}_k(n) - \hat{\mathbf{P}}_k(n). \tag{2.19}$$

Since an 802.11 OFDM symbol has few pilots, we group all the pilots in consecutive N_S OFDM symbols as in [25]. Specifically, a pilot group consists of $N_P \times N_S$ pilots, where N_P is the number of pilots per OFDM symbol.[6] We then define pilot

[6]We empirically set $N_S = 10$, which yields 40 pilots in a pilot group per spatial stream using 20 MHz band.

error vector magnitude (PEVM) of the ith pilot group as

$$\mathrm{PEVM}_i = \sqrt{\frac{1}{N_P \cdot N_S} \sum_{n=(i-1)N_S+1}^{i \cdot N_S} \sum_{k \in K_P} |\mathbf{e}_k(n)|^2}, \tag{2.20}$$

where K_P is the set of pilot subcarrier indexes, e.g., $K_P = \{6{,}20{,}34{,}48\}$ for 20 MHz bandwidth [27]. Using the measured PEVM, we approximate the SINR of the ith pilot group as [24]

$$\rho_i^{(\mathrm{dB})} \approx -2 \cdot \mathrm{PEVM}_i^{(\mathrm{dB})}, \tag{2.21}$$

where $x^{(\mathrm{dB})}$ represents x on the dB scale.[7]

CCI detection of QACK is based on the SINR variation. Specifically, if the SINRs of both ith and $(i{+}1)$th pilot groups are smaller than the SINR of the $(i{-}1)$th pilot group by exceeding a threshold, a new CCI is assumed to start when the ith pilot group is received. For better detection, SINR is smoothed using exponential weighted moving average (EWMA) as

$$\tilde{\rho}_{i(\mathrm{dB})} = \begin{cases} (1-a)\tilde{\rho}_{i-1}^{(\mathrm{dB})} + a\rho_i^{(\mathrm{dB})}, & \text{if } |\rho_i^{(\mathrm{dB})} - \tilde{\rho}_{i-1}^{(\mathrm{dB})}| < \Delta_\rho, \\ \rho_i^{(\mathrm{dB})}, & \text{otherwise,} \end{cases} \tag{2.22}$$

where $0 < a < 1$ is a smoothing factor and Δ_ρ is the SINR threshold for CCI detection. We use $a = 0.3$ unless stated otherwise. Then, the start and end of a CCI are determined by

$$i_{\mathrm{start}} = i, \ \text{ if } \ \tilde{\rho}_{i-1}^{(\mathrm{dB})} - \max\left(\rho_i^{(\mathrm{dB})}, \ \rho_{i+1}^{(\mathrm{dB})}\right) > \Delta_\rho, \tag{2.23}$$

$$i_{\mathrm{end}} = i, \ \text{ if } \ \min\left(\rho_i^{(\mathrm{dB})}, \ \rho_{i+1}^{(\mathrm{dB})}\right) - \tilde{\rho}_{i-1}^{(\mathrm{dB})} > \Delta_\rho, \tag{2.24}$$

where i_{start} and i_{end} are the indexes of the first and the last pilot groups affected by the CCI.

[7] If x represents power, e.g., S and I, we use $x^{(\mathrm{dBm})}$ instead.

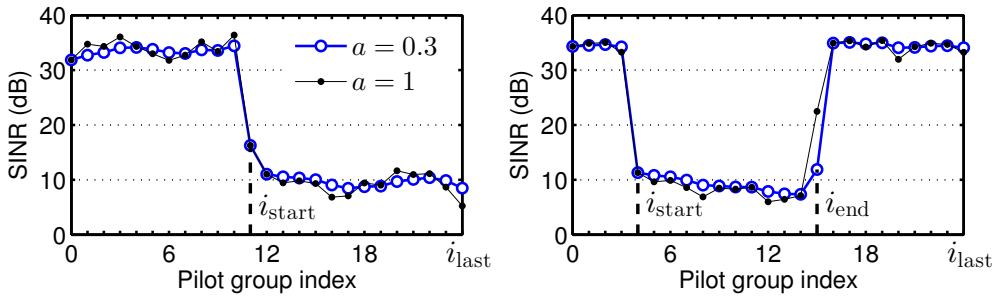

(a) CCI detected

(b) CCI detected but disappeared

Figure 2.8: Temporal variation in $\tilde{\rho}_i$ for two frames with 250 OFDM symbols: Measured by NI USRP-2943R, $\Delta_\rho = 5$ dB. When $a = 1$, SINR is not smoothed, thus fluctuating more than that with $a = 0.3$.

If a CCI is detected and does not end during a frame reception as shown in Fig. 2.8(a), which is the measurement result using NI USRP-2943R, the CCI power at aTX, i.e., $I_{\text{iTX}\to\text{aTX}}$, is estimated using the RSS[8] and average SINR as

$$\hat{I}^{(\text{dBm})}_{\text{iTX}\to\text{aTX}} = \text{RSS}^{(\text{dBm})} - 10\log_{10}\frac{\sum_{i'=i_{\text{start}}}^{i_{\text{last}}}\rho_{i'}}{i_{\text{last}} - i_{\text{start}} + 1}, \tag{2.25}$$

where i_{last} is the index of the last pilot group in the frame. If a CCI ends during the frame reception as shown in Fig. 2.8(b), on the other hand, the CCI is not likely to affect the impending ACK transmission from aTX, and hence, is considered as not detected. The CCI detection result and the estimated CCI power are used to estimate aRX's link margin, which determines how much ACK power aTX can reduce. The performance of the proposed CCI detection and CCI power estimation is evaluated using an SDR platform in Section 2.4.

[8] A frame's RSS is measured during the reception of the frame's preamble.

2.3.2 Link Margin Estimation

To make AFER of ACK transmissions from aTX to aRX with a CCI from iTX be under 1%, SIR at aRX should satisfy

$$\mathrm{SIR}_{\mathrm{aRX}}^{(\mathrm{dB})} = S_{\mathrm{aTX}\to\mathrm{aRX}}^{(\mathrm{dBm})} - I_{\mathrm{iTX}\to\mathrm{aRX}}^{(\mathrm{dBm})} \geq \rho_{\mathrm{A},1\%}^{*(\mathrm{dB})}, \tag{2.26}$$

where $\rho_{\mathrm{A},1\%}^{*}$ is the SIR value which yields 1% AFER. The link margin of aRX, denoted by λ_{aRX}, is then given as

$$\lambda_{\mathrm{aRX}}^{(\mathrm{dB})} \triangleq \mathrm{SIR}_{\mathrm{aRX}}^{(\mathrm{dB})} - \rho_{\mathrm{A},1\%}^{*(\mathrm{dB})}. \tag{2.27}$$

Before transmitting an ACK frame, aTX estimates $\lambda_{\mathrm{aRX}}^{(\mathrm{dB})}$ based on the information it has. Specifically, the estimated aRX's link margin, i.e., $\hat{\lambda}_{\mathrm{aRX}}$, is given as

$$\hat{\lambda}_{\mathrm{aRX}}^{(\mathrm{dB})} = \left(\hat{S}_{\mathrm{aTX}\to\mathrm{aRX}}^{(\mathrm{dBm})} - \hat{I}_{\mathrm{iTX}\to\mathrm{aTX}}^{(\mathrm{dBm})}\right) - \rho_{\mathrm{A},1\%}^{*(\mathrm{dB})} + C^{(\mathrm{dB})}. \tag{2.28}$$

The first term, i.e., estimated aRX's signal power, is calculated assuming the channel reciprocity and aTX's knowledge of aRX's transmit power (P_{aRX})[9] as

$$\hat{S}_{\mathrm{aTX}\to\mathrm{aRX}}^{(\mathrm{dBm})} = S_{\mathrm{aRX}\to\mathrm{aTX}}^{(\mathrm{dBm})} + \left(P_{\mathrm{aTX}}^{(\mathrm{dBm})} - P_{\mathrm{aRX}}^{(\mathrm{dBm})}\right). \tag{2.29}$$

The second term is the estimated CCI power at aTX given in (**??**). Since the locations and antenna gains of aTX and aRX are different, the estimated CCI power based on PEVM at aTX can be considerably different from the actual CCI power at aRX. *This difference, along with the inaccuracy of* $\hat{S}_{\mathrm{aTX}\to\mathrm{aRX}}$ *and the device & environment dependency of* $\rho_{\mathrm{A},1\%}^{*}$ *due to the different RF characteristics of devices, is compensated by adopting calibration factor* C, which is the last term in (2.28).

The value of calibration factor is adapted based on the statistics of AFER. Specifically, aTX collects AFER statistics using frame sequence number (SN). According to

[9] A STA can report its current transmit power using IEEE 802.11h Transmit Power Control function [27]. Even without the information, the inaccuracy of the estimation can be offset by the calibration described in the following.

the standard [27], SN increases by one (modulo 2^{12} operation) for every data/management frame transmission. After aTX sends an ACK frame to acknowledge a received data frame with SN equal to k, the next data frame's SN is $k+1$ if the ACK frame is successfully received by aRX, or k if the ACK frame is not successfully received by aRX. Using this characteristic, aTX measures AFER during a time interval T. Then, C is adapted according to the following four conditions.

1. **Increase:** If AFER $\leq 1\%$ it infers underestimated $\hat{\lambda}_{\mathrm{aRX}}$, thus increasing C by 1 dB.

2. **Decrease:** If AFER $> 1\%$ it infers overestimated $\hat{\lambda}_{\mathrm{aRX}}$, thus decreasing C by 1 dB.

3. **Fast decrease:** If consecutive ACK frame errors occur, C should be rapidly decreased in order to protect subsequent ACK transmissions. Therefore, if the number of consecutive ACK frame errors exceeds two, aTX decreases C by 1 dB and starts a new time interval.

4. **Steady state:** If i) and ii) occur in turns for more than two time intervals, the estimation margin is assumed to be around the optimal value. In order to prevent so-called *ping-pong effect*, in this case, aTX does not change C for T_{steady} after decreasing C.

In the following, we use $T = 200$ ms and $T_{\mathrm{steady}} = 10\ T$. Fig. 2.9 illustrates an example of calibration factor adaptation. The black solid curve shows the temporal change of λ_{aRX}, which is drawn using Jakes' fading model with Doppler velocity of 0.1 m/s. The blue solid line segments and the gray dashed curve represent C and $\hat{\lambda}_{\mathrm{aRX}}$, respectively. The green circle and the red X on the $\hat{\lambda}_{\mathrm{aRX}}$ curve indicate all successes and partial failures of a group of ACK frames, which are sent using the adjusted transmit power based on $\hat{\lambda}_{\mathrm{aRX}}$, respectively. If no ACK failure occurs, e.g., until 0.4 s, C is increased, while it is decreased after ACK failures, e.g., at 0.6 and 0.8 s. With the consecutive ACK failures around 1.2 s, C is decreased quickly, thus

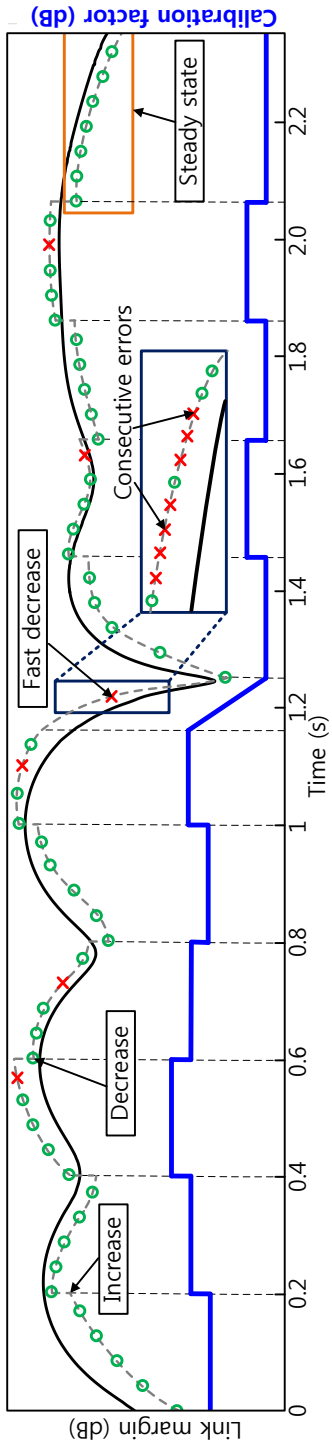

Figure 2.9: Example of link margin calibration.

decreasing $\hat{\lambda}_{\mathrm{aRX}}$. After repeated increase and decrease of C starting from 1.45 s to 2.05 s, the steady state starts.

2.3.3 ACK Power Adjustment

As long as the estimated link margin given by (2.28) is equal to or larger than 0 dB, AFER below 1% is expected. Accordingly, we adjust ACK power to make $\hat{\lambda}_{\mathrm{aRX}}$ 0 dB. Putting (2.29) into (2.28) and substituting $\hat{\lambda}_{\mathrm{aRX}}$ with 0 dB give

$$P_{\mathrm{aTX}}^{(\mathrm{dBm})} = P_{\mathrm{aRX}}^{(\mathrm{dBm})} + \hat{I}_{\mathrm{iTX}\to\mathrm{aTX}}^{(\mathrm{dBm})} - S_{\mathrm{aRX}\to\mathrm{aTX}}^{(\mathrm{dBm})} + \rho_{\mathrm{A},1\%}^{*(\mathrm{dB})} - C^{(\mathrm{dB})}. \tag{2.30}$$

It should be noted that we readjust C so as to make the resulting ACK power is in the range of the minimum and the maximum transmit power of aTX.

Meanwhile, if any CCI is not detected, it corresponds to one of the three cases: (i) there is no CCI, (ii) a CCI power is too small to be detected, and (iii) a CCI started before the frame reception. For the first two cases, the *necessity for using low ACK power* is less than when a CCI is detected, because there is no OBSS transmission to be protected or the receiver of the OBSS transmission may also get small CCI power from the ACK transmission. For the third case, *necessity for using high ACK power* is greater than when CCI is detected, since aTX cannot estimate the CCI power, thus having more uncertainty. Therefore, aTX uses $\hat{I}_{\mathrm{aTX,max}}$ instead of $\hat{I}_{\mathrm{iTX}\to\mathrm{aTX}}$ in (2.30), where $\hat{I}_{\mathrm{aTX,max}}$ is the maximum CCI power among the CCIs aTX has detected, to adjust ACK power conservatively. $\hat{I}_{\mathrm{aTX,max}}$ is updated whenever aTX detects a CCI and the estimated CCI power is greater than $\hat{I}_{\mathrm{aTX,max}}$.

It is worth mentioning that if multiple interferers exist for a single aRX, i.e., aRX is hidden to more than one OBSS device, C is mostly affected by the strongest interferer, i.e., the interferer whose interference is received with the highest power at aRX. Therefore, ACK power is set more conservatively to protect the ACK transmission. The performance of QACK with multiple BSSs will be examined in Section 2.5.2.

2.3.4 Conditional QACK Enabling/Disabling

If BSSs not performing QACK (legacy BSSs) and BSSs performing QACK (QACK BSSs) coexist, QACK BSSs may experience performance degradation. This is because ACK frames from QACK BSS do not harm the data transmissions in legacy BSS, while ACK frames from legacy BSS do so. This imbalance becomes severer due to the exponential increase of contention window after each failure of data transmission. thus resulting in fewer transmission attempts in QACK BSS. To prevent such unfair degradation of QACK BSSs' performance, we conditionally enable/disable QACK based on other BSSs' behavior. The basic philosophy is that "do not try to protect others unless you are protected." We stipulate that aTX is protected if $\widetilde{S}^{(\mathrm{dBm})}_{\mathrm{aRX}\rightarrow\mathrm{aTX}} - \widetilde{I}^{(\mathrm{dBm})}_{\mathrm{OA}} \geq \rho^{*(\mathrm{dB})}_{\mathrm{D},10\%}$ where $\widetilde{S}^{(\mathrm{dBm})}_{\mathrm{aRX}\rightarrow\mathrm{aTX}}$ and $\widetilde{I}^{(\mathrm{dBm})}_{\mathrm{OA}}$ are EWMA powers of the signals from aRX and the CCIs caused by OBSS ACK frames, respectively. Whenever aTX receives a data frame from aRX or an OBSS ACK frame, it updates the EWMA powers using the measured RSS. Then, aTX (i) disables QACK for aRX if $\widetilde{S}^{(\mathrm{dBm})}_{\mathrm{aRX}\rightarrow\mathrm{aTX}} - \widetilde{I}^{(\mathrm{dBm})}_{\mathrm{OA}} < \rho^{*(\mathrm{dB})}_{\mathrm{D},10\%}$ or (ii) enables QACK for aRX otherwise.

2.4 Prototyping-Based Feasibility Evaluation

We implement CCI detection and CCI power estimation in NI USRP-2943R, which has Xilinx Kintex-7 FPGA, using LabVIEW$^{\mathrm{TM}}$ Communication System Design Suite (CSDS$^{\mathrm{TM}}$) and 802.11 Application Framework, which is compliant to the IEEE 802.11 physical layer specifications [28].

2.4.1 Feasibility of CCI Detection and CCI Power Estimation

We first check whether the proposed CCI detection and CCI power estimation can work even with the presence of RF impairment. As mentioned in Section 3, CFO is

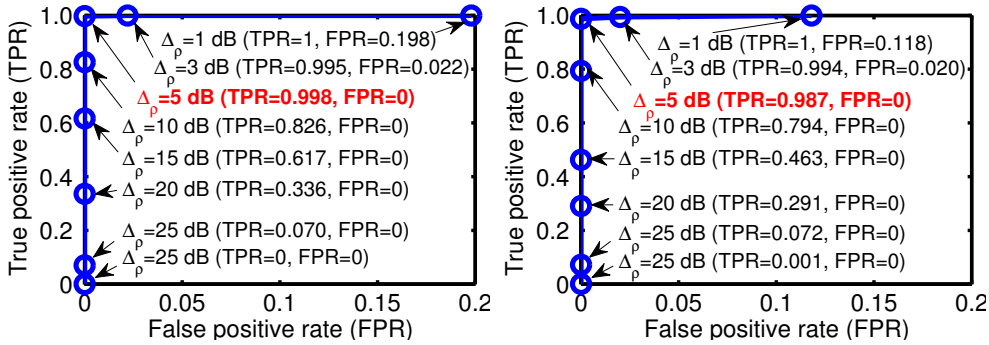

(a) Line of sight (b) No line of sight

Figure 2.10: ROC curve for CCI detection: RSS$= -60$ dBm, CCI power $= \{-\infty, -85, -80, -75, -70, -65\}$ dBm, and 6,000 frames per Δ_ρ.

the main impairment which affects PEVM.[10] CFO can be compensated using Schimidl and Cox algorithm [26], a widely used CFO estimation scheme. However, it leaves residual CFO (RCFO) with zero-mean and variance $\sigma^2 = \frac{1}{(\pi T)^2 \cdot L \cdot \mathrm{SNR}}$, where T is the duration (excluding cyclic prefix) of a training symbol consisting of two identical halves in time domain and L is the number of time samples in one-half of the training symbol.

Measurement setup: Three USRP-2943Rs are used each for aTX, aRX, and iTX. We configure aRX, i.e., data transmitter, and iTX not to sense each other. Changing the transmit power levels of aRX and iTX, we measure PEVM of a data frame for every 100 ms to calculate SINR at aTX. Additionally, the CFO between aRX and aTX is artificially set to the multiples of RCFO's standard deviation.

Results: Fig. 2.10 is the receiver operating characteristic (ROC) curve for CCI detection for different values of Δ_ρ in both line of sight (LOS) and no line of sight (NLOS)

[10] Symbol timing offset (STO) yields a phase offset proportional to subcarrier index. Without a significant sampling frequency offset (SFO), however, the phase offset incurred from STO is constant over time for a subcarrier. With a local oscillator tolerance stipulated by IEEE 802.11 standard [27], SFO is negligible, and hence, STO does not affect PEVM.

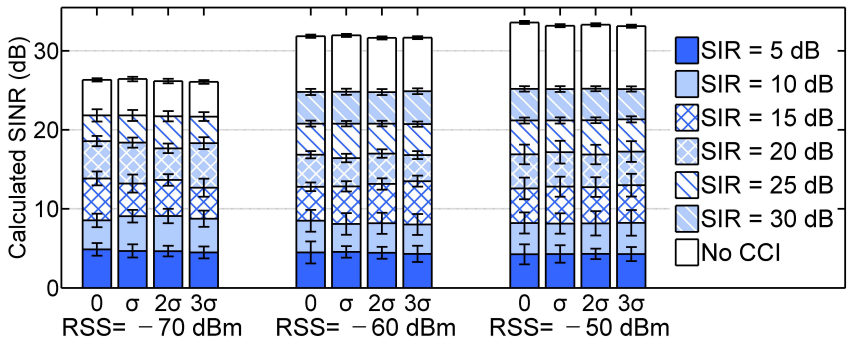

Figure 2.11: Calculated SINR using PEVM depending on RSS, CCI power, and RCFO: 1,000 frames in each case.

cases. It shows that, when $\Delta_\rho = 5$ dB, only 0.2% (1.3%) of CCIs are not detected with 0% false positive detection in LOS (NLOS) environment. Therefore, we use 5 dB for the detection threshold for the following measurements.

Fig. 2.11 shows the approximated SINR depending on the RSS, RCFO, and actual SIR, controlled by adjusting iTX's transmit power. The upper boundaries of boxes represent the average value, and the heights of error bars represent the standard deviation of calculated SINR for different CCI powers with given RSS and RCFO. For example, the leftmost boxes show the results when RSS $= -70$ dBm and RCFO $= 0$. The calculated SINRs in this case are about 27 dB when no CCI exists, and 22 dB when SIR is 25 dB, i.e., CCI power is smaller than RSS by 25 dB (CCI power $= -70 - 25 = -95$ dBm). It is shown that the effect of RCFO is marginal even for RCFO of 3σ.[11] In addition, the gap between the average calculated SINR and the actual SIR is 2.38 dB on average. This result shows that the proposed method estimates CCI power precisely.[12]

[11] For Gaussian distribution, the values less than 3σ away from the mean account for 99.73% of the set.

[12] It is worth mentioning that the proposed method slightly overestimates CCI power, which results in more conservative ACK power adjustment.

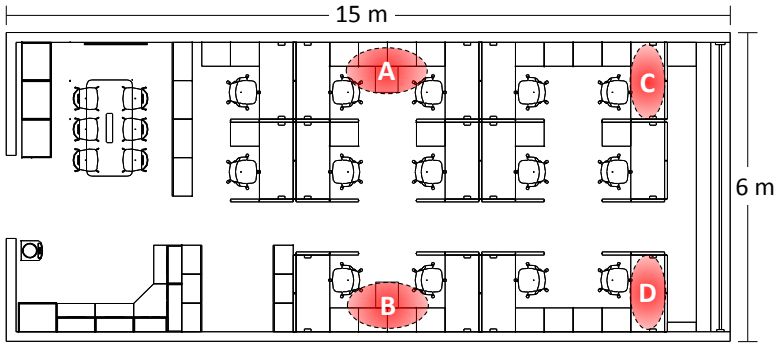

Figure 2.12: Office environment for throughput measurement: Each red oval represents the location of a pair of aTX and aRX.

2.4.2 Throughput Enhancement by QACK

Based on the estimated CCI power, we control ACK power and measure the throughput enhancement in two BSS scenario.

Topology description: Four USRP-2943Rs are used, two for each BSS, composed of one aRX and one aTX. We connect an antenna with high antenna gain to the aTXs, thus making ACK signal power relatively larger than data signal power in the air. Each pair of aTX and aRX is located at one of the four red ovals in Fig. 2.12. Accordingly, we conduct the measurement for 6 different topologies, i.e., A-B, A-C, A-D, B-C, B-D, and C-D. For each topology, the locations and orientations of aTX and aRX are determined within the regions such that i) aRXs are hidden to each other and ii) ACK interference power is larger than data interference power in both BSSs.

Results: Fig. 2.13 shows the average and standard deviation of each BSS's throughput for two different modulation and coding schemes (MCSs). Four cases are presented, namely, i) both aTXs use the maximum transmit power (Default), ii) both aTXs control ACK power based on QACK without link margin calibration (NoCalbr.), iii) both aTXs control ACK power based on QACK with link margin calibration (QACK), and iv) only one BSS is operating (BSS 1 or BSS 2 Only) which represents the upper limit. *It is*

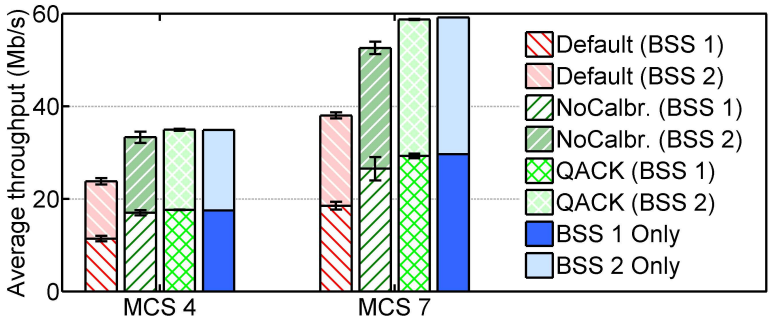

Figure 2.13: Measured throughput in 6 topologies: 1500-byte fully backlogged UDP traffic is generated from aRXs.

shown that the throughput using QACK *with link margin calibration becomes close to the upper limit, i.e., spatial reuse is almost maximized by lowering ACK power.* Compared with Default, QACK achieves 48% and 55% higher average throughput for MCS 4 and MCS 7, respectively.

Due to the scalability limitation of prototyping, we conduct simulations for more extensive performance evaluation.

2.5 Simulation-based Performance Evaluation

In this section, we evaluate the performance of QACK via ns-3 simulation [29]. We implement QACK in the simulator by reflecting the measurement in the previous section. Specifically, we assume that aTX can detect a CCI during a data frame reception only if the SINR is smaller than 35 dB. Otherwise, the CCI power is too small to be differentiated from the noise caused by RF imperfections. We assume that only the APs implement QACK and the STAs are the legacy devices with no modification.[13]

Minstrel rate adaptation algorithm [30] using 802.11ac data rates with a single

[13]For future work, we will also consider that STAs also implement QACK, thus enabling more cooperative operation on ACK power control.

[14]We consider hand-grip loss of mobile STAs as studied in [21].

Table 2.2: Common simulation parameters

Model & parameter	Value
Transmit power	0–20 dBm (AP), 15 dBm (STA)
Antenna gain	3 dBi (AP), -8 dBi (STA)[14]
Packet size	1,460 bytes (no aggreagation)
CCA threshold	-82 dBm
Simulation time	10 seconds

spatial stream and 20 MHz bandwidth, i.e., MCS 0–8[15], and Jakes' fading model with Doppler velocity of 0.1 m/s are adopted. We apply the common parameters in TGax simulation scenarios which focus on densely deployed WLANs [22]. The parameters which are not specified or different from the parameter in [22] are summarized in Table 2.2. We compare QACK with two comparison schemes: the default 802.11 using the maximum ACK power (Default) and the proposed scheme in [6] (MinPACK).

2.5.1 Two BSS Topology

Topology description: We first deploy two BSSs each with a single AP and a client STA, i.e., BSS 1 consisting of (AP 1, STA 1) and BSS 2 consisting of (AP 2, STA 2), as shown in Fig. 2.2. AP 1, STA 1, and AP 2 are located at $(0, 0)$, $(r, 0)$, and $(50\text{ m}, 0)$, respectively. The radius of the BSSs' region is 10 m,[16] and STA 2 is randomly located within the region of BSS 2. Each STA has fully-backlogged UL UDP traffic.

In this topology, according to the pathloss model in [22], if no CCI exists, APs can decode a data frame from a STA located at the edge of its region with a high probability, even with the highest data rate, i.e., MCS 8. In addition, if two STAs are over 35 m apart, they usually cannot sense each other, thus transmitting simultaneously. Adopting Jakes' fading model, however, the channel gain starts fluctuating dynamically by

[15]MCS 9 is not valid for 802.11ac in 20 MHz channel with a single stream.

[16]We use "region of a BSS" as the range where the BSS's STA is located.

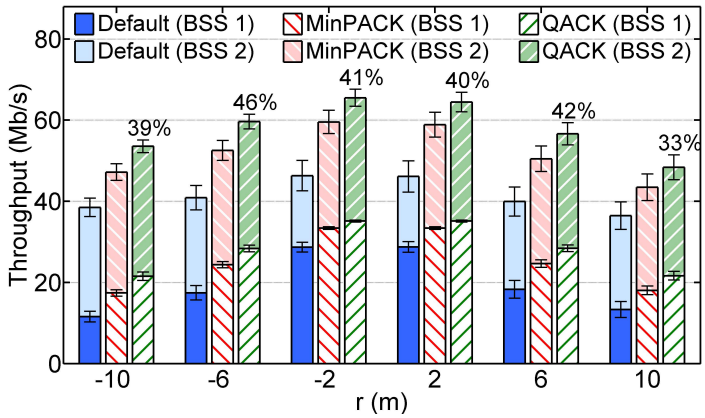

(a) Per-BSS throughput depending on r

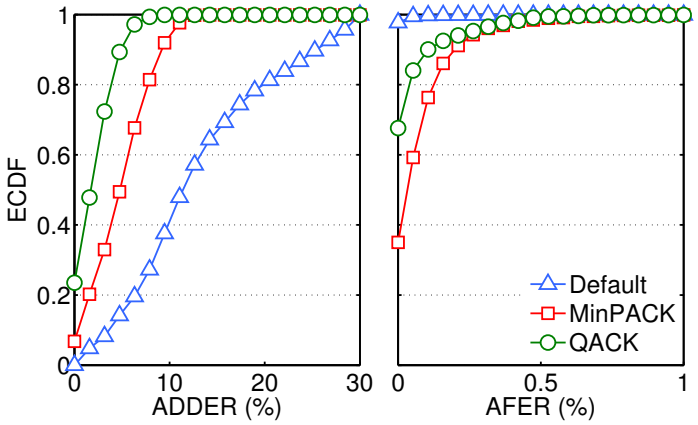

(b) ECDFs of per-BSS ADDER and AFER

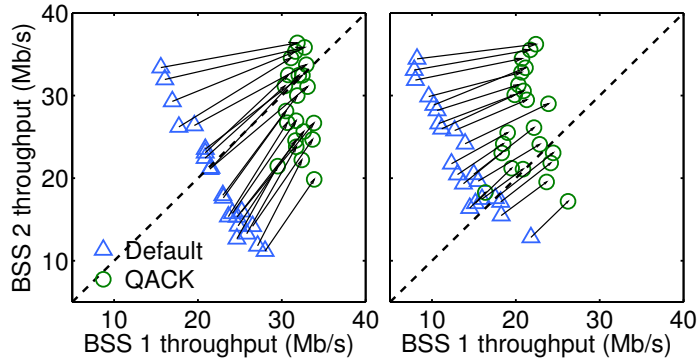

$r = 4$ m $\qquad$ $r = 10$ m

(c) Throughput change in each iteration

Figure 2.14: Simulation results in two BSS topology: $r = \{\pm 2, \pm 4, \pm 6, \pm 8, \pm 10\}$ m and 100 iterations per each r.

up to 20–30 dB during the simulation time. Accordingly, data frame error can occur without the presence of a CCI, and STAs can sense each other situationally.

Results: The bars in Fig. 2.14(a) show each BSS's average throughput depending on r, i.e., the location of STA 1 on the x-axis. The numbers above the bars show the throughput gain of QACK over Default, and the error bars represent standard deviation. For every r, QACK provides considerable throughput gain in both BSSs. Compared with Default, the average throughput gain of QACK over $r = -10$ to 10 m is 41%. Fig. 2.14(b), which shows empirical CDF (ECDF) of ACK-driven data error rate (ADDER)[17] and AFER, demonstrates that QACK significantly reduces ACK-driven data errors with a slight increase in AFER. In all cases, AFER of QACK is less than 1% and the average AFER is 0.05%. Fig. 2.14(c) illustrates the throughput enhancement for 20 random iterations in the cases of $r = 4, 10$ m. We draw an arrow from the point representing Default's throughput to the point representing QACK's throughput. All arrows point towards the upper right corner and the diagonal line, indicating that QACK improves not only throughput in both BSSs, but also the fairness among them for all iterations. The reason why QACK achieves higher throughput than MinPACK is twofold: (i) QACK converges to the appropriate level of ACK power more quickly than MinPACK, and (ii) MinPACK does not resolve ACK-driven data errors during its sampling period.

Discussion: In this topology, signal power decreases as $|r|$ increases, and data interference power between the BSSs increases as r increases. Therefore, throughput at ± 10 m, especially at 10 m, is lower than the others. With large r, in addition, AP 1 cannot lower ACK power much due to the lack of link margin, or two STAs become to sense each other, thus resulting in relatively low throughput gain. In this regard, QACK's gain is maximized in the environments with small BSSs where the distance between OBSSs is relatively larger than the BSSs's region, e.g, office environments

[17] ADDER is given by the ratio of the number of ACK-driven data errors to the number of total data frame transmissions.

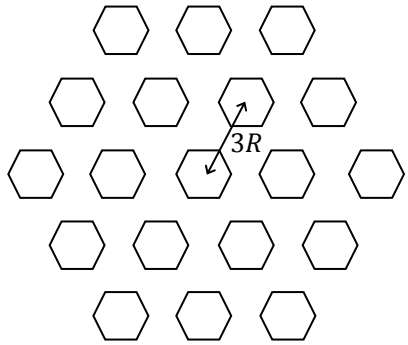

Figure 2.15: 19 BSS layout

with planned deployment of APs.

2.5.2 Multiple BSS Environment

Topology description: Next, we consider more general topology with multiple APs and STAs. We adopt the BSS layout of indoor small BSS scenario in [22], which represents real-world deployment with high density of WLAN devices. We deploy 19 APs in the hexagonal layout, which applies a frequency reuse of 3 as shown in Fig. 2.15. The radius of a BSS's region is R and the distance between adjacent OBSSs is $3R$. In each BSS, one STA is randomly located within the BSS's region and has fully-backlogged traffic.

Results: Fig. 2.16(a) presents each scheme's performance depending on R. The height of lower bar represents bottom 10% BSS throughput among 100 iterations, and the height of stacked bar indicates the average BSS throughput. The dots represent Jain's fairness index among the throughputs in (19 BSSs $\times$ 100 iterations). With Default, as R increases, more simultaneous data transmissions become viable, thus enhancing average throughput. However, the bottom 10% BSS throughput does not improve much, and the fairness decreases. This is because the STAs which belong to the BSS in the center hardly succeed in data transmissions due to the congested ACK interferences from surrounding OBSSs. By lowering ACK power, on the other hand, the fairness

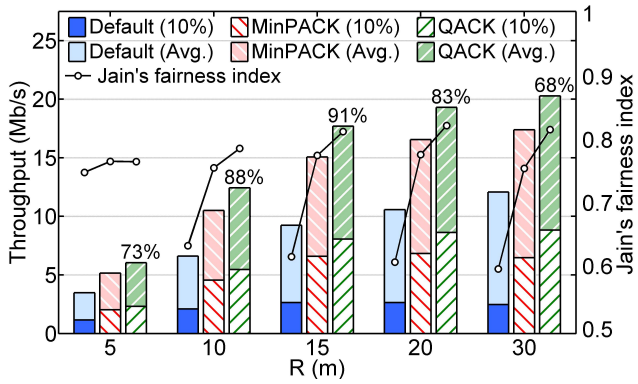

(a) Throughput depending on R

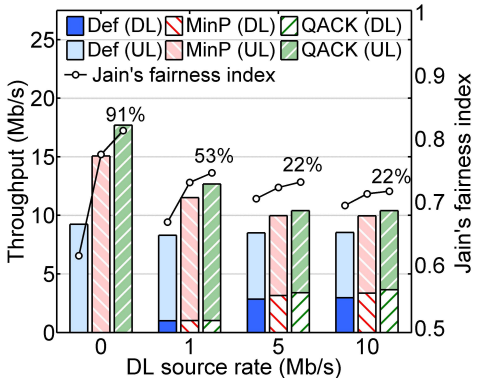

(b) Effect of DL traffic

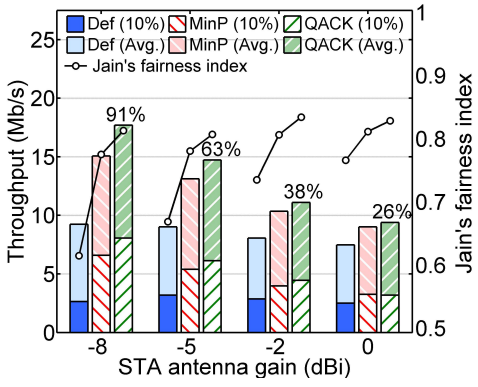

(c) Effect of AP–STA asymmetry

Figure 2.16: Simulation results in multiple BSS topology: 100 iterations per each x-axis value, R = 15 m for (b) and (c).

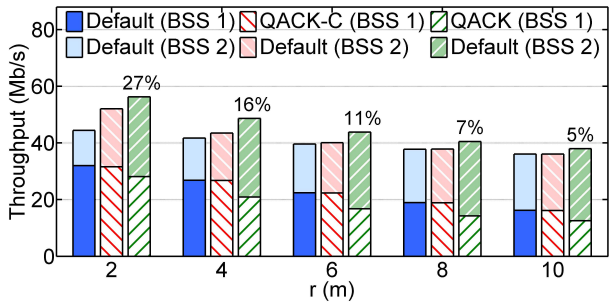

Figure 2.17: Performance of coexisting QACK BSS and legacy BSS.

among the BSSs, along with the average and bottom 10% throughput, is significantly enhanced. Compared with Default, QACK achieves 81% gain in average throughput and 190% gain in bottom 10% throughput, on average.

Discussion: Figs. 2.16(b) and (c) show the effect of DL traffic and the asymmetry between AP and STA devices. In Fig. 2.16(b), the lower and upper bars represent the average DL and UL throughput, respectively. We generate DL UDP traffic at each AP with the source rate of $\{1, 5, 10\}$ Mb/s. As DL source rate increases, both the average throughput and the gain of QACK decrease, because APs' DL data transmissions, generating strong data interference, prevent simultaneous transmissions in OBSSs. Since all APs become fully loaded with a source rate exceeding 5 Mb/s, increasing DL source rate no longer affects the average throughput.

Similarly, we change the STA's antenna gain to see the effect of RF asymmetry between AP and STA devices. As STA's antenna gain increases, both the average throughput and the gain of QACK decrease, because fewer simultaneous transmissions occur with more STAs sensing each other. Moreover, data interference and ACK interference become symmetric, and hence, the effect of ACK power control becomes less significant, while QACK still enhances the throughput by at least 27%. *In summary, the performance gain of* QACK *is more remarkable with severer imbalance between AP and STA devices in terms of both traffic and RF characteristics.*

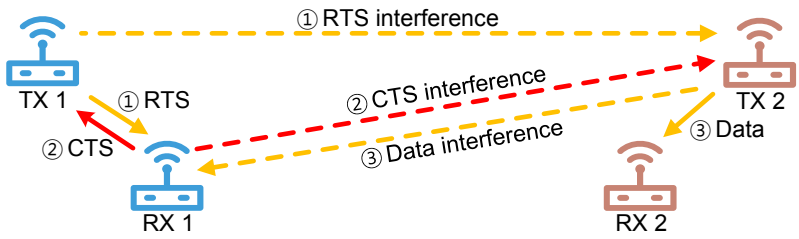

Figure 2.18: System model for CTS power control: Numbers in circle represent the order of occurrence.

2.5.3 Coexistence with Legacy Devices

The previous simulations assume that all BSSs use QACK, thus protecting each other. If legacy BSSs and QACK BSSs coexist, on the other hand, QACK BSSs may suffer performance degradation because only devices in QACK BSSs lower ACK power. Fig. 2.17 shows the performance of coexisting QACK BSS (BSS 1) and legacy BSS (BSS 2) in the two BSS topology. It is shown that QACK sacrifices QACK BSS's throughput for sum throughput enhancement without conditional enabling/disabling. QACK with conditional enabling/disabling (QACK-C), on the other hand, prevents QACK BSS's throughput loss by adaptively reducing ACK power depending on OBSS's behavior.

2.6 Quiet CTS: Proposed CTS Power Control

2.6.1 Problem Statement

We first show how the exchange of RTS/CTS, which aims to prevent the hidden terminal problem, limits simultaneous transmission opportunities. In the system model in Fig. 2.18, TX 1 transmits an RTS frame to reserve the medium before transmitting a data frame. We consider the case where another transmitter in an OBSS, i.e., TX 2, cannot sense the RTS frame. For ease of description, the RTS signal coming from OB-

SSs will be called the *RTS interference*. Also, the CTS signal coming from OBSSs will be called the *CTS interference*.

Next, RX 1 responds the RTS frame with a CTS frame, and it exerts CTS interference to TX 2. If TX 2 can sense the CTS frame from RX 1, the power of the CTS interference from RX 1 at TX 2 is given as

$$I_{\mathrm{RX1}\to\mathrm{TX2}} \geq C_{\mathrm{th,TX2}}, \tag{2.31}$$

where $C_{\mathrm{th,node}}$ represents the CCA threshold of the node. We assume that if a node senses a CTS frame, it can decode the frame with a high probability. Regardless of the viability of the following data transmission from TX 1, in this case, TX 2 may set network allocation vector (NAV) and defer its transmission. If RX 1 could successfully decode the data frame from TX 1 even with the existence of data interference from TX 2 and vice versa, it means that TX 2 missed out on a transmission opportunity. The performance degradation due to this case is well known as the *exposed terminal problem*. As shown in this example, the exchange of RTS/CTS can aggravate the exposed terminal problem at the cost of reducing the hidden terminal problem.

2.6.2 CTS Power Control

Assume that now RX 1 decreases its CTS power by a factor of $\Delta_{P,\mathrm{cts}}$ and TX 2 becomes impossible to sense the CTS interference, then the decreased power of the CTS interference from RX 1 at TX 2 is given as

$$I'_{\mathrm{RX1}\to\mathrm{TX2}} = \frac{I_{\mathrm{RX1}\to\mathrm{TX2}}}{\Delta_{P,\mathrm{cts}}} < C_{\mathrm{th,TX2}}. \tag{2.32}$$

Then, TX 2 may start its data transmission to RX 2 and it will exert a data interference to RX 1. Assuming the channel reciprocity, The data interference power from TX 2 at RX 1 and the CTS interference power from RX 1 at TX 2 have the following relation:

$$\frac{I_{\mathrm{TX2}\to\mathrm{RX1}}}{P_{\mathrm{TX2}} \cdot G_{\mathrm{comb,RX1}}} = \frac{I_{\mathrm{RX1}\to\mathrm{TX2}}}{P_{\mathrm{RX1}} \cdot G_{\mathrm{comb,TX2}}}, \tag{2.33}$$

where P_{node} and $G_{\mathrm{comb,node}}$ are the transmit power of a node without power control and the combining gain of a node, respectively. In the above equation, $G_{\mathrm{comb,RX1}}$ is assumed to be one, because when receiving the data interference from TX 2, RX 1 will be already tuned to the data frame from TX 1. Then (2.33) is rewritten as

$$\begin{aligned} I_{\mathrm{TX2}\to\mathrm{RX1}} &= \left(\frac{P_{\mathrm{TX2}}}{P_{\mathrm{RX1}}\cdot G_{\mathrm{comb,TX2}}}\right) I_{\mathrm{RX1}\to\mathrm{TX2}} \\ &\triangleq \zeta_{\mathrm{RX1,TX2}}\cdot I_{\mathrm{RX1}\to\mathrm{TX2}}, \end{aligned} \tag{2.34}$$

where $\zeta_{\mathrm{RX1,TX2}} = P_{\mathrm{TX2}}/(P_{\mathrm{RX1}}\cdot G_{\mathrm{comb,TX2}})$. Substituting (2.32) into (2.34) gives:

$$\begin{aligned} I_{\mathrm{TX2}\to\mathrm{RX1}} &= \zeta_{\mathrm{RX1,TX2}}\cdot I'_{\mathrm{RX1}\to\mathrm{TX2}}\cdot\Delta_{P,\mathrm{cts}} \\ &< \zeta_{\mathrm{RX1,TX2}}\cdot C_{\mathrm{th,TX2}}\cdot\Delta_{P,\mathrm{cts}} \end{aligned} \tag{2.35}$$

Using (2.35), the SIR at RX 1,where RX 1 is receiving a data frame from TX 1 and the data interference from TX 2, is given as

$$\widetilde{\mathrm{SIR}}_{\mathrm{RX1}} = \frac{S_{\mathrm{TX1}\to\mathrm{RX1}}}{I_{\mathrm{TX2}\to\mathrm{RX1}}} \tag{2.36}$$

$$> \frac{S_{\mathrm{TX1}\to\mathrm{RX1}}}{\zeta_{\mathrm{RX1,TX2}}\cdot C_{\mathrm{th,TX2}}\cdot\Delta_{P,\mathrm{cts}}} \tag{2.37}$$

and the worst case SIR is given as

$$\widetilde{\mathrm{SIR}}_{\mathrm{RX1,worst}} = \frac{S_{\mathrm{TX1}\to\mathrm{RX1}}}{\zeta_{\mathrm{RX1,TX2}}\cdot C_{\mathrm{th,TX2}}\cdot\Delta_{P,\mathrm{cts}}}. \tag{2.38}$$

If the worst case SIR is greater than the SIR threshold which yields almost no data frame error, we can expect that the probability that the hidden terminal problem happens is very low. We use an SIR threshold which yields 1% error rate according to [23] as the SIR threshold and denote it as ρ^*_m, where m is the MCS used for the data transmission. Then, the condition for preventing hidden terminal problem is given as

$$\frac{S_{\mathrm{TX1}\to\mathrm{RX1}}}{\zeta_{\mathrm{RX1,TX2}}\cdot C_{\mathrm{th,TX2}}\cdot\Delta_{P,\mathrm{cts}}} \geq \rho^*_m \tag{2.39}$$

and the possible range of $\Delta_{P,\mathrm{cts}}$ is given as

$$\Delta_{P,\mathrm{cts}} \leq \frac{S_{\mathrm{TX1}\to\mathrm{RX1}}}{\zeta_{\mathrm{RX1,TX2}}\cdot C_{\mathrm{th,TX2}}\cdot\rho^*_m}. \tag{2.40}$$

We need also consider the viability of CTS transmission. Because CTS frame has the same structure with an ACK frame, the viability of a CTS transmission is the same as the viability of an ACK transmission using the same data rate. In this sense, we compare the the maximum possible value in (2.40) and the ACK power decrease yields by QACK, and use the a lower value as

$$\Delta_{P,\mathrm{cts}} = \min\left(\frac{P_{\mathrm{RX1}}}{P_{\mathrm{aTX}}},\ \max\Big(1, \frac{S_{\mathrm{TX1}\to\mathrm{RX1}}}{\zeta_{\mathrm{RX1,TX2}}\cdot C_{\mathrm{th,TX2}}\cdot \rho^{*}_{m}}\Big)\right), \tag{2.41}$$

where P_{aTX} is the adjusted ACK power with the maximum CCI power among the previously detected CCI powers and given by (2.30) as

$$P^{(\mathrm{dBm})}_{\mathrm{aTX}} = P^{(\mathrm{dBm})}_{\mathrm{aRX}} + \hat{I}^{(\mathrm{dBm})}_{\mathrm{iTX,max}} - S^{(\mathrm{dBm})}_{\mathrm{aRX}\to\mathrm{aTX}} + \rho^{*(\mathrm{dB})}_{\mathrm{A},1\%} - C^{(\mathrm{dB})}. \tag{2.42}$$

It should be noted that we only consider the data interference from TX 2 when calculating the SIR at RX 1. This is because we assume that the RX 2 uses QACK, and hence the ACK interference from RX 2 is comparable with the data interference from TX 2.

2.6.3 Relationship with Quiet ACK

In (2.40), RX 1 does not know the values of $\zeta_{\mathrm{RX1,TX2}}$ and $C_{\mathrm{th,TX2}}$, and hence cannot determine $\Delta_{P,\mathrm{cts}}$. We tackle this by using the result of CCI power estimation in Section 2.3.1. Specifically, first let

$$\zeta_{\mathrm{RX1,TX2}}\cdot C_{\mathrm{th,TX2}} = K\cdot C_{\mathrm{th,RX1}}, \tag{2.43}$$

where K is a positive real number. Substituting (2.43) into (2.35) gives

$$I_{\mathrm{TX2}\to\mathrm{RX1}} < K\cdot C_{\mathrm{th,RX1}}\cdot \Delta_{P,\mathrm{cts}}. \tag{2.44}$$

In Section 2.3.1, the CCI power during frame reception is estimated as (2.35). The estimated CCI power is used to calibrate K as follows:

i) **Initialization:** Before initializing K, RX 1 transmits a CTS frame with its default power and wait for the data transmission from TX 1. Receiving the data transmission, RX 1 performs the CCI detection and estimation method. If CCI is detected and its power is estimated as $\hat{I}$, RX 1 initializes K using (2.44) as follows:

$$K = \frac{\hat{I}}{C_{\mathrm{th,RX1}}}. \tag{2.45}$$

It should be noted that $\Delta_{P,\mathrm{cts}} = 1$ in this case because RX 1 did not control the CTS power.

ii) **Increase:** After the initialization of K, RX 1 reduces its CTS power by $\Delta_{P,\mathrm{cts}}$ according to (2.41). During the reception of data frame from TX 1 after the CTS transmission with the reduced power, if the calculated CCI power, i.e., $\hat{I}$, is greater than the maximum expected value given by (2.44), K is updated as

$$K = \frac{\hat{I}}{C_{\mathrm{th,RX1}} \cdot \Delta_{P,\mathrm{cts}}}. \tag{2.46}$$

iii) **Decrease:** Let $\mathrm{d}t$ be the elapsed time since the most recent update of K, K is steadily decreased as

$$K^{(\mathrm{dB})} = K^{(\mathrm{dB})} - f(\mathrm{d}t), \tag{2.47}$$

where $f(\mathrm{d}T)$ is a linear function of $\mathrm{d}t$. This regression of K aims to prevent excessively conservative CTS power control due to too high K, which is set by either an overestimated CCI power or a CCI already disappeared.

2.6.4 Simulation Results

We evaluate the performance of the proposed CTS power control method, namely QCTS (Quiet CTS), via ns-3 simulation. We consider *RTS scenario*, i.e., the scenario that all STAs use RTS before transmitting a data frame, and the simulation parameters are the same as in Chapter 2.5. $f(\mathrm{d}t)$ in (2.47) is set to $3 \cdot \frac{\mathrm{d}t}{0.2}$, which corresponds to the 3 dB decrease per 200 ms.

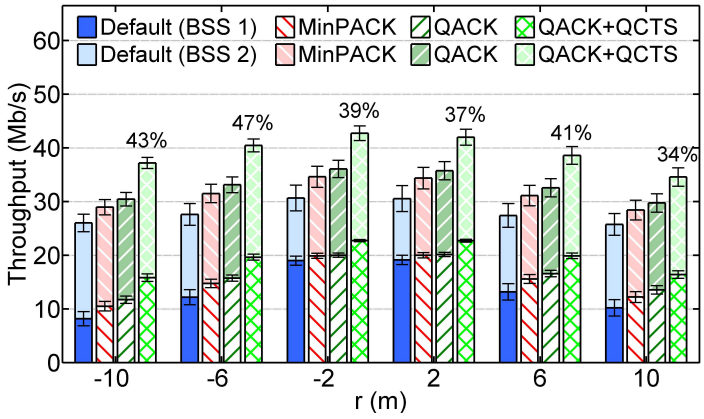

(a) Per-BSS throughput depending on r

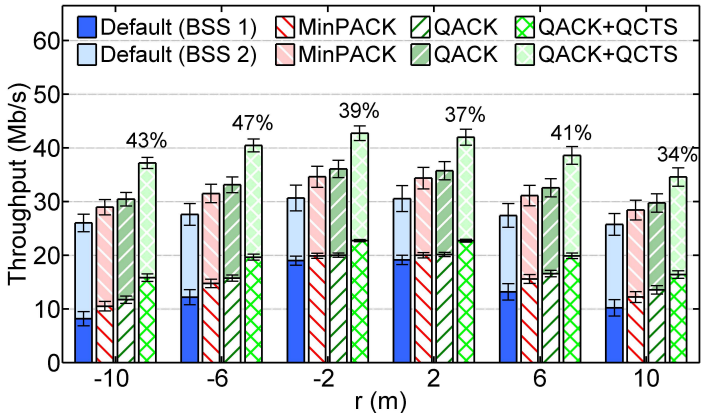

(b) ECDFs of per-BSS CFER and AFER

Figure 2.19: Simulation results in two BSS topology: $r = \{\pm 2, \pm 4, \pm 6, \pm 8, \pm 10\}$ m and 100 iterations per each r.

Two BSS Topology

We first deploy two BSSs each with a single AP and a client STA as in Chapter 2.5.1. All the parameters are the same as the parameters in Chapter 2.5.1 except for the distance between two APs; they are 60 m apart in this scenario instead of 50 m. Fig. 2.19(a), which is in the same format as Fig. 2.14(a), shows mean and standard deviation of each BSS's throughput. It is shown that in RTS scenario the throughput gain of QACK is relatively marginal compared with the previous results, which are obtained in the scenario without RTS usage. As explained in Chapter 2.6.1, this is because RTS/CTS exchange limits simultaneous transmission attempts, thus leaving little room for performance enhancement by QACK. On the other hand, QACK with QCTS considerably enhances the throughput by enriching simultaneous data transmissions. Fig. 2.19(b) shows the ECDF of a BSS's CTS frame error rate (CFER) in 600 iterations, i.e., total 1,200 samples of CFER. It is shown that among the 1,200 samples the worst case CFER is about 2%, and the average CFER is only 0.15%. This result demonstrates that QACK with QCTS effectively reduces exposed terminals with only a marginal damage in CTS delivery.

19 BSS Topology

Next, we consider 19-BSS topology which is shown in Chapter 2.5.2. Fig. 2.20 shows the average and the bottom 10% BSS throughputs as explained in 2.5.2. The performance of QACK with QCTS becomes more remarkable in 19-BSS topology, yielding up to 125% gain in average throughput and 413% gain in the bottom 10% throughput. This result demonstrates that the advantage of using reduced CTS power is more emphasized in the network with many BSSs.

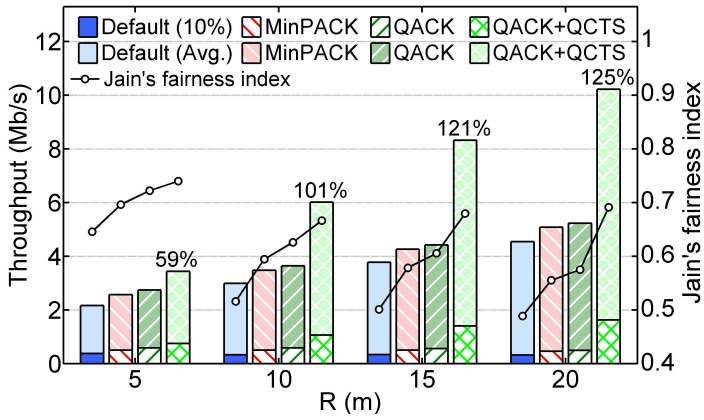

Figure 2.20: Per-BSS throughput depending on r

2.7 Summary

We have presented QACK, a novel power control algorithm for IEEE 802.11 MAC ACK frames. Our goal is to adjust ACK power to reduce ACK-driven data errors in OBSSs without compromising robust ACK frame delivery. We meet this goal by CCI detection and CCI power estimation during a data frame reception, which enables dynamic power adaptation for subsequent ACK frame transmission, and link margin estimation based on AFER statistics. We have also proposed a CTS power control method which enables more simultaneous data transmission with the usage of RTS. Our implementation and simulation confirm the feasibility and the performance of QACK in diverse environments.

Chapter 3

FACT: Fine-Grained Adaptation of Carrier Sense Threshold in IEEE 802.11 WLANs

3.1 Introduction

The exposed terminal problem [31] has been one of the main challenges in IEEE 802.11 wireless local area networks (WLANs) [27], which is based on carrier sense multiple access with collision avoidance (CSMA/CA). Specifically, if an access point (AP) and its client stations (STAs) are closely located, a transmission between them is viable even if there exists a co-channel interference (CCI) from overlapping basic service set (OBSS). Current clear channel assessment (CCA) mechanism in WLANs, however, prevents such viable transmission attempts if the CCI power is over a fixed carrier sense threshold (CST)[1], thus failing to obtain spatial reuse gain in many cases.

In this chapter, we propose a standard-complaint CST adaptation method, called FACT (Fine-grained Adaptation of Carrier sense Threshold). The main advantages of FACT are

1. Adaptivity: FACT adapts CST depending on both interferer and destination, thus eliminating exposed terminals. With marginal overhead, it also adapts to channel

[1] It is also called CCA threshold, and is generally -82 dBm.

variation in order to be more robust to channel fading.

2. Practicality: FACT utilizes functions defined in IEEE 802.11 standard to identify interferer and measure the effect of the interference at destination. Therefore, it is implementable in commercial WLAN devices via only firmware update.

We also propose a supplementary CCA method which reduces time overhead in identifying interferers. The performance of the proposed methods is evaluated via ns-3 simulation. Simulation results show that FACT adaptively enables simultaneous transmission when it is viable, thus yielding up to $1.8\times$ throughput in a two-cell environment compared with the legacy method which uses a fixed CST.

The rest of this chapter is organized as follows. In Section 3.2, we introduce IEEE 802.11 functions utilized in the proposed method. Section 3.3 and Section 3.4 describe the proposed CST adaptation method and CCA method, respectively. Simulation-based performance evaluation is presented in Section 3.5, and Section 3.6 summarizes this chapter.

3.2 Preliminaries

We first introduce preliminary functions of IEEE 802.11 WLAN, which are utilized in our proposed scheme.

3.2.1 IEEE 802.11h Transmit Power Control (TPC)

IEEE 802.11h is an amendment for spectrum and transmit power management extensions [32]. Among the amendment, TPC, which is originally designed to satisfy maximum transmit power regulation, provides a procedure for a STA to notify its *link margin* to the associated AP as shown in Fig. 3.1. Specifically, an AP triggers TPC by sending a *TPC request* frame to its STA. The STA upon the TPC request reception answers with a *TPC report* frame carrying the STA's link margin. According to the standard, a STA's link margin is defined as the ratio of the received signal strength of

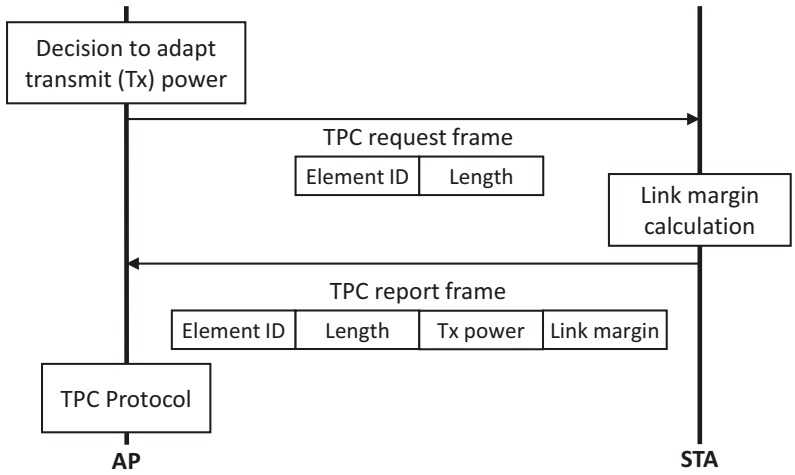

Figure 3.1: IEEE 802.11h TPC procedure.

the corresponding TPC request to the minimum desired signal strength by the STA. The specific algorithm for computing the link margin is implementation dependent.

In this dissertation, we define an algorithm determining link margin as follows. Firstly, with the existence of a CCI as shown in Fig. 3.2, link margin is redefined as the ratio of the received signal-to-interference ratio (SIR) during the reception of a TPC request to the desired SIR.[2] Secondly, assuming that STAs are aware of their radio frequency (RF) parameters such as receiver sensitivities[3] and noise floor, STA k estimates desired SIR using its RF parameters as

$$\mathrm{SIR}^{*}_{k,m} = \mathrm{RxSens}_{k,m} - \mathrm{NF}_{k} \tag{3.1}$$

where $\mathrm{SIR}^{*}_{k,m}$, $\mathrm{RxSens}_{k,m}$, and NF_{k} are STA k's desired SIR for modulation and coding scheme (MCS) m, receiver sensitivity for MCS m, and noise floor, on the dB scale, respectively.

[2]We assume that CCIs are much stronger than noise, thus using SIR instead of signal-to-interference plus noise ratio (SINR).

[3]Receiver sensitivity, i.e., receiver minimum input sensitivity, is defined as the input power level guaranteeing that the PER of 1000-byte packets shall be 10% or less. Therefore, the values are rate-dependent.

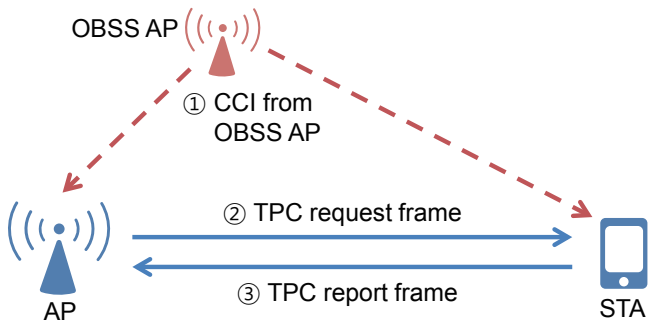

Figure 3.2: IEEE 802.11h TPC procedure in our target scenario.

Accordingly, STA k's link margin for MCS m with the existence of a CCI from node j, denoted by $\lambda^j_{k,m}$, is calculated as

$$\begin{aligned}\lambda^j_{k,m} &\triangleq (\text{Received SIR})_k - \text{SIR}^*_{k,m} \\ &= (S_{i\to k} - I_{j\to k}) - \text{SIR}^*_{k,m} \end{aligned} \tag{3.2}$$

where $S_{i\to k}$ and $I_{j\to k}$ are the signal power at STA k from AP i and the CCI power at STA k from interferer j, on the dB scale, respectively.

3.2.2 IEEE 802.11ah Basic Service Set (BSS) Color

IEEE 802.11ah is an amendment for providing extended range WLAN using sub 1 GHz bands [33]. Task group ah (TGah) proposed to place *color bits*, indicating which BSS the transmitter and receiver of a frame belong to, in the SIG field of the frame. The color bits enable other nodes to identify whether the frame is from their own BSS or from OBSS by reading the SIG field of the frame.

3.3 FACT: Proposed CST Adaptation Scheme

In this section, we present a CST adaptation method, called FACT.

Table 3.1: An example of CST table of AP i, consisting of $C_i(j,k)$'s.

Destination (k) / Interferer (j)	STA 1	STA 2	STA 3
AP 2	-70 dBm	-75 dBm	-72 dBm
AP 3	-80 dBm	-67 dBm	-82 dBm
AP 4	-77 dBm	-70 dBm	-81 dBm

3.3.1 Basic Principle

Unlike the principle of the original CCA, i.e., *"do not disturb others,"* FACT allows an AP to *"transmit if its transmission is viable."* The AP, therefore, adapts CST depending on both interferers and destinations. Specifically, AP i manages CST for pairs of interferer j and destination k, i.e., $C_i(j,k)$, using a *CST table* as shown in Table 3.1. For example, when the AP has a head-of-the-queue packet destined to STA 1 and the ongoing frame, generating a CCI, is from AP 2, it performs CCA with CST of -70 dBm.[4]

To determine CST for each destination, AP i needs to assess whether its destination can successfully receive its signal or not based on the CCI power, which itself experiences. If AP i learns the maximum power of the CCI from interferer j, which destination STA k can tolerate, it sets $C_i(j,k)$ as the maximum tolerable CCI power. It should be noted that the CCI power here refers to the received power at the AP, not the received power at the destination STA.

[4]We assume that an AP is the transmitter. However, STAs can also work in the same manner. When a STA is the transmitter, the only destination is its associated AP, and the CST table becomes one-dimensional.

3.3.2 Challenges and Solutions

There are two challenges for this operation. First, before receiving the MAC header of a frame, an AP cannot identify which interferer transmits the frame. Second, it is difficult for an AP to measure the tolerable CCI power at a remote STA, since the AP does not know the received powers of the desired signal and CCI at the remote STA.

We overcome these challenges using the above-described functions, i.e., BSS color and TPC, as follows. Firstly, assuming that BSS color is implemented, an AP can identify neighboring APs' transmissions by BSS color bits in the SIG field. Since SIG field is at the front part of a frame and easily decodable, the AP can identify an interferer in three time slots after starting receiving,[5] if the interferer is an OBSS AP. CCIs from OBSS STAs are also identifiable, for example, by decoding MAC header or putting transmitter's partial association ID (PAID) in SIG field. Because these procedures to identify CCIs from OBSS STAs are not defined in the current standard, we focus on CCIs from OBSS APs in this section.

Secondly, an AP is able to know the ratio of signal and CCI power at a remote STA using TPC request and TPC report. Specifically, by receiving a link margin measured by the remote STA with the existence of a CCI, the AP can expect whether the STA can decode AP's signal with the existence the CCI from the same interferer. Then, the CST for the pair of the interferer and the STA can be adapted according to the CCI power measured at the AP and the reported link margin.

3.3.3 Specification

Based on the two functions, the procedure of FACT is given as follows:

1. Initially, AP i sets $C_i(j,k) \leftarrow C_{\max}, \forall(j,k)$, where $C_{\max}$ is the maximum CST, e.g., -62 dBm. With this initial CST, AP i can transmit only TPC requests. Data

[5] According to IEEE 802.11ac, it takes 24 us, i.e., 8 us of L-STF + 8 us of L-LTF + 4 us of L-SIG + 4 us of VHT-SIG-A1.

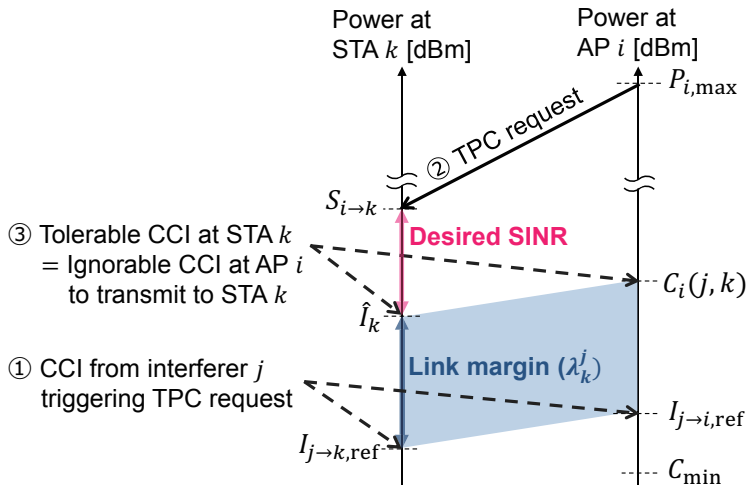

Figure 3.3: Illustration for CST adaptation.

and other control/management frame transmissions to STA k under a CCI from j are prohibited until $C_i(j,k)$ is updated.

2. If AP i senses a CCI from interferer j, it records the CCI power as reference power, i.e., $I_{j\to i,\mathrm{ref}}$, and unicasts or broadcasts a TPC request using a reference MCS, i.e., m_{ref}.[6]

3. STA k, upon successfully receiving the TPC request by *second frame capture* [34], calculates a link margin, i.e., $\lambda^j_{k,m_{\mathrm{ref}}}$, according to (3.2). Then, STA k reports the link margin via a TPC report when it first accesses channel afterward.

4. When AP i receives the TPC report from STA k, it sets

$$C_i(j,k) \leftarrow I_{j\to i,\mathrm{ref}} + \lambda^j_{k,m_{\mathrm{ref}}}. \tag{3.3}$$

If AP i does not receive TPC report from STA k within a timeout threshold, it sets the CST as $C_i(j,k) \leftarrow C_{\mathrm{def}}$, where C_{def} is the default CST, i.e., -82 dBm.[7]

[6]The reference MCS should be robust so that more STAs can receive it. However, it does not have to be the lowest MCS, because the required SIR for second frame capture is about 11 dB [34] and much higher than the desired SIR for the lowest MCS.

[7]If an AP has sent multiple TPC requests for various OBSS APs, and is waiting for multiple TPC

The reason for the calculation in (3.3) is illustrated in Fig. 3.3. Assuming that the channel between an interferer and AP i and the channel between the interferer and STA k are strongly correlated,[8] the CCI power increment at STA k is the same as the CCI power increment at AP i, i.e.,

$$I_{j\to k} = I_{j\to k,\mathrm{ref}} + (I_{j\to i} - I_{j\to i,\mathrm{ref}})\,. \tag{3.4}$$

Therefore, if $I_{j\to i} - I_{j\to i,\mathrm{ref}} \leq \lambda^{j}_{k,m_{\mathrm{ref}}}$, then $I_{j\to k} \leq I_{j\to k,\mathrm{ref}} + \lambda^{j}_{k,m_{\mathrm{ref}}}$, and thus STA k can successfully decode a signal from AP i according to the definition of link margin. Since the principle of FACT is "transmit if it can succeed," AP i can ignore CCI which satisfies:

$$I_{j\to i} \leq I_{j\to i+\mathrm{ref}} + \lambda^{j}_{k,m_{\mathrm{ref}}}. \tag{3.5}$$

Therefore, the maximum ignorable CCI power at AP i is given as the right side of (3.5), i.e., $(I_{j\to i,\mathrm{ref}} + \lambda^{j}_{k,m_{\mathrm{ref}}})$, and the value serves as CST.

3.3.4 Transmit Power Adjustment

The principle, however, can harm the fairness among OBSSs, since it does not protect ongoing transmissions. To enhance the fairness, we adjust both CST and transmit power as

$$C_i(j,k) \leftarrow I_{j\to i,\mathrm{ref}} + \alpha\lambda^{j}_{k,m_{\mathrm{ref}}}, \tag{3.6}$$

$$P_i(j,k) \leftarrow P_{i,\max} - (1-\alpha)\lambda^{j}_{k,m_{\mathrm{ref}}} \tag{3.7}$$

where $P_i(j,k)$ and $P_{i,\max}$ are AP i's adjusted power to STA k when interferer j is transmitting and AP i's maximum transmit power, respectively. $\alpha \in (0,1]$ is *egoism*

reports from a single STA, the AP distinguishes TPC reports by *dialog token*, which is included in both TPC request and TPC report frames.

[8] If AP i and STA k are closely located and distant from interferer j, j-to-i link and j-to-k link have positive correlation [35]. Due to independent fading at each link, however, the link correlation could become low. We consider the effect of fading later in this section.

parameter controlling the trade-off between AP i's own throughput and overall fairness. High α enables the AP to gain more transmission chances, while low α better protects ongoing transmissions. With the adjusted transmit power of AP i, the signal power at STA k becomes lower, and STA k's maximum tolerable CCI also becomes lower. Therefore, CST is also set lower than the CST without transmit power adjustment.

3.3.5 Conditional Update of CST

Since signal power fluctuates due to multi-path fading, CST should be adapted depending on the channel condition. To this end, AP i records the signal power of the latest TPC report from STA k for interferer j as the reference signal strength. i.e., $S^j_{k\to i,\mathrm{ref}}$. AP i also keeps track of subsequent $S_{k\to i}$ and $I_{j\to i}$, and calculates $\Delta S_i(j,k)$ and $\Delta I_i(j,k)$ as

$$\Delta S_i(j,k) = S_{k\to i} - S^j_{k\to i,\mathrm{ref}} \tag{3.8}$$

$$\Delta I_i(j,k) = I_{j\to i} - I^k_{j\to i,\mathrm{ref}} \tag{3.9}$$

where $I^k_{j\to i,\mathrm{ref}}$ is the reference CCI power from j which is measured when sending the latest TPC request to STA k. If AP i senses a CCI from j and the CCI power satisfies $|\Delta S_i(j,k)| + |\Delta I_i(j,k)| \geq \Delta_{\mathrm{thres}}$, it transmits a TPC request to STA k to update $C_i(j,k)$, where Δ_{thres} is *update threshold* on the dB scale. If the value is less than the update threshold, AP i updates $C_i(j,k)$ as $C_i(j,k) \leftarrow C_i(j,k) + \Delta S_i(j,k)$ without transmitting a TPC request.

3.4 Blind CCA and Backoff Compensation

In this section, we propose a supplementary CCA method compatible with all CST adaptation schemes considering both interferer and destination as FACT.[9]

[9]Unlike the previous section, in this section, we consider CCIs from both OBSS APs and OBSS STAs.

3.4.1 Blind CCA

As described in Section 3.3, AP spends three time slots to identify an interferer by reading SIG field. During the three time slots, the AP cannot use the interferer-dependent CST since the interferer is unknown. We name these time slots *blind-slots*, and name the CCA during blind-slots *blind CCA*. To differentiate CCIs during blind-slots, we first define a range of CCI powers at AP i from interferer j as $\mathbb{R}_i(j) \triangleq [I_{j\to i,\min}, I_{j\to i,\max}]$, where $I_{j\to i,\min}$ and $I_{j\to i,\max}$ are the minimum and the maximum $I_{j\to i}$ for a time interval, respectively. For example, if the CCI power at AP 1 from AP 2 ranges from -70 dBm to -65 dBm, $\mathbb{R}_1(2)$ is $[-70, -65]$.

Based on $\mathbb{R}_i(j)$ of each interferer j, we define *interferer sets*, i.e., $\mathbb{J}_{i,l}$ as the minimum set of interferers such that $\underset{j\in\mathbb{J}_{i,l}}{\cup} \mathbb{R}_i(j)$ is disjoint with $\underset{j\in\mathbb{J}_{i,l'}}{\cup} \mathbb{R}_i(j)$, $\forall l' \neq l$, where $l \in \{1, \cdots, l_{\max}\}$ is index for the interferer set and $l_{\max}$ is the total number of interferer sets. If $\mathbb{R}_1(3)$ is $[-67, -60]$ and $\mathbb{R}_1(4)$ is $[-80, -75]$, for example, $\underset{j=1,2}{\cup} \mathbb{R}_i(j) = [-70, 60]$ and is disjoint with $\mathbb{R}_1(4)$. Therefore $\mathbb{J}_{1,1}$ includes AP 2 and AP 3, and $\mathbb{J}_{1,2}$ includes AP 4.

When AP i senses a CCI power included in $\underset{j\in\mathbb{J}_{i,l}}{\cup} \mathbb{R}_i(j)$, it sets CST for blind CCA as

$$\hat{C}_{i,l}(k) = \min_{j\in\mathbb{J}_{i,l}} C_i(j,k). \tag{3.10}$$

If the CCI power is not included in any $\underset{j\in\mathbb{J}_{i,l}}{\cup} \mathbb{R}_i(j)$, C_{def} is used during the blind-slots.

Also, since destination is not specified for post backoff, CST for post backoff is given as

$$\hat{C}_{i,l} = \min_{k\in\mathbb{K}_i} \hat{C}_i(k) \tag{3.11}$$

where $\mathbb{K}_i$ is a set of AP i's client STAs. When AP i has no packet to send, it performs CCA with C_{def} to gather information about new interferers.

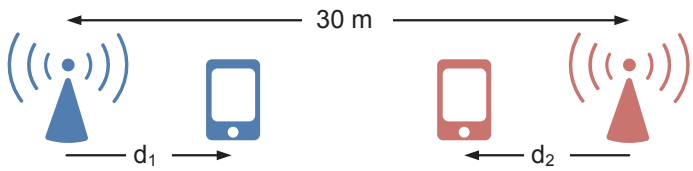

Figure 3.4: Simulation topology for performance evaluation of CST adaptation.

3.4.2 Backoff Compensation

In addition to blind CCA, we propose a simple method, named *backoff compensation* to compensate overhead in backoff. When a CCI power at AP i from interferer $j \in \mathbb{J}_{i,l}$ is lower than $C_i(j,k)$ and higher than $\hat{C}_{i,l}(k)$, AP i could have reduced backoff counter (BC) during blind-slots if it identified j earlier. To reduce the temporal overhead, we perform backoff compensation after identifying the interferer. Specifically, AP i reduces BC by $\min(\mathrm{BC}_{\mathrm{curr}}, \Delta_{\mathrm{BC}})$, where $\mathrm{BC}_{\mathrm{curr}}$ is the current BC and $\Delta_{\mathrm{BC}} \in \{0,1,2,3\}$ with uniform probability. This random compensation mitigates collisions among the APs which simultaneously finish backoff by backoff compensation.

3.5 Performance Evaluation

The performance of the proposed schemes is evaluated via ns-3 simulation [29]. Fig. 3.4 shows a network topology with two APs 30 m apart from each other. Two STAs are located d_1 and d_2 away from their associated APs, respectively. Positive distance refers that the STA is on the side of the OBSS, and negative distance means the opposite side of the OBSS. To see how FACT works depending on the locations of a destination and an interferer, we iteratively locate STAs at every combination of (d_1, d_2), $d_1, d_2 \in \{-15, 14, \cdots, 13, 14\}$ (m). Saturated downlink UDP traffic is generated at both APs and throughput is measured for 1 second. Jakes' fading model and Minstrel rate adaptation algorithm using 802.11n data rates with a single spatial stream is

adopted. Other simulation parameters follow the common parameters in TGax simulation scenarios which consider densely deployed WLANs [22].

Fig. 3.5 shows the throughput for (d_1, d_2) by color at the coordinate; red color represents high throughput and blue color represents low throughput. Upper five diagrams show the sum throughput of the two BSSs, while lower five diagrams show the minimum throughput of the both, i.e., a BSS's throughput which is lower than that of the other BSS's.j Doppler velocity is 0.1 m/s and the throughput is averaged out over 100 iterations.

In Fig. 3.5(a), i.e., when CST is fixed to -82 dBm,[10] throughput is consistent regardless of the locations of STAs. For every (d_1, d_2), the sum throughput is about 32 Mb/s and the minimum throughput is about 16 Mb/s. Since the signal strength between the two APs is about -64 dBm according to TGax pathloss model, the APs share the channel. On the other hand, if CST is fixed to -62 dBm, APs do not sense each other, thus transmitting simultaneously. Consequently, the throughput is almost doubled when STAs are close to the associated AP since the simultaneous transmissions are viable. As either STA gets far from the associated AP, however, the throughput drops rapidly due to decreased SIR.

Meanwhile, as shown in Fig. 3.5(d)–(e), FACT works as -62 dBm when STAs and the associated APs are close enough to achieve successful simultaneous transmissions, and works as -82 dBm when STAs are relatively far from the APs, respectively. In addition, by lowering α, i.e., reducing transmit power, higher gain is achieved, especially in terms of the minimum throughput. The average gains of sum throughput over -82 and -62 dBm are about 9% and 17%, respectively.

The PER-based scheme, which increases CST with PER smaller than $p_{\min}$ and decreases CST with PER greater than $p_{\max}$ [9],[11] shows a similar trend as FACT. As

[10] IPCS is the proposed CST adaptation scheme in [8]. To eliminate hidden terminals, IPCS sets CST very conservatively. Therefore, resulting CST is equivalent to -82 dBm.

[11] The plotted throughput is the average of the results with four target parameters used in [9], i.e., $(p_{\max}, p_{\min}) = \{(0.2, 0.1), (0.3, 0.2), (0.4, 0.3), (0.5, 0.4)\}$. Also, we update CST based on the PER

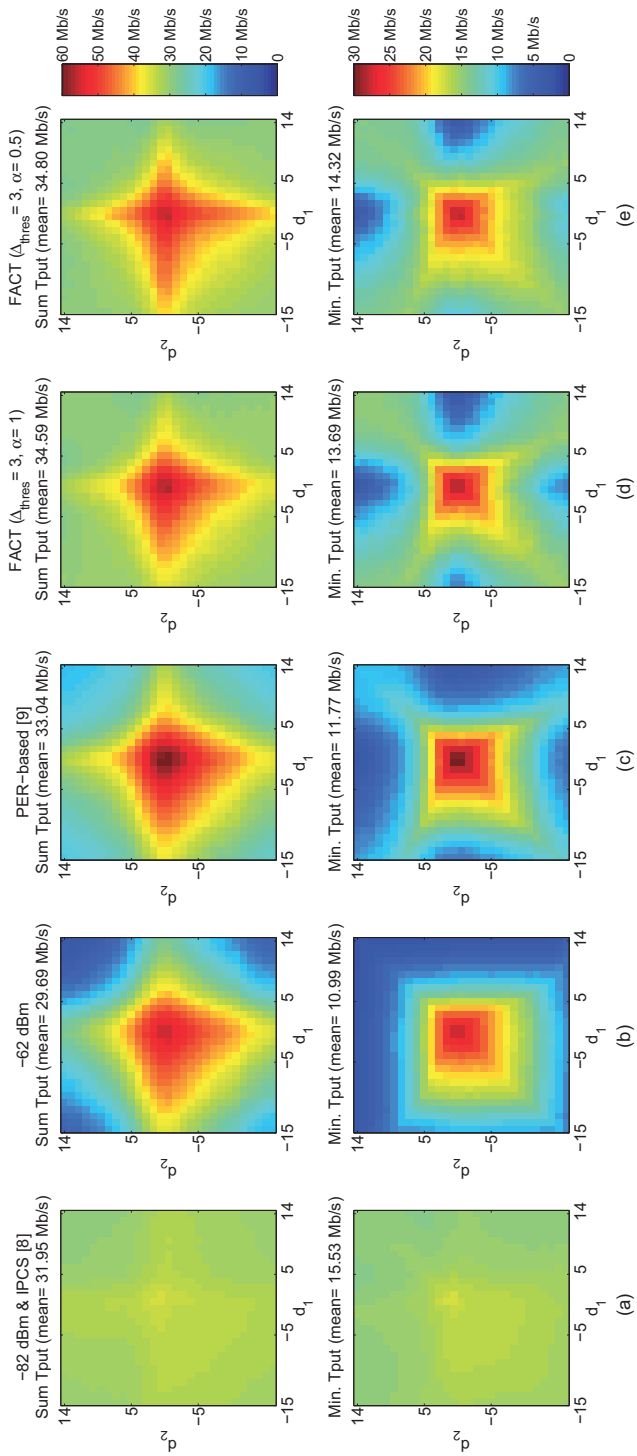

Figure 3.5: Sum and minimum throughput of CST adaptation methods.

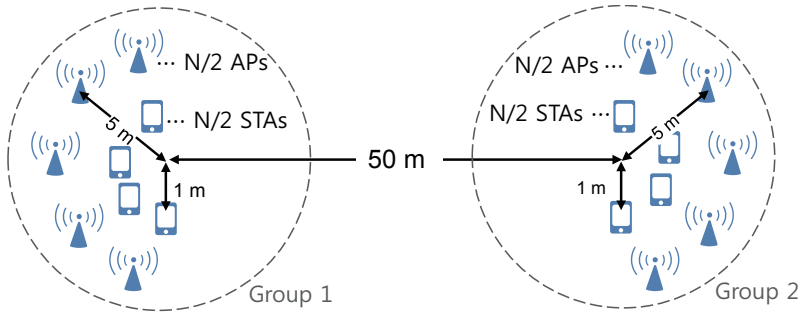

Figure 3.6: Simulation topology for performance evaluation of blind CCA and backoff compensation.

shown in the edge region of Fig. 3.5(c), however, it gets lower throughput, because it aggressively tries transmissions, which harms the other cell, while enduring a certain degree of PER.

Fig. 3.6 shows a network topology used for performance evaluation of blind CCA and backoff compensation. There are N BSSs consisting of one AP and one STA, and the BSSs are divided into two groups. If an AP in Group 1 starts a transmission, the APs in Group 2 can reduce BC by using a CST adaptation method considering interferer after identifying the interferer, while the APs in Group 1 cannot. Therefore, the APs in Group 2 can perform backoff compensation.

Fig. 3.7 shows the sum throughput and the average collision error rate of all BSSs for various N, when CWmin$=$ 15 and 31, respectively. The numbers in the legend represent the mean values of the corresponding performance metrics across N BSSs. Doppler velocity is 0 m/s and the throughput is averaged out over 20 iterations. For all cases, blind CCA shows the best performance by eliminating time overhead in identifying OBSS. Full compensation (FullCompen.), i.e., reducing BC by 3, gains high throughput when $N = 2$. However, as N increases, its throughput drops rapidly due to many collisions among APs in the same group, thus being worse than no compensation (NoCompen.). Random compensation (RndCompen.), on the other hand, ameliorates

of every 50 packets as in [10] instead of the CST updating period of 20 s used in [9].

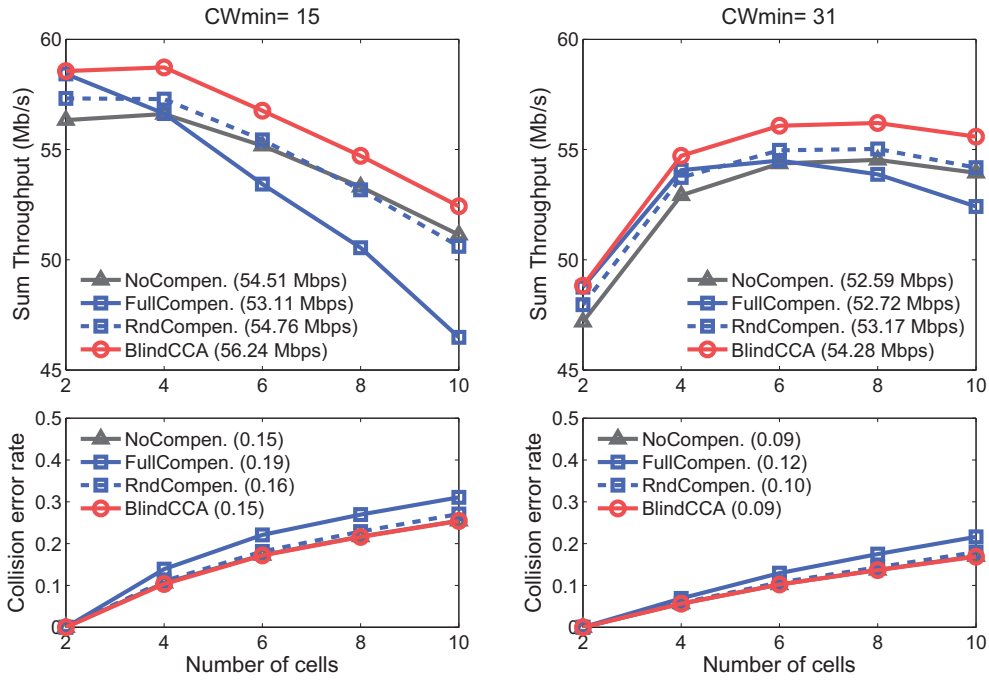

Figure 3.7: Sum throughput and collision rate of blind CCA and backoff compensation schemes for different CWmin's

collisions, thus achieving higher throughput than NoCompen., especially when contention window is large, i.e., CWmin= 31.

3.6 Summary

In this chapter, we have proposed a standard-compliant CST adaptation method considering both interferer and destination for better spatial reuse. The proposed CST adaptation scheme utilizes existing standard's functions to identify interferers and to assess the channel between interferers and destinations. We also proposed a CCA scheme for CST adaptations to reduce time overhead in backoff. Simulation results demonstrate that the proposed schemes considerably enhance network throughput by conditionally promoting simultaneous transmissions among OBSSs.

Chapter 4

MASTaR: MAC Protocol for Access Points in Simultaneous Transmit and Receive Mode

4.1 Introduction

The ability of a node to successfully receive a signal while transmitting another signal is referred to as in-band simultaneous transmit and receive (STR) or in short STR.[1] STR is considered a promising technology to increase network capacity in wireless communication systems including IEEE 802.11 wireless local area network (WLAN), a.k.a. Wi-Fi [27]. The main challenge, however, to realize STR has been self-interference (SI). For successful reception during transmission in the same band, a node should be capable of reducing the SI to the noise floor level. This capability is known as self-interference cancellation (SIC). Without perfect SIC, the achievable capacity of STR is restricted to less than the full-duplex limit, which is double the half-duplex capacity. How SIC can be brought to real radios is studied in [13, 36–41].

STR transmission is classified as either *symmetric mode* or *asymmetric mode*, depending on the nodes engaged in the transmission. In the symmetric mode, as shown in Fig. 4.1(a), two nodes transmit and receive signals to/from each other simultane-

[1] It is also often referred to as in-band full duplex, but we use the term STR in this dissertation.

(a) Symmetric mode (b) Asymmetric mode

Figure 4.1: Operational modes of STR in WLANs.

ously. In the asymmetric mode, as shown in Fig. 4.1(b), a node transmits and receives to/from different nodes. The node that initiates the first transmission—*primary transmission*—is called the *primary transmitter (PTX)*; the corresponding receiver is called the *primary receiver (PRX)*. Similarly, the transmitter and receiver of the subsequent transmission—the *secondary transmission*—are called the *secondary transmitter (STX)* and *secondary receiver (SRX)*, respectively. In Fig. 4.1(b), for instance, if station (STA) 1 transmits first, and access point (AP) subsequently transmits to STA 2, {PTX, PRX, STX, SRX} are given by {STA 1, AP, AP, STA 2}, respectively.

In IEEE 802.11 WLAN, the asymmetric mode is more feasible because the STR capability cannot be easily implemented in mobile STAs, especially in small devices such as smartphones. AP devices, however, are more likely to be capable of STR thanks to their relatively larger size and higher performance in comparison to mobile devices. Thus, we will mainly focus on the asymmetric mode in this dissertation.

In the asymmetric mode, there are three possible scenarios: (i) *Uplink (UL) First* (where STA transmits first and its associated AP follows), (ii) *Downlink (DL) First* (where AP transmits first and its client STA follows), and (iii) *Coincidence* (where both start transmission at the same time). In the UL First case, AP starts new transmission while receiving UL signal. This is challenging because the SI after analog SIC can saturate the AP's automatic gain control (AGC) [15]. A possible solution is to set the AGC conservatively in advance so that the SI power is within the dynamic range of the AP's analog-to-digital converter (ADC) to secure enough dynamic range for the uncancelled SI in advance when the AP starts a reception. This solution increases the

quantization noise caused by ADC, thus requiring high-cost ADC with many bits for reliable quantization. Another challenge is that the AP has to estimate the *SI channel after analog SIC* to perform digital SIC. However, due to the presence of the ongoing UL signal, the SI channel estimation can be inaccurate. In the latter part of this chapter, we quantitatively analyze this issue.

In the DL First and Coincidence cases, AP starts receiving new UL signal while transmitting. Likewise, the dynamic range of the AP's AGC should accommodate the SI before digital SIC, and hence, a high-performance ADC is required to suppress the quantization noise added to a newly receiving signal. What is worse, in order to decode the UL signal after the digital SIC, the orthogonal frequency-division multiplexing (OFDM) symbol of the UL signal must align with the OFDM symbol of the DL signal within the cyclic prefix (CP) duration [39, 40]. To make this possible, the AP must notify in advance when to start the UL transmission to the STA. Such notification causes protocol overhead.

In this chapter, we analyze the SIC performance achievable with the 802.11 physical layer convergence protocol (PLCP) frame structure without any modification. By using 3D-ray tracing results and adopting the notion of *dirty estimation* and *clean estimation* as the estimation method for SI channel, we measure the physical (PHY) layer feasibility of STR in the 802.11 WLANs.

Along with the PHY layer issues, to bring STR to the current 802.11 WLAN, we need to address the following problems concerning medium access control (MAC) layer:

- With carrier sensemultiple access with collision avoidance(CSMA/CA) based channel access, a node cannot, regardless of its SIC capability, start new transmission during reception since its channel status is indicated as *BUSY*.

- The current Acknowledgment (ACK) mechanism faces a new problem. Assuming that, STA 1, as in Fig. 4.1(b), finishes its transmission successfully earlier than AP,

the AP should transmit an ACK frame in short inter-frame space (SIFS) time according to the current standard. However, the AP cannot start the ACK transmission because it is still transmitting data to STA 2. On the other hand, if the AP finishes its transmission first, STA 2 transmits an ACK frame, but the ACK frame may collide with the data frame transmitted by STA 1. In this case, the AP can receive either the data frame, the ACK frame, or neither.

- If PTX (or STX) causes significant interference to SRX (or PRX), the secondary transmission fails due to low received signal-to-interference-plus-noise ratio (SINR). This type of interference is called *inter-node interference (INI)*. Note that the existence of INI is a disadvantage of the asymmetric mode compared with the symmetric mode.

We thus propose a novel protocol for APs supporting STR in WLANs, named MASTaR (MAC protocol for Access point in Simultaneous Transmit and Receive mode). MASTaR solves the aforementioned MAC layer problems by enabling (i) access to busy channel after identifying PTX, (ii) *dummy data frame* and *explicit block ACK (BA)*, and (iii) transmission scheduling based on *link map*. The three key components will solve the above-mentioned three problems. Moreover, designed based on the current IEEE 802.11 standard, MASTaR's main advantage is standard-compliant operation of STAs, i.e., it only requires legacy devices of existing IEEE 802.11 functions and does not change the PLCP/MAC frame structures. To the best of our knowledge, this is the first standard-compliant STR MAC protocol in the 802.11 WLANs, supporting the asymmetric mode with legacy STAs.

The rest of this chapter is organized as follows. We introduce the 802.11 functions utilized in the proposed protocol in Section 4.2. In Section 4.3, we present the detailed operation of MASTaR. In Section 4.4, we look at the feasibility of MASTaR and Section 4.5 evaluates its performance. Finally, Section 4.6 presents the summary of this chapter.

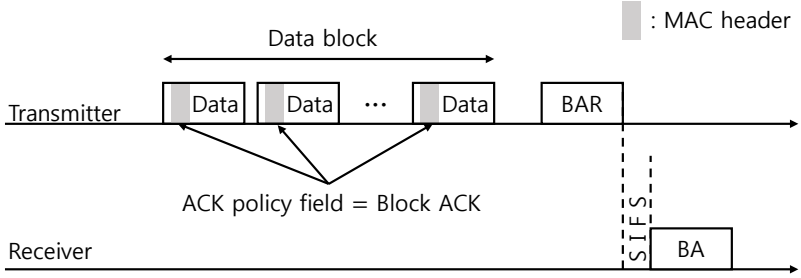

Figure 4.2: Explicit block ACK procedure.

4.2 Preliminaries

We first introduce preliminary IEEE 802.11 functions and RF capability, which are utilized in the proposed protocol.

4.2.1 Explicit Block ACK

In baseline IEEE 802.11 ACK policy, every single unicast frame should be individually acknowledged. IEEE 802.11e [27], published in 2005, defines block ACK (BA) which acknowledges multiple frames at once. Depending on the ACK policy field in a MAC header, two different BA policies, i.e., *implicit BA* and *explicit BA*, can be applied. With the implicit BA policy, the transmitter sets a frame's ACK policy field to "Normal ACK," and the receiver sends a BA immediately after the reception of the frame. With the explicit BA policy, on the other hand, the ACK policy field is set to "Block ACK," and the receiver should wait for a BA request (BAR) before sending a BA as shown in Fig. 4.2. In this way, the explicit BA policy makes it possible for the transmitter to control when the receiver should send a BA. It is worth mentioning that both IEEE 802.11h and IEEE 802.11e have been incorporated into the revised 802.11 standard published in 2007. Accordingly, the majority of the legacy devices should be compliant with the functionalities defined in IEEE 802.11h and 802.11e.

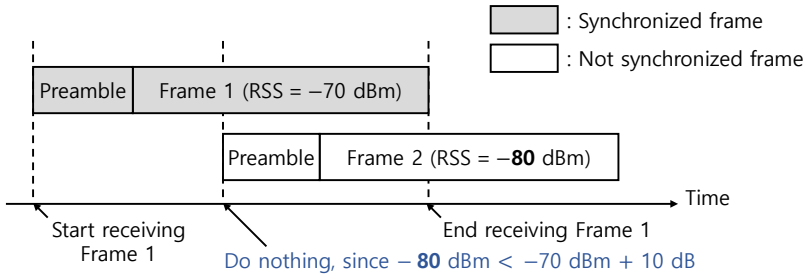

(a) First frame capture

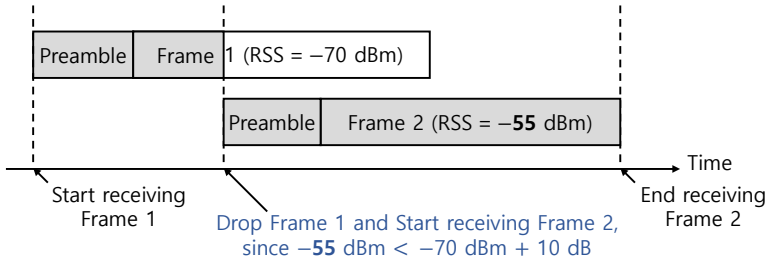

(b) Second frame capture

Figure 4.3: Illustration for capture effect.

4.2.2 Capture Effect

In wireless networks, if more than one frame is being transmitted on the same channel, a node can receive no frame or only the strongest frame depending on the relative signal power and the arrival timings of the colliding frames. Assuming that a frame with a greater signal power arrives at a node which is already receiving a frame as shown in Fig. 4.3(b), the node should stop the current reception and synchronize with the stronger frame to decode at least one frame correctly. This behavior for the successful reception of the later-arriving frame is referred to as *second frame capture. First frame capture*, in contrast, refers to the phenomenon that the already-synchronized frame has a greater signal power than the later-arriving frame such that it is successfully decoded by the receiver enduring the interference from later-arriving frames as shown in Fig. 4.3(a).

It has been found that approximately 10 dB signal-to-interference ratio (SIR) is

required for second frame capture [34], and commercial WLAN devices generally have the second capture capability [21]. Therefore, a later-arriving frame can be decoded if its signal power is higher than that of the already-synchronized frame by at least 10 dB. In contrast, first frame capture does not have such criteria because a receiver may keep synchronizing with the already-synchronized frame unless a later-arriving frame has a signal power greater than 10 dB stronger. It should be noted that the actual decodability of both the already-synchronized frame and the later-arriving frame depends on the MCS of the frames.

4.3 MASTaR: Proposed MAC Protocol

In this section, we propose a novel MAC protocol, namely MASTaR. We focus on the asymmetric mode with DL secondary transmission. That is, an AP starts secondary transmission after identifying the transmitter of UL transmission. We assume that STR capability is implemented in APs, and STAs are the legacy devices supporting the preliminary functions.[2] It should be noted that MASTaR can also consider the STAs with STR capability, by prioritizing the symmetric mode transmission.[3] In the followings, however, we focus on the asymmetric mode. Based on the two existing functions in the 802.11 standards, i.e., TPC and explicit BA, MASTaR consists of the components described below.

4.3.1 PTX Identification

To initiate secondary transmission, the STX—an AP—should identify that the PTX is one of its client STAs. We propose two PTX identification methods, each for the primary transmission initiated with/without request-to-send (RTS). This is because the AP cannot force the legacy STAs to use or not to use RTS; each STA has *RTS threshold*

[2]If a STA does not support IEEE 802.11h TPC or second capture, the STA is excluded from the candidate SRX.

[3]The symmetric mode transmission is prioritized, since no INI problem exists in the symmetric mode.

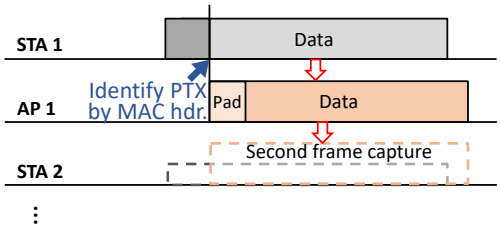

(a) PTX identification by MAC header

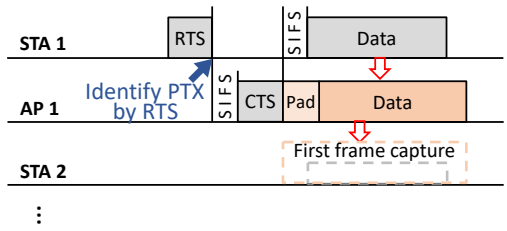

(b) PTX identification by RTS

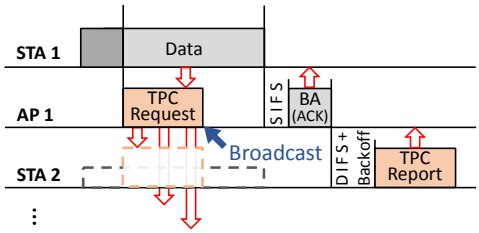

(c) Broadcasting TPC request

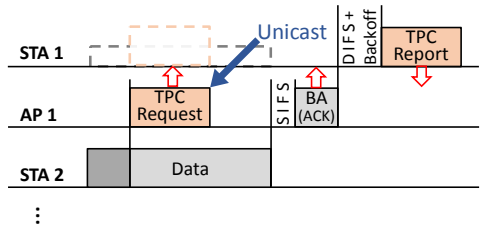

(d) Unicasting TPC request

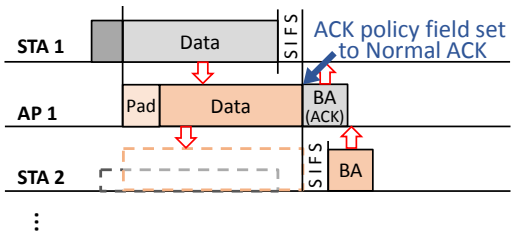

(e) Simultaneous (implicit) BA

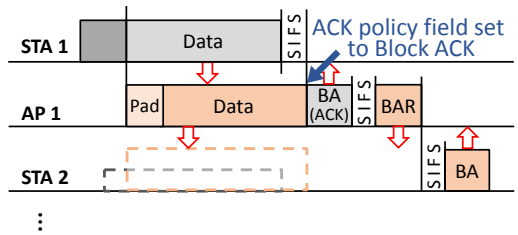

(f) Explicit BA using BAR

Figure 4.4: Basic operation of MASTaR.

and uses RTS only before transmitting data frames with lengths longer than its RTS threshold.

For UL data transmission without RTS, the AP peeks the MAC header of the frame on the primary transmission as shown in Fig. 4.4(a).[4] In a strict sense, since bit errors can occur, the AP is not convinced of the PTX before checking cyclic redundancy check (CRC). However, the probability is quite low that the erroneous MAC address becomes the same as one of the client STAs' addresses. For this reason, the next IEEE 802.11 WLAN standard, i.e., IEEE 802.11ax, will also use the MAC header of a frame to determine from which basic service set (BSS) the frame is being transmitted [44]. If the source address in the primary transmission's MAC header does not agree with any of the AP's client STAs,[5] PTX identification fails; no secondary transmission is initiated, making it possible to prevent erroneous operations. If the source address corresponds to one of the AP's client STAs, the AP initiates secondary transmission. At this stage, the AP is also aware of the duration of the primary transmission by reading the LENGTH and RATE field in the PLCP header, and uses it for scheduling the secondary transmission.

On the other hand, if PTX sends RTS before its data transmission, the AP can clearly identify PTX before the primary transmission as shown in Fig. 4.4(b). In this case, the AP schedules secondary transmission right after CTS so that its transmission precedes the UL transmission. This enables (i) clean SI channel estimation for the BA

[4] According to IEEE 802.11ac [42], the VHT-SIG-A field in the PLCP header for DL frames contains partial AID, which indicates individual client STA. However, for UL frames, only BSS ID is contained in VHT-SIG-A field; thus the transmitter of the UL transmission cannot be identified by reading the PLCP header. If a new IEEE 802.11 standard defines a new PLCP header conveying transmitter identifier as suggested in [43], an AP can identify PTX before decoding MAC header.

[5] By utilizing IEEE 802.11ah *BSS color*, which is also adopted in 802.11ax, the AP can know that a frame is transmitted from other BSSs if the BSS color bit in the frame's PLCP header does not match the AP's own BSS color. In this case, the AP can verify that the frame is not transmitted from its client STA without reading the frame's MAC header.

transmission at the AP,[6] and (ii) first frame capture of the BA frame for the primary transmission at the target receiver, i.e., PTX. In this case, the AP can discern the duration of the primary transmission from the DURATION field in the MAC header of the RTS frame.

4.3.2 Initial Training

To choose the best SRX for a given PTX, an AP manages a link map. For each pair of STAs i and j, a link map is defined as

$$\mathcal{L}(j,i):\ (j,i) \rightarrow (\lambda^{j}_{i,0}, \lambda^{j}_{i,1}, \cdots, \lambda^{j}_{i,m_{\max}}),\ \ \forall i,j \in \mathbb{I}, \tag{4.1}$$

where $\mathbb{I}$ is the set of all client STAs and $m_{\max}$ is the maximum MCS, e.g., 8 for IEEE 802.11ac with a single spatial stream.

To build a link map, the AP sends a TPC request frame after the PTX identification using reference MCS, i.e., m_{ref}. The required SINR of the reference MCS should be low so that more STAs can receive the TPC request frame. However, it need not be lower than the required SIR for second frame capture, which is about 10 dB. Initially, the TPC request frame is broadcast as shown in Fig. 4.4(c), since $\mathcal{L}(\mathrm{PTX}, i)$ is empty for $\forall i$. At a STA, if the signal power of the TPC request frame is sufficiently stronger than the signal power from PTX, the STA can receive the TPC request frame, calculate the SINR, and report it via a TPC report frame. If the AP receives the TPC report frame before the *TPC report timeout*, the AP estimates link margins for other MCSs and populates the link map.

4.3.3 Link Map Management

Since the signal power changes due to multi-path fading and STAs' mobility, a link map is adapted depending on the channel condition as follows. Let the time when the

[6]Within SIFS time, i.e., 16 μs [42], the AP can estimate the SI channel for the BA frame without interference, by using the 8 μs legacy long training field (L-LTF), which is sent after the 8 μs legacy short training field (L-STF).

AP sends the latest TPC request to STA i during the reception from PTX j be τ_i^j. The AP records the signal power of PTX j at that time as $S_j(\tau_i^j)$, and the signal power of the corresponding TPC report frame from STA i as $S_i(\tau_i^j)$. The AP also keeps track of subsequent received signal power from all its client STAs, and calculates

$$\Delta S_{i,\mathrm{srx}} = S_i - S_i(\tau_i^j) \text{ and } \Delta S_{j,\mathrm{ptx}} = S_j - S_j(\tau_i^j), \tag{4.2}$$

where S_i and S_j are the recently measured signal power from STAs i and j, respectively. Then the link map is updated as follows:

- If the AP senses primary transmission from STA j and the signal power satisfies $|\Delta S_{i,\mathrm{srx}}| + |\Delta S_{j,\mathrm{ptx}}| \geq \Delta_{\mathrm{thres}}$, it unicasts a TPC request to STA i as shown in Fig. 4.4(d) to update $\mathcal{L}(j,i)$, where Δ_{thres} is the *update threshold* on the dB scale and is set to 3 dB for the simulations.
- If the value is less than the update threshold, the AP updates $\lambda_{i,m}^j$ as $\lambda_{i,m}^j \leftarrow \lambda_{i,m}^j + \Delta S_{i,\mathrm{srx}}$ without unicasting a TPC request.

In the second case, only $\Delta S_{i,\mathrm{srx}}$ is used for the link margin update because if S_i changes by $\Delta S_{i,\mathrm{srx}}$, $S_{\mathrm{AP}\to i}$ also changes by $\Delta S_{i,\mathrm{srx}}$ assuming channel reciprocity and no transmit power control at STA i. $\Delta S_{j,\mathrm{ptx}}$, on the other hand, cannot be utilized to estimate $I_{j\to i}$, since the channel between the AP and STA j and the channel between STA i and STA j are not always correlated.

4.3.4 Secondary Transmission

After populating the link map, the AP initiates secondary transmission based on the link map. Various scheduling and rate selection algorithms can be adopted for the secondary transmission depending on the purpose (e.g., maximizing throughput or achieving fairness.) In this work, we present a simple scheduling and rate selection algorithm for reliable secondary transmission while trying to achieve high throughput gain. Specifically, MASTaR schedules secondary transmission to a STA which is most

robust to the interference from the current PTX. For a given PTX j, the AP searches the link map to find the SRX whose link margin with respect to the PTX is the greatest, i.e.,

$$i^* = \underset{i \in \mathbb{I}, i \neq j}{\operatorname{argmax}} \lambda^j_{i,m_{\mathrm{ref}}}. \tag{4.3}$$

Used for the secondary transmission is the highest order of MCS satisfying $\lambda^j_{i^*,m} \geq 0$. The AP then aggregates multiple MAC protocol data units (MPDUs) destined to i^* so that the aggregated MPDU (A-MPDU) can be transmitted within the remaining duration of the primary transmission.

Next, the AP pads a dummy data frame before the first subframe in the A-MPDU, and sends, as shown in Fig 4.4(e), the A-MPDU with the padded dummy data. The dummy data frame contains random bit and out-of-order sequence number, so that the receiver drops the dummy data frame. Using the dummy data padding serves two purposes. First, it prevents UL transmission from a node that failed to sense the primary transmission, thus resolving hidden terminal problem. Second, it makes the secondary transmission end SIFS after the end time of the primary transmission so that the BA from the AP to PTX (i.e., BA for the primary transmission) is transmitted SIFS earlier than the BA from SRX to the AP (i.e., BA for the secondary transmission). This also enables clean SI channel estimation and first frame capture of the BA transmission for the primary transmission.

Finally, if PTX can receive the AP's BA (or legacy ACK) with the simultaneous SRX's BA transmission after PTX's data transmission, i.e., $\lambda^{i^*}_j \geq 0$ for the BA (or legacy ACK) data rate, the AP sets ACK policy of the A-MPDU to *Normal ACK*, so that, as shown in Fig. 4.4(e), there is a partial overlapping of the acknowledgement transmissions responding to primary and secondary transmissions. If $\lambda^{i^*}_j < 0$ for the BA (or legacy ACK) data rate, on the other hand, PTX may fail to decode the BA (or legacy ACK) from the AP due to the INI caused by the BA from SRX. To prevent the failure, the AP sets ACK policy of the A-MPDU to "Block ACK", indicating the explicit BA policy, to make the BAs be transmitted in a consecutive order as shown in

Fig. 4.4(f). If the BA from SRX fails despite the use of explicit BA, the AP reduces the link margin for the link by 3 dB to apply stricter criteria for the secondary transmission on the link.

It should be noted that, in MASTaR, STR happens when a STA wins the channel and starts UL transmission. If the AP wins the channel, on the other hand, STR is not possible. Therefore, if the AP uses a longer contention window (CW) than do the STAs, the probability that a STA wins the channel increases, thus potentially acquiring more STR opportunities. The effect of CW size of the AP is studied in Section 4.5.

4.4 Feasibility Study

In this section, adopting the PHY layer perspective, we verify the feasibility of STR in WLAN. As mentioned in prior studies, the feasibility of STR is directly related to the performance of SIC [13, 36–41]. Therefore, we introduce analog and digital SIC schemes which fit for WLAN, and evaluate the SIC performance in indoor environments.

4.4.1 Analog SIC and Channel Modeling

The primary purpose of analog SIC is to attenuate SI sufficiently and prevent the ADC from being saturated by SI. Researchers have developed several analog SIC designs including passive and active cancellation [13, 37–40]. As a solution for isolation, we employ the dual-polarized antenna introduced in [39, 40]. Since a dual-polarized antenna is a passive device, there is no power consumption or tuning process. Further cancellation can be achieved by active analog SIC using tunable circuits [38].

To evaluate the performance of digital SIC, we should model an SI channel including the effect of analog SIC. Therefore, we generate an SI channel model with the dual-polarized antenna. We use Wireless System Engineering (WiSE)—a 3D ray-tracing tool developed by Bell Labs [46]—to obtain non-line of sight (NLOS) SI chan-

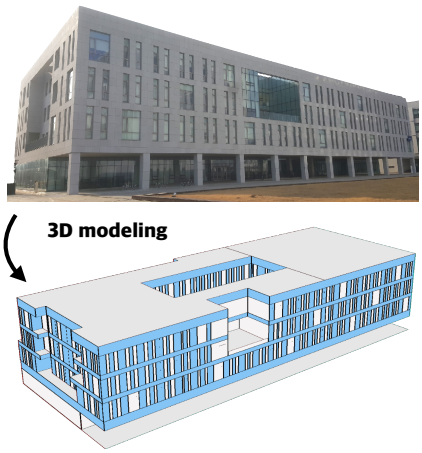

(a) 3D modeling of a four-story building (Veritas C of Yonsei University)

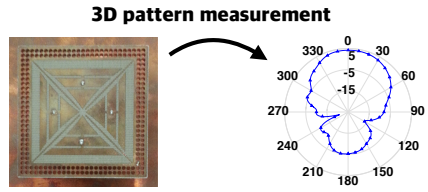

(b) Dual-polarized antenna and its radiation pattern [45]

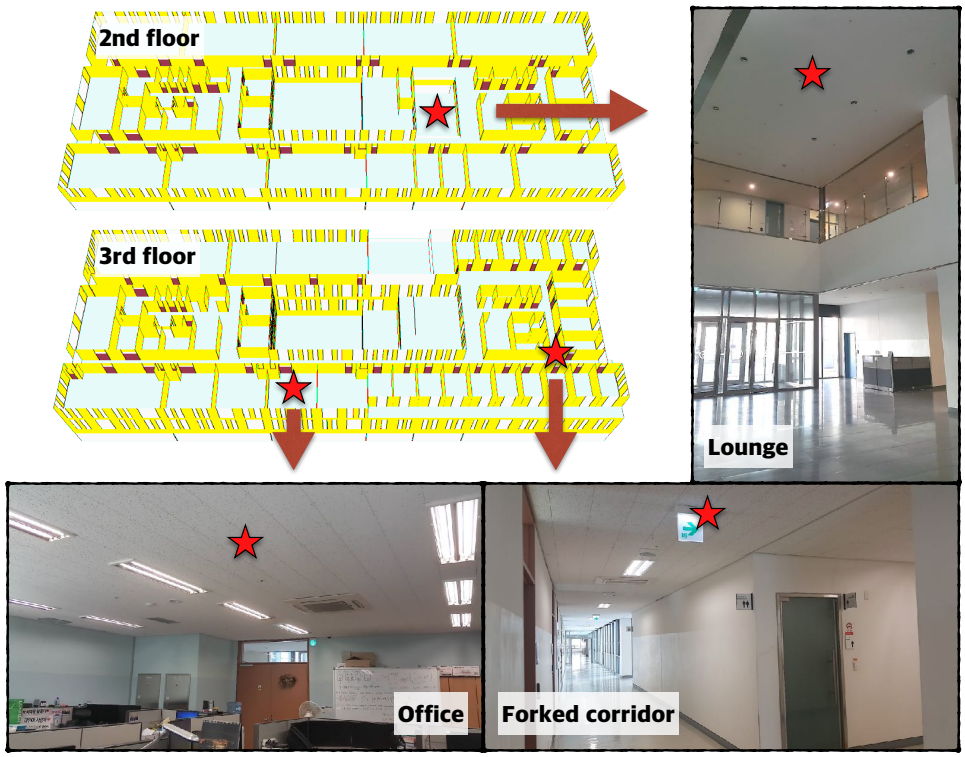

(c) Pictures of AP-deployed locations

Figure 4.5: The building modeling and the antenna for 3D ray-tracing

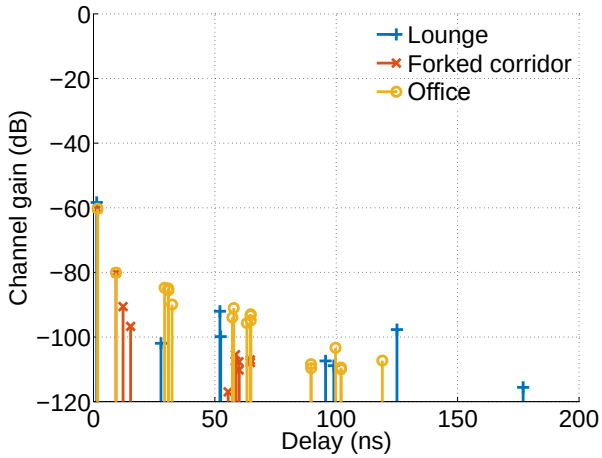

Figure 4.6: Power delay profile of each scenario.

nel taps, which represent the SI components returning after being reflected off of the wall, floor, and ceiling. Specifically, we have modeled a four-story building as shown in Figs. 4.5(a) and (c), and deploy an AP in three different scenarios: (i) Lounge, (ii) Forked-corridor, and (iii) Office. It should be noted that in the Lounge scenario, there is no ceiling between the first and the second floors in the lounge area, and the AP is mounted on the ceiling of the second floor. In the Forked-corridor and Office scenarios, the APs are mounted on the ceiling of the third floor. The APs are modeled with the measured radiation pattern of the dual-polarized antenna as shown in Fig. 4.5(b), and the center frequency is 5.2 GHz.

Fig. 4.6 shows the resulting power delay profiles (PDPs) for the three scenarios. The first tap of each scenario with a delay of 1.33 ns is the reflection from a ceiling, and its channel gain is around -60 dB. Since the dual-polarized antenna provides 43 dB SIC in an indoor environment [39, 40], we add a zero-delay tap with a channel gain of -43 dB to each PDP; this zero-delay tap represents the direct path leakage between two polarizations. Also, since most active analog SIC techniques target line of sight (LOS) path or leakage [38], active analog SIC can be modeled by attenuating the zero-delay tap, i.e., for analog SIC of 60 dB, the zero-delay tap has a channel gain

Table 4.1: Simulation parameters for feasibility studies.

Parameter	Value
FFT size	64
Number of data subcarriers	52
Sample period	50 ns
Max frame length	5.484 ms
Noise level	-94 dBm

of -60 dB instead of -43 dB. We take into account the channel mobility by applying Rayleigh fading model to each tap. Since the first two taps are the LOS component and the reflection from a ceiling,[7] respectively, the two taps are considered static.

4.4.2 Digital SIC for WLAN

Since the digital SIC performance is strongly related to the accuracy of SI channel estimation, the first step of digital SIC is determining what signal to use as a reference signal. Recalling that backward compatibility is one of the most important features of WLAN, it is impossible to modify PLCP framework. Thus, unlike LTE-based STR systems introduced in [39–41], the orthogonality of UL and DL reference signals cannot be guaranteed in WLAN systems. Also, employing a signal in the data part as the reference signal is not proper because the UL signal will behave as interference. As the reference signal for SI channel estimation, therefore, we employ the two-OFDM-symbol L-LTF signal as the reference signal for SI channel estimation. With the L-LTF signal, the SI channel is estimated by the per-subcarrier least square method.

To evaluate the SIC performance in WLAN systems, we have simulated a single-input single-output (SISO) OFDM system with the parameters in 20 MHz WLAN systems as listed in Table 4.1. Since the SI channel is estimated at PLCP preamble,

[7] Since the AP is mounted on the ceiling, we assume no mobility between the AP and the ceiling.

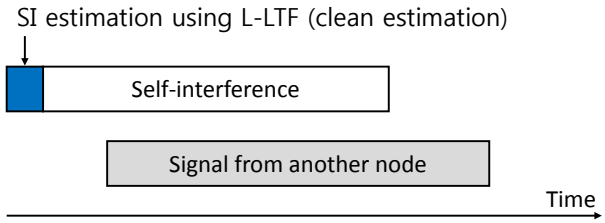

(a) SIC with clean estimation

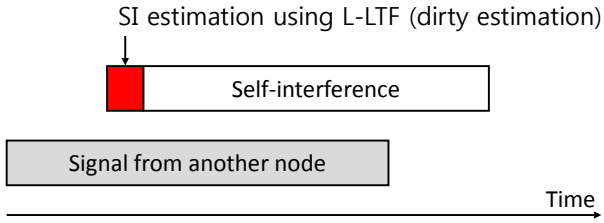

(b) SIC with dirty estimation

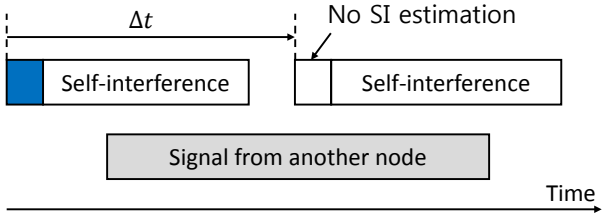

(c) SIC with clean estimation Δt before

Figure 4.7: Two cases of SI channel estimation and SIC utilizing previous clean estimation.

which is the beginning part of a frame, the SIC performance will degrade at the latter part of the frame. As a worst case, therefore, we assume a frame length of 5.484 ms, i.e., the maximum frame length in the 802.11ac WLAN, and evaluate the average SIC performance over one frame. We consider the following two cases of SI channel estimation.

- *Clean estimation*: SI channel estimation *without* the presence of signals from other nodes, i.e., interference, sharing the medium.
- *Dirty estimation*: SI channel estimation *with* the presence of interferences.

Fig. 4.7 shows the cases of clean and dirty estimation. In clean estimation, the SI channel can be accurately estimated, and hence high digital SIC performance can be achieved. In MASTaR, however, clean estimation is not always possible because, as shown in Fig. 4.4(a), AP needs to start transmission while receiving a signal.

Therefore, we first check how the digital SIC performance degrades as time goes by after clean estimation. We assume the AP performs clean estimation at a certain time, and after Δt, it transmits a new frame using the previously estimated SI channel instead of performing new SI estimation. Fig. 4.8(a) shows the average digital SIC performance during frame transmission, which is sent Δt after clean estimation, with different values of Doppler spread (f_D). We consider Δt of less than 100 ms, because AP can perform clean estimation at least once in 100 ms thanks to its beacon transmission; AP transmits a beacon every 100 ms. We also consider f_D of less than 6 GHz, since the value of Doppler spread in indoor environments is experimentally found to be *up to* 6 Hz at 5.25 GHz [47].

The solid lines in Fig. 4.8(a) show the results with analog SIC of 43 dB, i.e., with only passive SIC based on the dual-polarized antenna, and dashed lines show the results with analog SIC of 60 dB, i.e., with both passive and active SICs. It should be noted that there exists a trade-off relationship between the analog and digital SIC performances. When $\Delta t = 0$, the sums of the analog and digital SIC performances

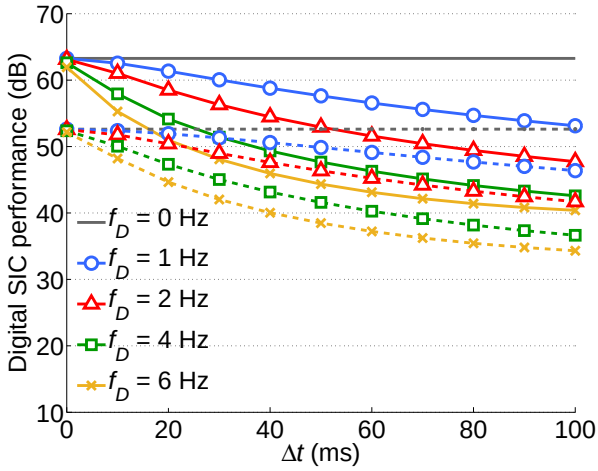

(a) SIC performance with clean estimation

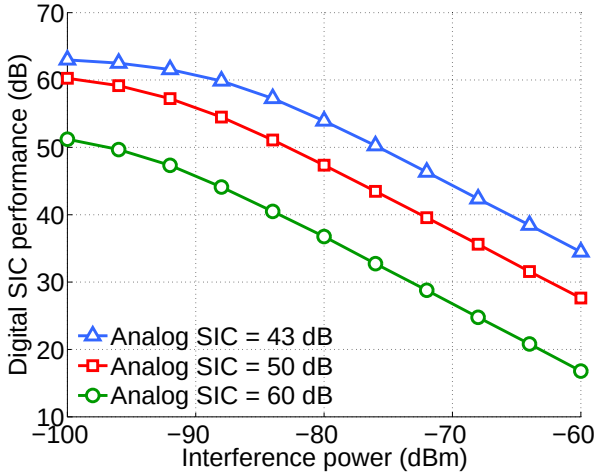

(b) SIC performance with dirty estimation

Figure 4.8: Ray-tracing based measured/simulated results.

with the analog SIC performances of 43 dB and 60 dB are about 106 dB and 113 dB, respectively. If the transmit power is 20 dB, the power of residual SI, i.e., SI after SIC, is then given by -86 dBm and -93 dBm, which are comparable to the noise floor, i.e., -94 dBm in 20 MHz band with noise figure of 7 dB [22]. As Δt increases, the digital SIC performance degrades, and the slope becomes steeper with a higher Doppler spread. In a static environment, however, the performance degradation is not significant. This result also agrees with the experiment result in [36], whose authors argued that the periodic estimation with a period of few hundred milliseconds provides good performance in static environments.[8]

Fig. 4.8(b) shows the results with dirty estimation. In this case, no matter what interferences exist, the AP performs SI estimation with L-LTF of each frame as a reference signal. As shown in Fig. 4.8(b), as the interference power increases, the digital SIC performance decreases. To identify PTX by reading MAC header in MASTaR, the UL signal power at AP should be greater than clear channel assess (CCA) threshold, which is -82 dBm in general. If the UL signal is encoded with high order MCSs, the signal power should be even greater for successful decoding. This UL signal acts as the interference during SI estimation, thus significantly damaging digital SIC. Compared with the result of clean estimation, this performance degradation of digital SIC caused by interference is much more significant. Therefore, we reuse the SI channel, estimated without the presence of interferences, when there exists a detectable interference, i.e., the interference with a power greater than the CCA threshold.

4.5 Performance Evaluation

The performance of MASTaR depends on the viability of secondary transmission. Therefore, the level of the interference between PTX and SRX is crucial for a reli-

[8]The coherence time of SI channel also depends on the tuning period active SIC. Since we do not assume a specific active SIC design in this work, the effect of tuning period is not studied. However, existing active SIC designs, e.g., [36, 38], use a tuning period of greater than 100 ms.

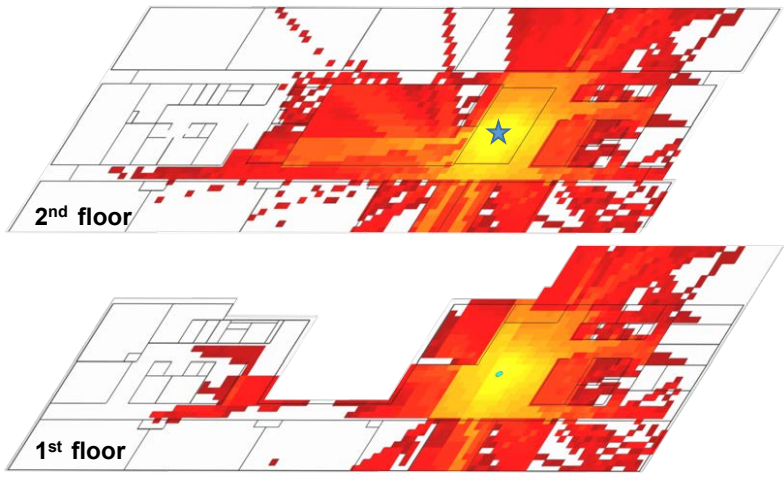

(a) Lounge scenario (1^{st} and 2^{nd} floors)

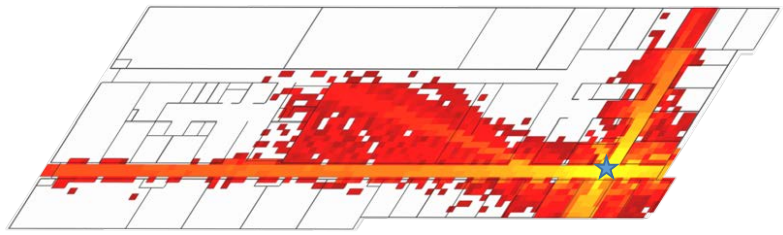

(b) Forked-corridor scenario (3^{rd} floor)

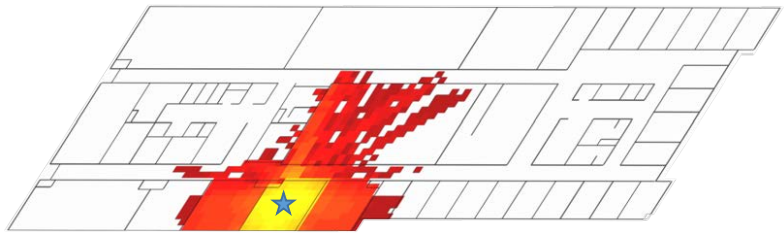

(c) Office scenario (3^{rd} floor)

Figure 4.9: 3D ray tracing results in three scenarios.

able performance evaluation. In this regard, we use the 3D ray-tracing tool again to calculate propagation loss in the three scenarios described in Section 4.4. Fig. 4.9 shows the result of the ray-tracing; the colored area represents the location in which a STA (with 0 dBi antenna gain) received a signal from the AP (located at the location marked with the star) greater than CCA threshold. In the colored area, the location with a greater signal power is colored more brightly than the location with a smaller signal power. It is shown that in the Lounge scenario (Fig. 4.9(a)), the signal propagates wider than other scenarios thanks to the spatial openness. In the Forked-corridor scenario (Fig. 4.9(b)), on the other hand, the building structure blocks signal propagation, thus spatially separating the shaded area. Meanwhile, the Office scenario (Fig. 4.9(b)) shows the most limited signal propagation because the AP is deployed in an enclosed room.

We implement the 3D ray-tracing result in ns-3 [29], and deploy STAs at random positions satisfying the condition that the signal power from the STAs to the AP is greater than the CCA threshold. For further reliable simulation results, we elaborately implement STR and second frame capture capabilities in the simulator. We also reflect the results in Section 4.4 to make the digital SIC performance fluctuate depending on Δt and interference power, for a given analog SIC performance which is 60 dB in the following simulation.

The common parameters in TGax simulation scenarios focusing on densely deployed WLANs [22] are applied. Also, we adopt Jakes' fading model, and use Minstrel rate adaptation algorithm [30] to adapt 802.11ac data rates with a single spatial stream and 20 MHz bandwidth, i.e., MCS 0–8.[9] With a 50-50 chance, each STA's antenna is modeled by one of two omnidirectional antennas with antenna gains of -2 dBi and -8 dBi. The former antenna follows the parameter in [22], and the latter one considers the hand-grip loss of mobile STAs as studied in [21]. The parameters not specified are summarized in Table 4.2.

[9]MCS 9 is not defined for 802.11ac in the 20 MHz channel.

Table 4.2: Simulation parameters for performance evaluation.

Parameter	Value
CW size	CWmin $= 15$, CWmax $= 1023$
A-MPDU bound	65535 bytes, 5.484 ms
Transmit power	20 dBm (AP), 15 dBm (STA)
CCA threshold	-82 dBm
Capture threshold	10 dB

We compare MASTaR with the following three protocols:

- HD: Current half duplex-based 802.11 MAC protocol.
- BusyTone: Transmitting busy tone during secondary transmission for hidden terminal resolution as proposed in [36].
- RTS/FCTS [18]: Three-way handshake before primary transmission using RTS and FCTS frames.
- A-Duplex [19]: Using SIR information to initiate the secondary transmission after an RTS frame ($\theta = 1/3$).

Since the original A-Duplex does not consider A-MPDU for its scheduling method and uses a fixed data rate, its performance is too low in our simulation environment which includes both A-MPDU and rate adaptation. For a fair comparison with MASTaR, thus, we apply the scheduling and rate selection algorithm which is adopted in MASTaR. Also, because RTS/FCTS and A-Duplex are based on STAs' RTS transmission, they are compared only in the RTS scenario. A more detailed description of them is presented in Section 1.2. It should be noted that we thoroughly implement the comparison protocols and MASTaR in ns-3, and hence the overhead in each protocol is reflected in the simulation results.

4.5.1 Simulation with UDP Data Traffic

We first generate UDP data traffic and measured throughput for 1 second by changing the following parameters:

- Doppler spread (f_D)
- Number of STAs (N)
- Ratio of DL traffic source rate to total traffic source rate (r_{DL})
- Total fixed SIC performance (*SIC*)
- AP's minimum CW size ($CWmin_{\mathrm{AP}}$).

Except for the simulation with various DL traffic ratios, each STA has both DL/UL fully-backlogged UDP traffic with 1460-byte payload MPDU. We carry out simulations for the following two cases: (i) *no-RTS case*, where STAs do not use RTS and (ii) *RTS case*, where STAs use RTS before A-MPDU transmission. All results are averaged out over 100 random topologies.

Results Depending on the Number of STAs (Figs. 4.10–4.12)

Figs. 4.10– 4.12 shows the performances with different values of N in all three scenarios. The lower and upper bars represent the average UL throughput and DL throughput. The dots represent the average Jain's fairness index among all links in a topology, and the numbers above bars show the throughput gain of MASTaR over HD. We first focus on the comparison of the protocols for the no-RTS case in the Lounge scenario, and then later address the effect of RTS and the characteristic of each scenario.

In the no-RTS case, as shown in Fig. 4.10(a), the throughput of HD rapidly decreases as N increases because of more collisions of UL frames. Since the rate adaptation algorithm works, accordingly, STAs are more likely to use a robust data rate,

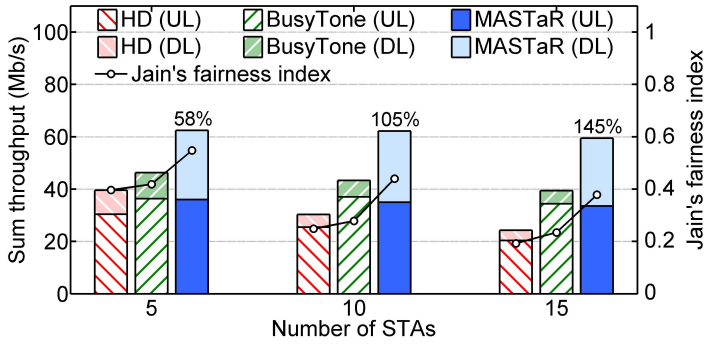

(a) no-RTS case

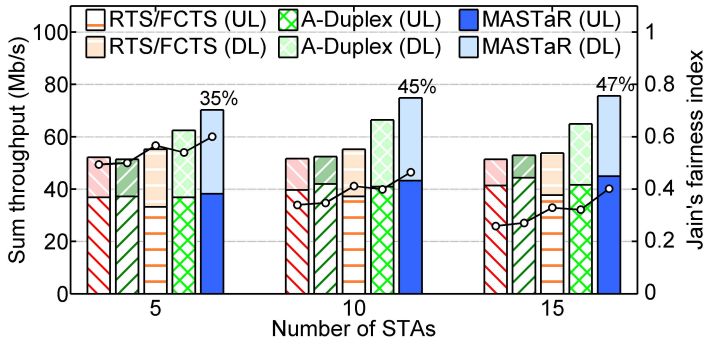

(b) RTS case

Figure 4.10: Performance depending on N in Lounge scenario: $f_D = 2$ Hz, $r_{\mathrm{DL}} = 0.5$, and $CWmin_{\mathrm{AP}} = 15$.

i.e., a low order MCS, thus longer occupying the medium during each transmission attempt. This affects DL transmission, which shares the medium with UL transmission, and results in very low DL throughput. Figs. 4.14(a) and (c) show how many UL and DL packets are transmitted with each MCS in the Lounge scenario with 10 STAs. The lower and upper bars represent the average numbers of packet successes and packet errors, respectively. It is shown that a considerable number of UL packet transmission fail due to collisions,[10] and much fewer packets are transmitted in DL.

[10]If the transmission failures are due to channel errors, the error ratio should be smaller with lower order MCSs. However, it is shown that the error ratio is even greater with lower order MCSs, especially with MCS 0. This shows that the main cause of the UL transmission failures is collisions.

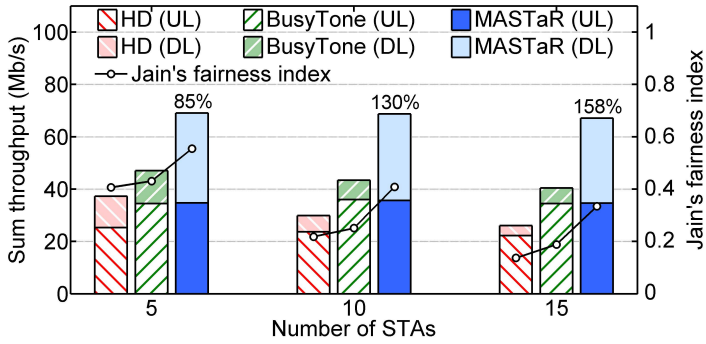

(a) no-RTS case

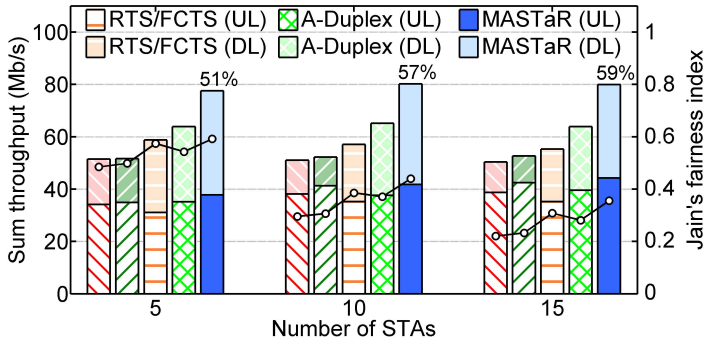

(b) RTS case

Figure 4.11: Performance depending on N in Forked-corridor scenario : $f_D = 2$ Hz, $r_{\mathrm{DL}} = 0.5$, and $CWmin_{\mathrm{AP}} = 15$.

BusyTone improves the throughput by resolving hidden terminals, but it does not prevent, as shown in Fig. 4.14(a), all collisions caused by hidden terminals. This is because the AP cannot transmit a busy tone before identifying PTX. In addition, some UL transmissions to the AP using BusyTone fail owing to the residual SI, i.e., SI after SIC.

On the other hand, in spite of the residual SI, MASTaR achieves a much higher sum throughput thanks to the DL secondary transmission. Fig. 4.14(c) illustrates that many more DL packets are transmitted using MASTaR. MASTaR also improves UL throughput by preventing collisions as BusyTone. In the other results shown below, MASTaR achieves, for the same reason, much higher throughput than the other protocols.

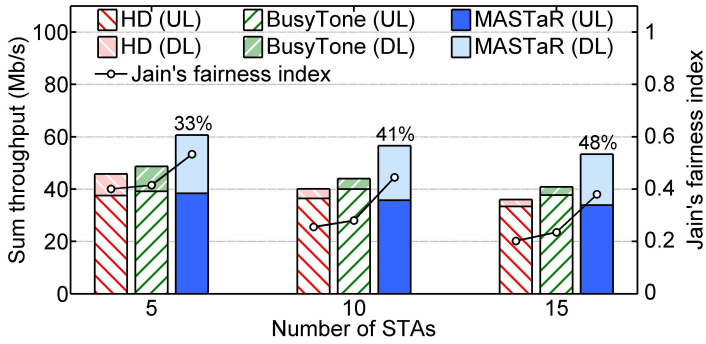

(a) no-RTS case

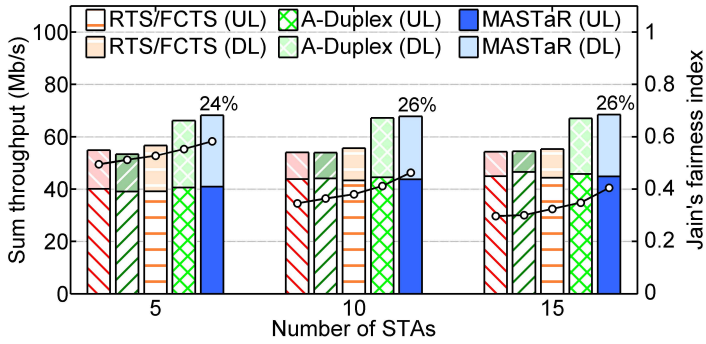

(b) RTS case

Figure 4.12: Performance depending on N in Office scenario: $f_D = 2$ Hz, $r_{\mathrm{DL}} = 0.5$, and $CWmin_{\mathrm{AP}} = 15$.

Meanwhile, MASTaR's throughput gain increases as N increases for two reasons: First, more collisions occur with larger N; the effect of hidden terminal resolution becomes significant. Second, better scheduling for secondary transmission is possible as the number of candidate SRXs increases. It should also be noted that MASTaR improves not only the sum throughput but also the fairness among the links. This is because MASTaR resolves the severe imbalance between UL and DL links, as described more specifically with the result depending on the DL traffic ratio (Fig. 4.15).

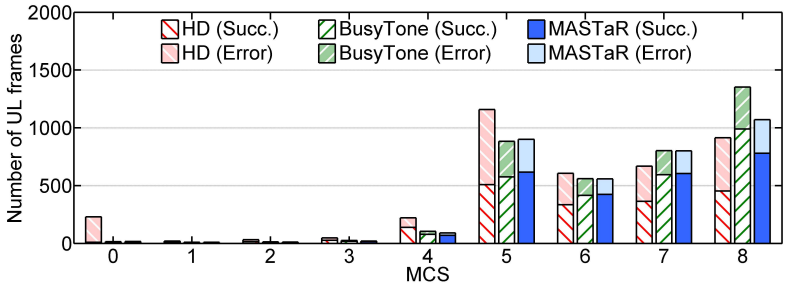

(a) UL data packet statistics (no-RTS case)

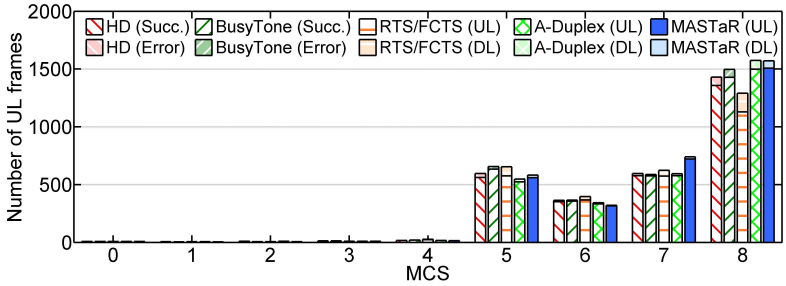

(b) UL data packet statistics (RTS case)

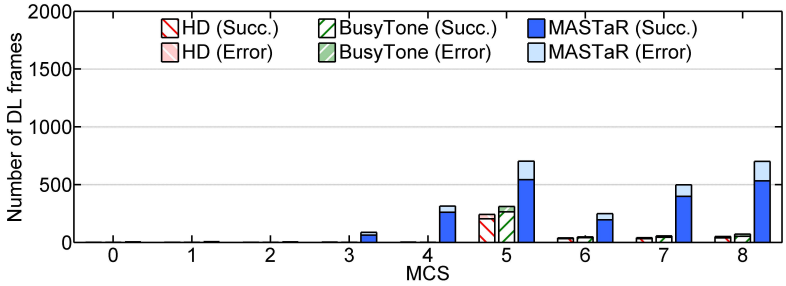

(c) DL data packet statistics (no-RTS case)

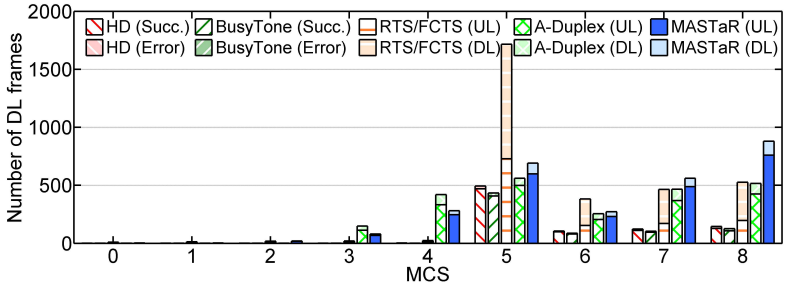

(d) DL data packet statistics (RTS case)

Figure 4.13: Packet success and error statistics depending on MCS in Lounge scenario: $f_D = 2$ Hz, $N = 10$, $r_{\mathrm{DL}} = 0.5$, and $CWmin_{\mathrm{AP}} = 15$.

Effect of RTS (Fig. 4.10–4.12)

Using RTS, the overall throughput increases and becomes less dependent on N since hidden terminals are resolved by CTS, as shown in Figs. 4.10(b) and 4.14(b). Meanwhile, RTS/FCTS enhances DL throughput by simultaneous transmission after exchanging one RTS frame and two consecutive FCTS frames. Since RTS/FCTS does not consider the INI between PTX and SRX, however, secondary transmission fails frequently due to the strong INI as shown in Fig. 4.14(d). Also, since the two ACK transmissions after the primary and secondary transmissions entirely overlap with each other, AP cannot estimate SI channel in a clean wireless medium. This makes much stronger SI remain uncancelled, thus causing ACK reception failures at the AP. Owing to the failures caused by both strong INI and residual SI, as well as the additional overhead of three-way handshaking for every UL transmission, RTS/FCTS achieves marginal performance gain over HD.

In A-Duplex, STAs report the SIR information of the previous transmission to the AP using a modified RTS frame, and the AP uses the SIR information to arrange the secondary transmission considering INI. Also, two ACK frames are always transmitted consecutively, and hence A-Duplex shows better throughput than RTS/FCTS. However, since each STA can report only the SIR measured during the previous transmission at its UL transmission opportunity, it takes long to collect the SIR information of the possible pairs of PTX and SRX. This leads to less optimal scheduling, thus making the performance of A-Duplex lower than MASTaR's.

The reasons why the throughput gain of MASTaR is higher in the no-RTS case than in the RTS case are twofold: First, the considerable gain of MASTaR in the no-RTS case comes from resolving hidden terminals, which is already achieved by using RTS and CTS in the RTS case. Second, due to the overhead of RTS and CTS, the channel occupancy time of UL *data* transmission decreases, and thus fewer secondary transmissions are carried out.

Results in Different Scenarios (Fig. 4.10–4.12)

When comparing Figs. 4.10(a), 4.11(a), and 4.12(a), or comparing Figs. 4.10(b), 4.11(b), and 4.12(b), we can see that the throughput gains of the STR protocols depend on the location of the AP, i.e., lounge, forked corridor, or office. The Lounge and Forked-corridor scenarios show a similar trend; the throughput gain of MASTaR increases rapidly as N increases and MASTaR achieves approximately double the throughput than HD when $N = 10$.

In the Office scenario, on the other hand, the throughput gain less depends on N, because fewer hidden terminals exist in this scenario; the STAs are distributed in a relatively small area around the APs' location. The dense deployment of STAs also aggravates INI, and hence, lower MCSs are used for secondary transmissions and fewer secondary transmissions occur. It should be noted that, however, the cubicles and office equipment, which are not modeled in the 3D ray-tracing, can reduce INI, while they have little influence on the signal propagation between STAs and the AP mounted on the ceiling. Thus, higher throughput gain is expected in a real office environment with office equipment and APs on the ceiling.

This result shows that the performance enhancement achieved by an STR-capable AP is expected to be more significant in the environments where the AP serves many STAs distributed in a wide area. In the following simulations, we present the graphs only for the Lounge scenario, which show the intermediate throughput gain.

Results Depending on the DL Traffic Ratio (Fig. 4.15)

Fig. 4.15 shows each protocol's performance depending on the DL traffic ratio. In this case, the source rate is 10 Mb/s per STA, and the number of STAs is ten. Therefore, the total source rate is fixed at 100 Mb/s and each link's source rate is given by the product of the traffic ratio and the total source rate, e.g., 20 Mb/s and 80 Mb/s for DL and UL, respectively when DL traffic ratio is 20%.

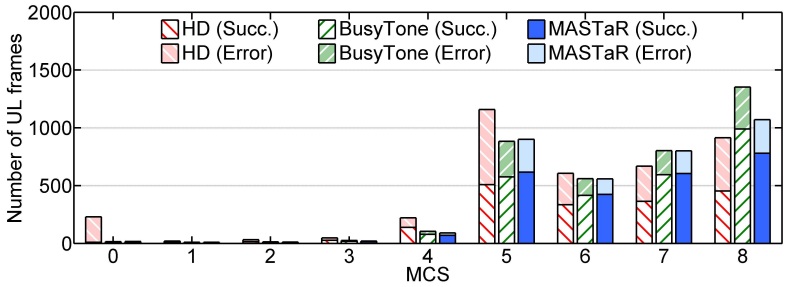

(a) UL data packet statistics (no-RTS case)

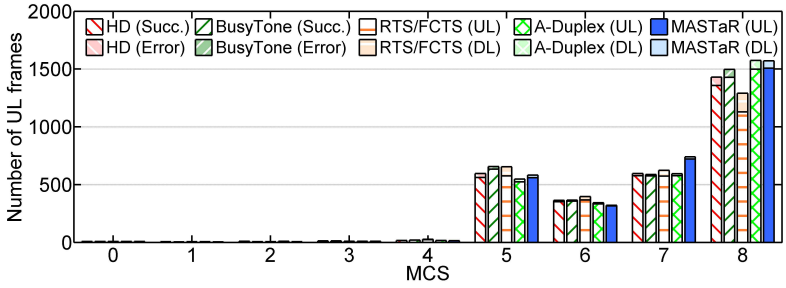

(b) UL data packet statistics (RTS case)

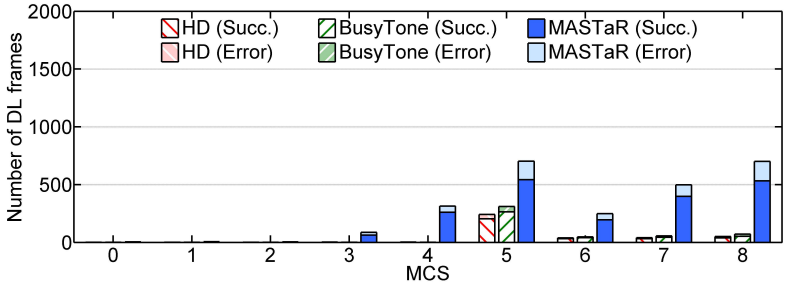

(c) DL data packet statistics (no-RTS case)

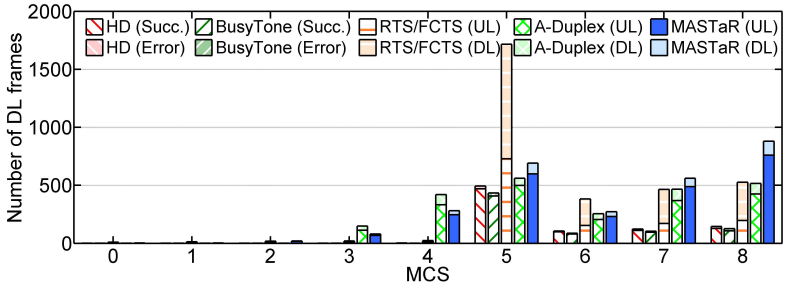

(d) DL data packet statistics (RTS case)

Figure 4.14: Packet success and error statistics depending on MCS in Lounge scenario: $f_D = 2$ Hz, $N = 10$, $r_{\mathrm{DL}} = 0.5$, and $CWmin_{\mathrm{AP}} = 15$.

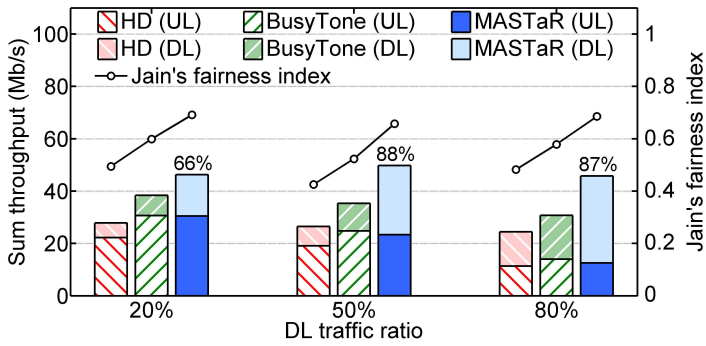

(a) no-RTS case

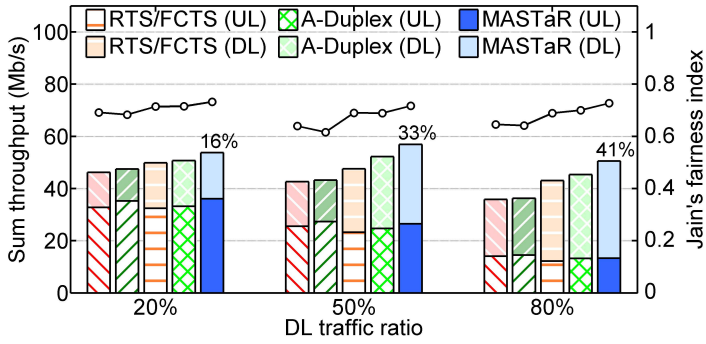

(b) RTS case

Figure 4.15: Performance depending on r_{DL} in Lounge scenario: $f_D = 2$ Hz, $N = 10$, and $CWmin_{\mathrm{AP}} = 15$.

For HD and BusyTone, as shown in both Figs. 4.15(a) and (b), the ratio of the achieved DL throughput to the total throughput is much smaller than the ratio of DL source rate to the total source rate, except for when the DL traffic ratio is 20%. This *starvation in DL* is because the AP cannot win the channel as often as it needs to when multiple STAs with UL traffic coexist. On the other hand, MASTaR delivers more DL traffic successfully thanks to the secondary transmission during the UL channel access. The portion of MASTaR's DL throughput, therefore, increases proportionally with the given DL traffic ratio. It is also worth mentioning that the throughput gain of MASTaRover HD stands out when DL traffic ratio is equal to or greater than 50%, that is, when DL traffic is more congested than UL traffic.

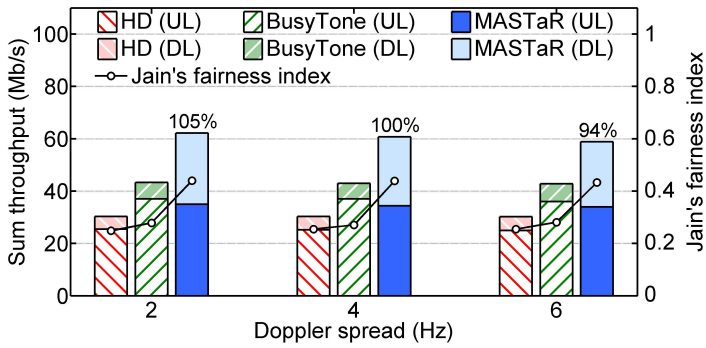

(a) no-RTS case

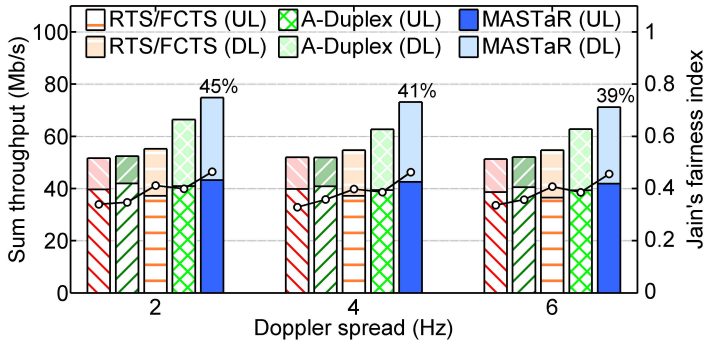

(b) RTS case

Figure 4.16: Performance depending on f_D in Lounge scenario: $N = 10$, $r_{\mathrm{DL}} = 0.5$, and $CWmin_{\mathrm{AP}} = 15$.

Results Depending on Doppler Spread (Fig. 4.16)

The effect of f_D on each protocol's performance is shown in Fig. 4.16. High f_D is harmful to MASTaR in two aspects. First, digital SIC performance becomes poor due to the short coherence time of the SI channel. Second, many TPC request transmissions for updating link map are required due to the short coherence time of the channel between nodes. Thus, it is shown in Fig. 4.16 that the throughput gain of MASTaR decreases as f_D increases. However, with $f_D = 6$ Hz, corresponding to high mobility in indoor environments, MASTaR still achieves significant throughput gain compared with other protocols.

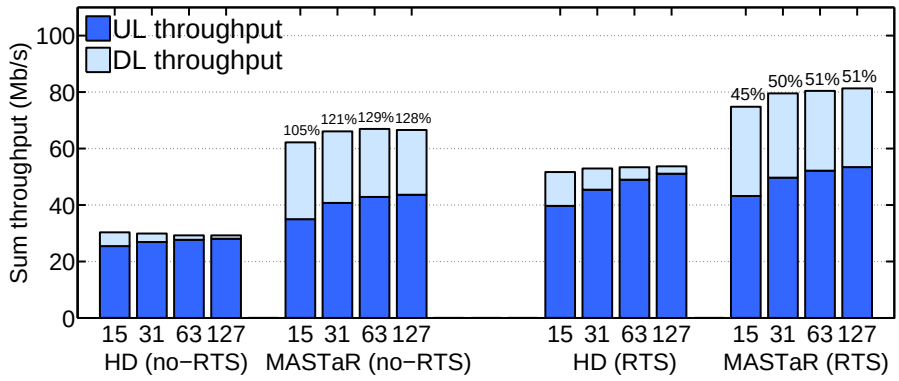

Figure 4.17: Performance depending on *CWmin*$_{\mathrm{AP}}$ in Lounge scenario: $f_D = 2$ Hz, $N = 10$, and $r_{\mathrm{DL}} = 0.5$.

Results Depending on the AP's CW Size (Fig. 4.17)

Fig. 4.17 shows the throughput of HD and MASTaR with different values of AP's minimum CW size (*CWmin*$_{\mathrm{AP}}$), where the numbers in the x-axis, i.e., 15, 31, 63, 127, represent *CWmin*$_{\mathrm{AP}}$. With a greater *CWmin*$_{\mathrm{AP}}$, the probability that the AP wins the channel becomes even lower, and the lower probability results in severer DL starvation in HD. In MASTaR, on the other hand, the AP can deliver DL traffic via secondary transmission simultaneously with UL transmission. Thus, the total throughput further increases and no DL starvation happens with a greater *CWmin*$_{\mathrm{AP}}$. When the channel is heavily occupied by STAs, therefore, AP can adjust its CW size depending on the viability of secondary transmission. For example, if heavy UL traffic exists and the average link margin in the link map is high, then larger CW size can be used.

Results with Fixed SIC Performance (Fig. 4.18)

In the previous simulations, we assume that analog SIC performance is fixed to 60 dB and digital SIC performance changes depending on Δt and interference power. In Fig. 4.18, we make the performance of digital SIC also fixed to certain values, i.e., $20, 30, 40, 50, 60$ dB. Then the total SIC performance (*SIC*) corresponds to 80, 90,

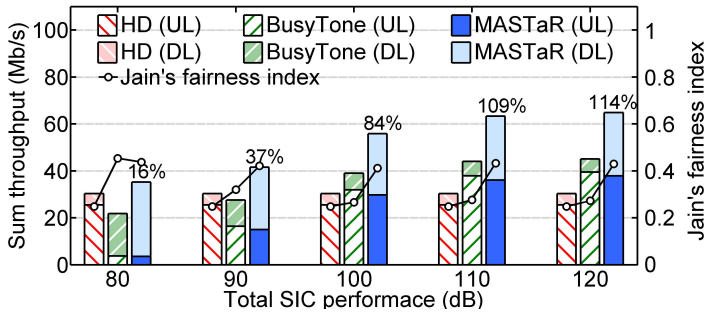

Figure 4.18: Performance depending on *SIC* in Lounge scenario (no-RTS case): $f_D = 2$ Hz, $N = 10$, $r_{\mathrm{DL}} = 0.5$, and $CWmin_{\mathrm{AP}} = 15$.

100, 110, 120 dB, respectively.

With low *SIC*, primary UL transmission fails due to the strong residual SI. When $SIC = 80$ dB, for instance, the residual SI power is about -60 dBm, which is comparable to the received power of the intended signals. The failures cause retransmissions and make the rate adaptation algorithm choose more robust MCS for UL transmission. Therefore, the UL throughput of BusyTone and MASTaR is worse than that of HD if *SIC* is low. As SIC performance increases, the UL throughput of the STR protocols increases, and becomes greater than the UL throughput of HD if $SIC \geq 100$ dB. Meanwhile, the DL throughput of MASTaR depends less on the SIC performance. The results demonstrate that if an *SIC* of approximately 100 dB or higher is possible, significant performance enhancement for both UL and DL is possible in WLANs with MASTaR.

Result in Two-BSS topology (Fig. 4.5.1)

In multi-BSS scenarios, however, the performance gain of STR protocols may be decreased due to the CCI among the BSSs. To check the performance of STR protocols via ns-3 simulation, we deploy two BSSs each with a single AP and 10 client STAs as shown in Fig. 4.19. The distance between two APs is d_{AP} and the STAs are randomly distributed within 10 m from its associated AP. All the other parameters are identical

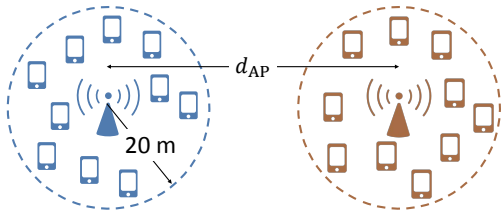

Figure 4.19: Two-BSS topology.

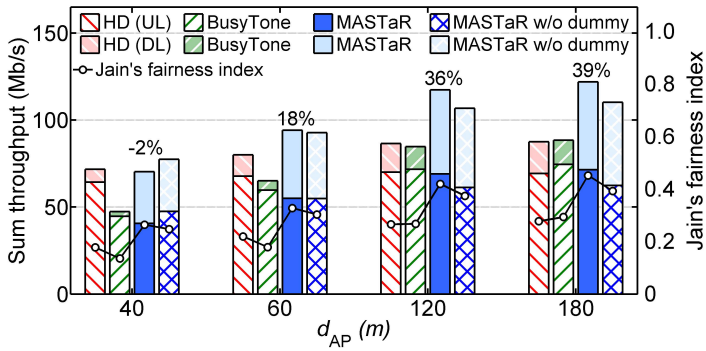

Figure 4.20: Performance depending on d_{AP}(no-RTS case): $f_D = 2$ Hz, $r_{\mathrm{DL}} = 0.5$, and $CWmin_{\mathrm{AP}} = 15$.

to the parameters in the previous simulations.

Fig. shows the performances with different values of d_{AP}, where the lower and upper bars represent the average UL throughput and DL throughput, respectively. When d_{AP} is small, it is shown that the STR protocols, i.e., BusyTone and MASTaR, yield even lower throughput than HD. This is because the secondary transmission in a BSS causes a strong CCI to the other BSS, thus either limiting transmission attempts or deteriorating SINR in the other BSS. The harmful effect of secondary transmission is reflected in the data packet statistics in Fig. 4.21. Unlike the previous statistics in Fig. 4.14, it is shown that less UL transmission attempts happen with STR protocols. Also, the UL packet error rate reduction of STR protocols thanks to hidden terminal resolution is no more observed. When the performance loss is the most, i.e., $d_{\mathrm{AP}} = 40$ m, we can slightly enhance the throughput of MASTaR by disabling dummy data frame padding. As d_{AP} increases, however, the performance gain of MAS-

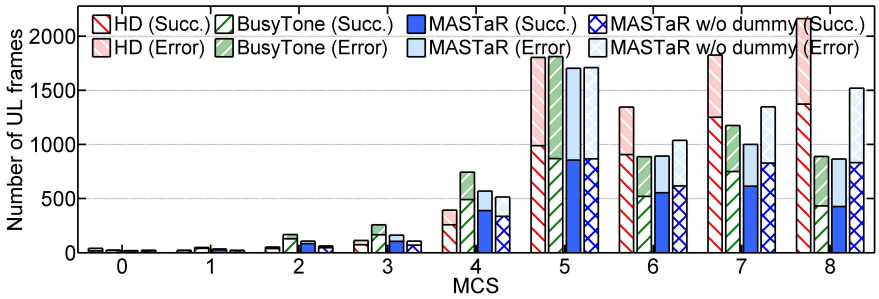

(a) UL data packet statistics (no-RTS case)

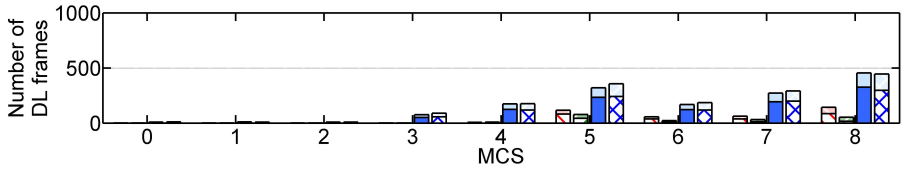

(b) DL data packet statistics (no-RTS case)

Figure 4.21: Packet success and error statistics depending on MCS in two-BSS topology: $f_D = 2$ Hz, $r_{\mathrm{DL}} = 0.5$, and $CWmin_{\mathrm{AP}} = 15$.

TaR grows and disabling dummy data frame padding yields no advantage. This result demonstrates the need for a joint power control, rate selection, and carrier sensing, which is our future work.

4.5.2 Simulation with Voice and Data Traffic

Next, we randomly distribute 20 STAs in each scenario, and give UDP traffic with a source rate of 1 Mb/s to all STAs. We also generate voice traffic using G.711 codec without silence compression, and change the number of the voice over internet protocol (VoIP) clients. The G.711 codec generates constant bit rate (CBR) traffic with 208-byte payload and inter-packet interval of 20 ms. Frame aggregation is not used for voice packet transmission, and RTS is also not utilized for voice packet because of the small packet size. As a performance metric of VoIP, we measure *R-score* [48]. For a given number of VoIP clients, we create 100 random topologies, and the number of VoIP clients ranges one to five. Accordingly, 500 random topologies are created in

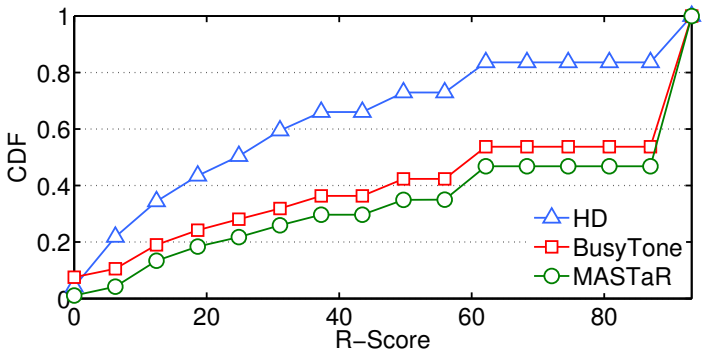

(a) CDF of R-score for voice traffic

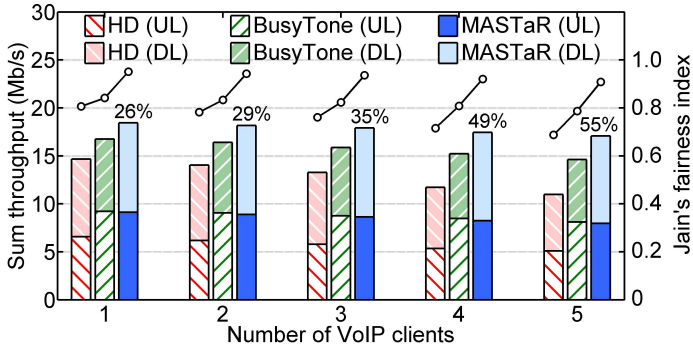

(b) Throughput for data traffic

Figure 4.22: Voice and data performance in Lounge scenario: $f_D = 2$ Hz, $r_{\mathrm{DL}} = 0.5$, and $CWmin_{\mathrm{AP}} = 15$.

total.

Fig. 4.22(a) shows the cumulative distribution function (CDF) of voice clients' R-score in the 500 topologies in Lounge scenario, where a STA's R-score is given by the minimum of R-scores for DL and UL. It is shown that MASTaR significantly enhances R-score by the reasons explained in the previous subsection, i.e., by resolving hidden terminals and DL starvation. Fig. 4.22(b), which shows the throughput for data traffic depending on the number of VoIP clients, demonstrates that the performance enhancement for voice traffic is achieved without sacrifice of data traffic since the throughput is also improved with MASTaR.

4.6 Summary

We have introduced MASTaR, a novel MAC protocol for STR in IEEE 802.11 WLAN. Since MASTaR was designed based on the existing functions of the current standards, it is standard-compliant in terms of STA's operation. The feasibility of MASTaR from the PHY layer perspective has been extensively evaluated using a 3D ray-tracing based simulator and the measurement data from a real-time full-duplex radio prototype. Also, the evaluation results based on 3D ray-tracing and ns-3 simulation under the various conditions. confirmed that the proposed protocol was able to achieve up to $2.58\times$ higher throughput than the current 802.11 MAC protocol. The results underscored the notion that a noteworthy performance enhancement will be achieved in WLAN with STR-capable APs.

Chapter 5

Concluding Remarks

5.1 Research Contributions

In this dissertation, we have addressed various strategies to enrich simultaneous transmission in WLAN.

In Chapter 2, we have presented QACK, a novel power control algorithm for IEEE 802.11 MAC ACK frames. We have also introduced link margin estimation based on AFER statistics. Our implementation and simulation confirm the feasibility and the performance of QACK and QCTS in diverse environments.

In Chapter 3, we have proposed a standard-compliant CST adaptation method considering both interferer and destination for better spatial reuse. We also proposed a CCA scheme for CST adaptations to reduce time overhead in backoff. Simulation results demonstrate that the proposed schemes considerably enhance network throughput by conditionally promoting simultaneous transmissions among OBSSs.

In Chapter 4, We have introduced MASTaR, a novel MAC protocol for STR in IEEE 802.11 WLAN. The feasibility of MASTaR from the PHY layer perspective has been extensively evaluated using a 3D ray-tracing based simulator and the measurement data from a real-time full-duplex radio prototype. Also, the evaluation results based on 3D ray-tracing and ns-3 simulation under the various conditions. confirmed

that the proposed protocol was able to achieve up to $2.58\times$ higher throughput than the current 802.11 MAC protocol.

5.2 Future Work

Based on the results of this dissertation, there are several new research directions which require further investigation. We highlight some of them as follows.

First, regarding ACK power control, out future work will include the performance evaluation of QACK and QCTS considering frame aggregation, which is anticipated to reduce the performance gain of them.

Second, regarding the CST adaptation, we will extend our work to be compatible with the newly defined function in IEEE 802.11ax, of which standardization process is in the final stage.

Lastly, regarding STR MAC protocol, Our future work will consider transmit power control and adaptive carrier sensing considering multi-cell environments. We also plan to carry out trace-based simulation using the SIC trace obtained from full duplex testbed.

Bibliography

[1] "Cisco visual networking index: Global mobile data traffic forecast update, 2015-2020," Feb. 2016. [Online]. Available: http://www.cisco.com/go/vni

[2] K. Ramachandra *et al.*, "Symphony: Synchronous two-phase rate and power control in 802.11 WLANs," in *Proc. ACM MobiSys*, 2008.

[3] T.-S. Kim, H. Lim, and J. C. Hou, " Improving spatial reuse through tuning transmit power, carrier sense threshold, and data rate in multihop wireless networks," in *Proc. ACM MobiCom*, 2006.

[4] V. P. Mhatre, K. Papagiannaki, and F. Baccelli, "Interference mitigation through power control in high density 802.11 WLANs," in *Proc. IEEE INFOCOM*, 2007.

[5] V. Shrivastava *et al.*, "CENTAUR: Realizing the full potential of centralized WLANs through a hybrid data path," in *Proc. ACM MobiCom*, 2009.

[6] W. Wang *et al.*, "Uncovering a hidden wireless menace: Interference from 802.11x MAC Acknowledgment frames," in *Proc. IEEE SECON*, 2014.

[7] J. Z. *et al.*, "Leveraging spatial reuse in 802.11 mesh networks with enhanced physical carrier sensing," in *Proc. IEEE ICC*, 2004.

[8] L. Fu, S. C. Liew, and J. Huang, "Effective carrier sensing in CSMA networks under cumulative interference," *IEEE Trans. Mobile Comput.*, vol. 12, no. 4, pp. 748–760, Apr. 2013.

[9] J. Z. *et al.*, "Adaptive CSMA for scalable network capacity in high-density WLAN: A hardware prototyping approach," in *Proc. IEEE INFOCOM*, Barcelona, Spain, 2006.

[10] P. Kulkarni and F. Cao, "Taming the densification challenge in next generation wireless LANs: An investigation into the use of dynamic sensitivity control," in *Proc. IEEE WiMob*, Oct. 2015.

[11] D. Kim, H. Lee, and D. Hong, "A survey of in-band full-duplex transmission: From the perspective of PHY and MAC layers," *IEEE Comm. Surveys Tut.*, vol. 17, no. 4, pp. 2017–2046, 2015.

[12] J. Kim, O. Mashayekhi, H. Qu, M. Kazandjieva, and P. Levis, "Janus: A novel MAC protocol for full duplex radio," Stanford University, Tech. Rep., 2013.

[13] M. Duarte, A. Sabharwal, V. Aggarwal, R. Jana, K. K. Ramakrishnan, C. W. Rice, and N. K. Shankaranarayanan, "Design and characterization of a full-duplex multiantenna system for WiFi networks," *IEEE Trans. Veh. Technol.*, vol. 63, no. 3, pp. 1160–1170, Mar. 2014.

[14] X. Xie, and X. Zhang, "Concise paper: Semi-synchronous channel access for full duplex wireless networks," in *Proc. IEEE ICNP*, Oct. 2014.

[15] A. Sahai, G. Patel, and A. Sabharwal, "Pushing the limits of full-duplex: Design and real-time implementation," 2011, arXiv preprint. [Online]. Available: https://arxiv.org/abs/1107.0607.

[16] S. Goyal, P. Liu, O. Gurbuz, E. Erkip, and S. Panwar, "A distributed MAC protocol for full duplex radio," in *Proc. Asilomar*, Nov. 2013.

[17] W. Zhou, K. Srinivasan, and P. Sinha, "RCTC: Rapid concurrent transmission coordination in full DuplexWireless networks," in *Proc. IEEE ICNP*, Oct. 2013.

[18] X. Zhang, W. Cheng, and H. Zhang, "Full-duplex transmission in PHY and MAC layers for 5G mobile wireless networks," *IEEE Wireless Commun. Mag.*, vol. 22, no. 5, pp. 112–121, 2015.

[19] A. Tang, and X. Wang, "A-Duplex: Medium access control for efficient coexistence between full duplex and half duplex communications," *IEEE Trans. Wireless Commun.*, vol. 14, no. 10, pp. 5871–5885, 2015.

[20] M. O. Al-Kadri, A. Aijaz, and A. Nallanathan, "An energy-efficient full-duplex MAC protocol for distributed wireless networks," *IEEE Wireless Commun. Lett.*, vol. 5, no. 1, pp. 44–47, 2016.

[21] S. Yoo, Y. Shin, S. Kim, and S. Choi, "Toward realistic WiFi simulation with smartphone "Physics"," in *Proc. IEEE WoWMoM*, June 2014.

[22] IEEE P802.11, *TGax Simulation Scenarios*, July 2015.

[23] D. Qiao, S. Choi, and K. G. Shin, "Goodput analysis and link adaptation for IEEE 802.11a wireless LANs," *IEEE Trans. Mobile Comput.*, vol. 1, no. 4, pp. 278–292, Oct. 2002.

[24] H. A. Mahmoud and H. Arslan, "Error vector magnitude to SNR conversion for nondata-aided receivers," *IEEE Trans. Wireless Commun.*, vol. 8, no. 5, pp. 2694–2704, 2009.

[25] O. Lee *et al.*, "SIRA: SNR-aware intra-frame rate adaptation," *IEEE Commun. Lett.*, vol. 19, no. 1, pp. 90–93, 2015.

[26] T. M. Schmidl and D. C. Cox, "Robust frequency and timing synchronization for OFDM," *IEEE Trans. Commun.*, vol. 45, no. 12, pp. 1613–1621, 1997.

[27] IEEE 802.11-2012, *Part 11: Wireless LAN Medium Access Control (MAC) and Physical Layer (PHY) specifications*, IEEE std., Mar. 2012.

[28] "LabVIEW Communications 802.11 application framework white paper," National Instruments, Technical Report, 2015.

[29] The network simulator ns-3. [Online]. Available: http://www.nsnam.org/.

[30] MadWiFi, Minstrel rate control. [Online]. Available: http://madwifi-project.org/browser/madwifi/trunk/ath_rate/minstrel.

[31] V. B. *et al.*, "MACAW: A media access protocol for wireless LAN's," in *Proc. ACM SIGCOMM*, 1994.

[32] IEEE 802.11h-2003, *Part 11: Wireless LAN Medium Access Control (MAC) and Physical Layer (PHY) specifications. Amendment 5: Spectrum and Transmit Power Management Extensions in the 5 GHz band in Europe*, IEEE std., Oct. 2003.

[33] Status of IEEE TG 802.11ah. [Online]. Available: http://www.ieee802.org/11/Reports/tgah_update.htm.

[34] J. Lee, W. Kim, S.-J. Lee, D. Jo, J. Ryu, T. Kwon, and Y. Choi, "An experimental study on the capture effect in 802.11a networks," in *Proc. ACM WiNTECH*, Montreal, Canada, Sep. 2007.

[35] K. Srinivasan *et al.*, "The κ factor: Inferring protocol performance using inter-link reception correlation," in *Proc. ACM MobiCom*, 2010.

[36] M. Jain, J. I. Choi, T. M. Kim, D. Bharadia, S. Seth, K. Srinivasan, P. Levis, S. Katti, and P. Sinha, "Practical, real-time, full duplex wireless," in *Proc. ACM MobiCom*, Sep. 2011.

[37] E. Aryafar, M. A. Khojastepour, K. Sundaresan, S. Rangarajan, and M. Chiang, "MIDU: Enabling MIMO full duplex," in *Proc. ACM MobiCom*, Aug. 2012.

[38] D. Bharadia, E. McMilin, and S. Katti, "Full duplex radios," in *Proc. ACM SIGCOMM*, Aug. 2013.

[39] M. Chung, M. S. Sim, J. Kim, D. K. Kim, and C.-B. Chae, "Prototyping real-time full duplex radios," *IEEE Commun. Mag.*, vol. 53, no. 9, pp. 56–64, 2015.

[40] M. Chung, M. S. Sim, D. K. Kim, C.-B. Chae, "Compact full duplex MIMO radios in D2D underlaid cellular networks: From system design to prototype results," submitted to *IEEE J. Select. Areas Commun.*, arXiv preprint. [Online]. Available: https://arxiv.org/abs/1612.06112.

[41] M. S. Sim, M. Chung, D. Kim, J. Chung, D. K. Kim, and C.-B. Chae, "Nonlinear self-interference cancellation for full-duplex radios: From link- and system-level performance perspectives," to appear in *IEEE Commun. Mag.*, arXiv preprint. [Online]. Available: https://arxiv.org/abs/1607.01912.

[42] IEEE 802.11ac-2013, *Part 11: Wireless LAN Medium Access Control (MAC) and Physical Layer (PHY) specifications. Amendment 4: Enhancements for Very High Throughput for Operation in Bands below 6 GHz*, IEEE std., Dec. 2013.

[43] S. Yoo, S. Kim, J. Yi, Y. Son, and S. Choi, "ProCCA: Protective clear channel assessment in IEEE 802.11 WLANs," *IEEE Commun. Lett.*, vol. PP, no. 99, 2016.

[44] IEEE P802.11, *Proposed TGax draft specification*, Mar. 2016.

[45] T. Oh, Y.-G. Lim, C.-B. Chae, and Y. Lee, "Dual polarization slot antenna with high cross polarization discrimination for indoor small MIMO systems," *IEEE Antennas Wireless Propag. Lett*, vol. 14, no. 2, pp. 374–377, 2015.

[46] R. A. Valenzuela, D. Chizhik, and J. Ling, "Measured and predicted correlation between local average power and small scale fading in indoor wireless communication channels," in *Proc. IEEE VTC*, 1988.

[47] IEEE P802.11, *TGn Channel Models*, May 2004.

[48] IEEE 802.20 WG on Mobile Broadband Wireless Access, VoIP evaluation for mobile broadband wireless Access (MBWA): Rev. 1, Sept. 2005.

초 록

무선 통신에 대한 수요가 증가함에 따라, Wi-Fi로 흔히 알려진 IEEE 802.11 표준 기반 무선랜(WLAN, Wireless Local Area Network)은 어디에서나 찾아볼 수 있는 기술로 거듭났다. 이로 인해 무선랜의 고밀화, 즉 공간적으로 인접한 많은 AP(Access Point)와 STA(station)들이 동일한 주파수 채널을 사용하며 이로 인해 한 단말이 얻을 수 있는 성능이 제한되는 현상이 두드러지고 있다. 따라서 이러한 고밀도 무선랜 환경에서는 단일 전송에 대한 스펙트럼 효율 뿐만 아니라 주파수 자원의 공간 재사용(spatial reuse)의 중요성 또한 강조된다. 즉, 특정 공간 내에서 얼마나 많은 동시 전송이 가능한지가 중요한 이슈로 자리매김하고 있다.

본 학위논문에서는 고밀도 무선랜 환경에서 더 많은 동시 전송을 성공시키기 위하여 다음과 같은 세 가지 전략을 고려한다. (i) 매체접근제어(MAC, Medium Access Control) 계층의 ACK(Acknowledgment) 및 CTS(Clear-To-Send) 프레임에 대한 송신 전력 제어, (ii) 반송파 감지 임계값(CST, Carrier-Sense Threshold) 적응, (iii) 동시 송신 및 수신 (STR, Simultaneous Transmit and Receiver), 즉 동일대역 전이중 통신 (in-band full duplex).

첫번째로, 본 학위 논문에서는 데이터 프레임에 의한 동일 채널 간섭(CCI, Co-Channel Interference)보다 덜 조명되어 왔던 MAC ACK 프레임에 의해 발생하는 CCI에 주목한다. 확률적 기하 분석(stochastic geometry analysis)을 기반으로 ACK 프레임의 송신 전력 조절의 필요성을 확인하였으며, 이를 바탕으로 동적 ACK 프레임 송신 전력 제어 알고리즘인 Quiet ACK(QACK)을 제안한다. QACK은 데이터 프레임 수신 중 수행되는 CCI 검출 및 CCI 전력 추정 기법과 ACK 프레임 전송 통계를

활용하여 세밀하고 신속하게 ACK 프레임의 송신 전력을 조절한다. 더불어, QACK을 바탕으로 CTS 프레임 송신 전력을 조절하여 더 많은 동시 전송이 시도될 수 있게 하는 Quiet CTS(QCTS)라는 알고리즘 또한 제안한다. QACK의 실현 가능성과 성능은 SDR(Software-Defined Radio) 기반 프로토타입을 통해 검증하며 기존 방식 대비 약 1.5배 높은 수율을 얻을 수 있음을 확인한다. 보다 일반적인 무선랜 환경에서의 QACK 및 QCTS의 성능은 ns-3를 사용한 다양한 시뮬레이션을 통해 평가한다.

다음으로, 동시에 더 많은 동시 전송이 시도될 수 있도록 간섭원(interferer node)과 목적 노드(destination node)에 따라 CST를 제어하는 CST 적응 방법, FACT(Fine-grained Adaptation of Carrier-sense Threshold)를 제안한다. 제안하는 방법은 무선랜 표준에서 이미 정의되어 있는 기능을 사용하므로 상용 무선랜 기기에서 쉽게 구현할 수 있다. 또한 FACT 및 다른 CST 적응 기법과 함께 동작할 수 있는 CCA(Clear Channel Assessment) 오버헤드 감소 기법을 제안하며, 제안한 기법들의 성능을 ns-3 시뮬레이션을 통해 비교평가한다. 시뮬레이션 결과를 통해 제안한 방법이 기존 방법에 비해 네트워크 전체 수율을 큰 폭으로 향상시킬 수 있음을 확인한다.

마지막으로, 무선랜에서 STR을 가능하게하는 새로운 MAC 프로토콜, 즉 MASTaR(MAC Protocol for Access points in Simultaneous Transmit and Receive mode)를 기존 무선랜 표준을 준수하는 방법으로 제안한다. 또한 MASTaR 동작을 위해 필요한 물리계층에서 디지털 자가 간섭 상쇄(SIC, Self-Interference Cancellation) 전략을 제안하며 그 실현 가능성과 성능을 3차원 광선 추적(3D-ray tracing) 기반 시뮬레이션을 통해 다양한 측면에서 평가한다. 시뮬레이션 결과는 현재 무선랜 MAC 프로토콜보다 최대 2.58배 높은 수율이 MASTaR를 통해 얻어질 수 있음을 보인다.

요약하면, 본 학위논문에서는 ACK 및 CTS 프레임의 송신 전력 제어 알고리즘과 CST 적응 및 STR을 위한 프로토콜을 제안한다. 제안한 알고리즘 및 프로토콜의 실현 가능성과 성능은 수치 해석, 3차원 광선 추적, ns-3 기반 시스템 수준(system-level) 시뮬레이션, SDR 기반 프로토타입 등 다양한 방법론을 통해 입증한다.